Biosynthesis and Function of Glycosylphosphatidylinositol in *Saccharomyces cerevisiae*

January 2006

Morihisa FUJITA

Biosynthesis and Function of Glycosylphosphatidylinositol in *Saccharomyces cerevisiae*

A Dissertation Submitted to

the Graduate School of Life and Environmental Sciences,

the University of Tsukuba

in Partial Fulfillment of the Requirements

for the Degree of Doctor of Philosophy in Science

(Doctoral Program in Functional Biosciences)

Morihisa FUJITA

TABLE OF CONTENTS

TABLE OF CONTENTS.....i

ABBREVIATIONS.....v

ABSTRACT.....1

GENERAL INRODUCTION.....3

GENERAL METHODS.....10

Escherichia coli strain.....10

Yeast strain.....10

Media.....10

Transformation of *E. coli* cells.....11

Preparation of plasmid DNA from *E. coli* cells.....11

Transformation of *S. cerevisiae* cells.....11

Recovery of plasmid DNA from transformed yeast cells.....12

Disruption of genes in yeast.....12

Tetrad dissection.....13

Western blotting.....14

Fluorescence microscopy.....15

Measurement of cell viability.....15

CHAPTOR I

***GPI7* is essential for yeast cell separation.....16**

I-1. Summary.....17

I-2. Introduction.....18

I-3. Materials and methods.....20

Strains and media.....20

Plasmids.....20

Genetic screens.....22

[2-^{3}H]*myo*-inositol labeling of GPI intermediates.....23

Western blotting.....23

Flow cytometry.....24

Fluorescence microscopy.....24

I-4. Results.....26

Isolation and characterization of *gpi7-2* mutants.....26

Multicopy suppressors of *gpi7-2* mutant.....29

Microscopic observation and flow cytometric analysis of *gpi7* mutants carrying multicopy suppressors.....30

Genetic interaction between GPI biosynthesis and Cbk1p pathway.....30

Localization of Egt2p in *gpi7* mutants.....32

I-5. Discussion.....35

Roles for multicopy suppressors in *gpi7* mutants.....36

Relationship between *GPI7* and Cbk1p-Ace2p pathway.....37

Specificity of cell separation control by *GPI7*.....39

CHAPTOR II

***BST1* is required for the quality control of GPI-anchored proteins.....41**

II-1. Summary.....42

II-2. Introduction.....43

II-3. Materials and methods.....45

Strains and media.....45

Plasmids.....45

Immunoblotting.....48

Subcellular fractionation and glycosylation of Gas1*p.....49

Cycloheximide chase analysis.....50

Inositol labeling and immunoprecipitation of HA-Gas1p.....51

Fluorescence microscopy.....52

Immunoprecipitation.....52

II-4. Results.....53

Construction and characterization of misfolded Gas1 proteins.....53

Gas1* proteins are modified by GPI, but degraded via proteasome.....55

ER-associated degradation pathway of Gas1* proteins.....56

Degradation of Gas1* protein requires GPI inositol deacylation.....58

Degradation of Gas1* protein in mutants of

GPI biosynthesis, concentration, and *N*-glycosylation.....61

Misfolded Gas1 proteins associate with both

the chaperone BiP/Kar2p and GPI inositol deacylase *in vivo*.....64

II-5. Discussion.....66

Increases in the molecular weight of Gas1* proteins.....66

Effect of *N*-glycan processing on the degradation of Gas1* proteins.....67

ER-associated degradation of Gas1* proteins.....67

Folding of GPI-anchored proteins.....69

Bst1p is involved in the quality control of GPI-anchored proteins.....69

GENERAL DISCUSSION.....72

Overview of this thesis.....72

Roles of a side chain ethanolaminephosphate of GPI anchor added by Gpi7p.....73

Roles of inositol deacylation of GPI anchor by Bst1p.....74

Contribution of this thesis to GPI anchor research.....76

Perspectives.....78

ACKNOWLEDGEMENT.....80

REFERENCES.....82

FIGURES AND TABLES.....100

ABBREVIATIONS

CFW	calcofluor white
CHX	cycloheximide
CPY	carboxypeptidase Y
DAPI	4,6-diamidino-2-phenylindole
ER	endoplasmic reticulumn
ERAD	ER-associated degradation
ERAD-C	ERAD-cytosolic
ERAD-L	ERAD-luminal
EtN-P	ethanolaminephosphate
5-FOA	5’-fluoroorotic acid
GlcN	glucosamine
GlcNAc	*N*-acetylglucosamine
GPI	glycosylphosphatidylinositol
HA	hemagulutinin
HRP	horseradish peroxidase
Ins	*myo*-inositol
kb	kilo base
kDa	kilo Dalton
LiAc	lithium-acetate
Man	mannose
mRFP	monomeric red fluorescent protein
ORF	open reading frame

PAGE	polyacylamide gel electrophoresis
PCR	polymerase chain reaction
PEG	polyethylene glycol
PI	propidium iodide
RNase	ribonuclease
SC	synthetic complete
SDS	sodium dodecyl sulfate
TNSALP	tissue-nonspecific alkaline phosphatase
WT	wild type

ABSTRACT

Protein glycosylation is a well-known post-translational modification in all eukaryotes. Protein glycosylation contributes to several biological functions including protein activity, quality control, stability, correct targeting, interaction between proteins, and cell-cell interaction. A number of cell surface proteins are modified by glycosylphosphatidylinositol (GPI). GPI-anchored proteins are important for the host's self-defense, signal transduction, and cell adhesion in mammalian cells, and for the cell wall biogenesis and cell wall assembly in yeast. The biosynthesis of GPI and its modification to proteins are carried out in the endoplasmic reticulum. The biosynthesis of GPI is essential for growth in yeasts and bloodstream forms of protozoan, and for embryonic development in mammals. In spite of the functional importance of GPI modification, studies on the physiological functions of GPI are little known. The work in this thesis focused on the physiological roles of the GPI moiety by studying genes involved in the GPI biosynthesis and modification in yeast *Saccharomyces cerevisiae*.

First, I characterized the role of a side chain ethanolaminephosphate to the second mannose on the GPI core structure, which is added by Gpi7p. The *gpi7* mutants have defects in cell separation and a daughter cell-specific growth defect at the non-permissive temperature. I isolated *WSC1*, *RHO2*, *ROM2*, *GFA1* and *CDC5* as multicopy suppressors of the *gpi7* mutants, suggesting that *gpi7* mutant cells may have defects in cell wall integrity and/or the cell cycle. Multicopy suppressors could suppress the growth defect of *gpi7* mutants, but not the cell separation defect. Mutations in the Cbk1p-Ace2p pathway, which activates the expression of daughter-specific genes for cell separation after cytokinesis, bypassed the temperature-sensitive growth defect of

gpi7 mutants. A GPI-anchored protein, Egt2p, that is required for cell separation, was not transported to the septum correctly in *gpi7* mutants. These results suggest that side chain EtN-P of the GPI anchor added by Gpi7p is important for the correct targeting of the GPI-anchored proteins in yeast cell separation. To my. knowledge, this is the first report indicating that a complete GPI structure is essential for the correct targeting of GPI-anchored proteins.

Second, I investigated the function of acyl portion on inositol of GPI moiety. After attachment of GPI to proteins, the acyl group on inositol of the GPI is eliminated by Bst1p. Because inostiol deacylation of GPI-anchored proteins by Bst1p is a first reaction after GPI attachment to proteins and a trigger of the ER exit of them, I speculated that the inositol deacylation of GPI by Bst1p mediates ER quality control of GPI-anchored proteins. To confirm this notion, I constructed and characterized a misfolded model of GPI-anchored protein, Gas1*p. Gas1*p was modified with a GPI anchor but retained in the ER and was degraded rapidly *via* the proteasome. Disruption of *BST1* caused a delay in the degradation of Gas1*p. This delay was due to the effect on the deacylation activity of Bst1p. Further, Gas1*p associated with Bst1p *in vivo*. My data suggests that a deacylation of the inositol on GPI plays a crucial role in the degradation of GPI-anchored proteins. This is the first report on molecular mechanisms of the quality control and degradation of GPI-anchored proteins, indicating that the GPI anchor itself is involved in the quality control process.

GENERAL INTRODUCTION

Worldwide genome sequencing projects from the beginning of 1990s enabled us to understand whole genome information of various living organisms. Whole genome information of more than 100 species is now available. In particular, the information of the model organisms, such as *Escherichia coli, Saccharomyces cerevisiae, Caenorhabditis elegans, Drosophila melanogaster,* and *Mus musculus,* were collected on databases in order, and we can access them anytime through the worldwide web. The accumulated knowledge accelerates the experimental research and reveals the molecular mechanisms of living organisms more rapidly. By the human genome-sequencing project that has been completed in 2003, we are able to obtain whole human blueprint. Based on the integrated information, we are demanded to understand more advanced living phenomena, such as regulation of transcription, protein-protein interaction and post-translational modification, which are thought to be major points to be uncovered in the post-genome sequencing era. In eukaryotes, almost all proteins are further modified after translation: acetylation, glycosylation, palmitylation, ubiquitination and so on (Han and Martinage, 1992).

Protein glycosylation is one of the most well known modifications in eukaryotes. From human genome-sequencing project, it is estimated that the number of proteins coded in human genome is about 26,000. It is presumed that about 50% of these proteins are modified by glycan (Kawasaki, 2003). Protein glycosylation is known to be important for the protein activity, quality control, stability, correct targeting, interaction between proteins, and cell-cell interaction in many living cells. More than 300 genes are involved in the glycan modification (glycogenes) including

glycosyltransferases, glycosidases, and glycan binding proteins (lectins) in human genome (Taniguchi, 2003). There are many reports that the defects in glycogenes cause diseases (e.g., congenital disorder of glycosylation, paroxysmal nocturnal hemoglobinuria, lysosomal diseases, and congenital muscular dystrophies).

Protein glycosylation is classed into three groups based on the types of binding between oligosaccharide and protein: asparagine (*N*)-linked glycosylation, serine/threonine (*O*)-linked glycosylation, and glycosylphosphatidylinositol (GPI)-anchoring. *N*-linked oligosaccharides are bound to asparagine residues in the sequence of Asn-X-Ser/Thr in proteins by *N*-glycosidic bonds. *O*-linked oligosaccharides are bound to serine or threonine residues in proteins by *O*-glycosidic bonds. The structural regularity of *O*-linked oligosaccharides is low relative to that of *N*-linked oligosaccharides. On the other hand, the bound form of GPI moiety is more unique. A carboxyl-terminal peptide of the substrate protein is cleaved by GPI transamidase complex, and an ethanolamine-phosphate of the GPI moiety is bound to the nascent carboxyl terminus of the protein.

GPI anchoring is one of the conserved post-translational modifications to many cell surface proteins in all eukaryotes. More than 150 proteins at the plasma membrane are anchored by GPI in human. GPI-anchored proteins are important for the host's self-defense, signal transduction, cell-cell interaction, and cell adhesion. Besides, some of them function as receptors for viruses and toxins. In the genome of *S. cerevisiae*, more than 60 open reading frames (ORFs) are predicted to encode GPI-anchored proteins. The GPI-anchored proteins play important roles for cell wall biogenesis and cell wall assembly in *S. cerevisiae*. Some of GPI-anchored proteins are localized at the plasma membrane. The others are further processed at the plasma

membrane and are covalently linked to β-1,6-glucan of the cell wall component through the GPI portion (Figure 1).

GPI has the conserved structure, NH_2-CH_2-CH_2-PO_4-6Manα1,2-Manα1,6-Manα1,4-GlcNα1,6Ins-PO_4-lipid (Figure 2). The biosynthesis of GPI is essential for growth in yeasts (Leidich *et al*., 1994) and bloodstream forms of protozoan (Ilgoutz *et al*., 1999; Nagamune *et al*., 2000), and for embryonic development in mammals (Hyman, 1988; Hirose *et al*., 1992). GPI is synthesized in the endoplasmic reticulum by sequential reactions (Kinoshita and Inoue, 2000; Eisenhaber *et al*., 2003). The identification of the genes required for the GPI biosynthesis has been performed actively in several mammalian and yeast groups by the genetic screening. In 1993, Dr. Taroh Kinoshita and his colleagues first cloned PIG-A, a catalytic component of the initial step for GPI biosynthesis (Takeda *et al*., 1993). Until now, 24 genes involved in the biosynthesis of GPI have been identified (Table I).

Phosphatidylinositol is modified by the stepwise additions of sugars and ethanolaminephosphates (EtN-P), thus forming a complete precursor lipid in the ER (Figure 3). The first step, the transfer of *N*-acetylglucosamine (GlcNAc) to PI generating GlcNAc-PI, is catalyzed by an enzyme complex consisting of at least seven components, Gpi3p (mammalian orthologue: PIG-A), Gpi2p (PIG-C), Gpi15p (PIG-H), Gpi19p (PIG-P), Gpi1p (GPI1), and Eri1p (PIG-Y). Mammalian DPM2 is also involved in this step. In the second step, GlcNAc moiety is de-*N*-acetylated by Gpi12p (PIG-L). These two reactions occur on the cytoplasmic surface of the ER. GPI intermediate is then flipped into the luminal side of the ER, where inositol moiety is acylatd by Gwt1p (PIG-W) generating GlcN-acyl-PI. Next, three Man and three EtN-P are sequentially added to GlcN-acyl-PI. Three distinct mannosyltransferases, Gpi14p (PIG-M), Gpi18p

(PIG-V) and Gpi10p (PIG-B), were identified, and Gpi14p (PIG-M) required the essential counterpart Pbn1p (PIG-X). In yeast and several parts of mammalian tissues, Smp3p (hSMP3) is involved in the addition of the fourth Man. The donor substrate dolichol-phosphate-mannose is synthesized by the Dpm1p enzyme in yeast but by the enzyme complex of DPM1, DPM2 and DPM3 in mammailan cells, and its translocation into the luminal side of the ER is mediated by SL15 in mammalian cells. The transfer of EtN-P to the first, third and second Man are catalyzed by Mcd4p (PIG-N), Gpi13p (PIG-O) and Gpi7p (GPI7). Gpi11p (PIG-F), an essential subcomponent, binds Gpi13p (PIG-O) and Gpi7p (GPI7) independently. The amido-group of EtN-P added by Gpi13p/Gpi11p (PIG-O/PIG-F) is finally transferred to the carboxyl terminus of proteins by GPI-transamidase generating GPI-anchored proteins. This reaction is catalyzed by the enzyme complex of the catalytic subunit Gpi8p (GPI8) and the four essential subcomponents, Gaa1p (GAA1), Gpi17p (PIG-S), Gpi16p (PIG-T) and Gab1p (PIG-U). The resulting GPI-anchored proteins are inositol-deacylated by Bst1p (PGAP1), and depart from the ER and are transported to the plasma membrane via Golgi apparatus.

Studies on the GPI-anchored proteins are interesting in both medical aspects and basic studies in biology. In medical aspects, first, GPI-anchored proteins DAF and CD59, which are complement regulatory proteins, are important for self-protection from complement. Mutations in PIG-A gene cause paroxysmal nocturnal hemoglobinuria due to the abnormality of the GPI anchor biosynthesis and deficiency in the surface expression of DAF and CD59 (Takeda *et al.*, 1993). Second, the abnormality of some GPI-anchored proteins causes unique diseases. Tissue-nonspecific alkaline phosphatase (TNSALP) is a GPI-anchored protein. Mutations in TNSALP are reported to be

associated with hypophosphatasia (Mornet, 2000). Prion diseases including Creuzfeldt-Jakob disease, Gerstmann-Straussler-Scheinker disease, and fatal familial insomnia are caused by conformational changes of prion protein, which is also a GPI-anchored protein (Prusiner, 1998). Third, genes involved in GPI biosynthetic pathways and modifications will be a target for the antifungal drugs and antiprotozoal drugs, because GPI structure is variable in the side chains and lipid moieties of GPI from yeast and protozoan to human, although GPI anchoring is essential for cell viability of fungi and for viability of protozoan in host cells (Kinoshita and Inoue, 2000). For example, in a particular stage of the life cycle of the protozoan parasite *Trypanosoma brucei*, the palmitic-acid residues of the GPI anchors are replaced with myristic-acid residues before the anchor is attached to proteins (Nagamune and Kinoshita, 2002). In yeast and other fungi, the diacylglycerol moieties of the GPI anchors are extensively replaced with ceramides after attachment of the GPI anchor to protein (Reggiori *et al.*, 1997).

Investigation of GPI-anchored proteins is also attractive in basic research area because they have unique properties that are different from soluble or membrane proteins. First, GPI-anchoring to protein confers a specific association with detergent-resistant membranes (DRM), which implies an association with a lipid-dependent structural unit that has a functional significance (Brown and Rose, 1992). Several biochemical studies proposed that GPI-anchored proteins are present in specialized membrane domains that have become known as lipid rafts, which are sphingolipid- and sterol-rich microdomains in membrane (Simons and Ikonen, 1997). Second, GPI-anchored proteins are transported from the ER to the Golgi apparatus in vesicles distinct from those containing non-GPI proteins (Muniz *et al.*, 2001). Several particular components are required for sorting GPI-anchored proteins from other secretory

proteins upon exit from the ER. The p24 family including Emp24p and Erv25p are directly required for efficient packaging of GPI-anchored proteins into ER-derived vesicles (Muniz *et al.*, 2000). Uso1p, a small GTPase Ypt1p, and COG complex are probably directly involved in cargo sorting before, or during, exit from the ER. v-SNAREs Bos1p, Bet1p, and Sec22p are also involved in the cargo sorting (Morsomme *et al.*, 2003). Ceramide synthesis also affects the transport of GPI-anchored proteins from the ER to the Golgi (Barz and Walter, 1999; Watanabe *et al.*, 2002). Third, although most of endocytic pathways require at least one of the numerous dynamin isoforms for the purpose of pinching-off at the cell surface, several GPI-anchored proteins are selectively internalized through a dynamin-independent pathway. GPI-anchored proteins are endocytosed through the GPI-anchored-proteins-enriched early endosomal compartments (GEEC) pathway (Fivaz *et al.*, 2002). The GPI anchor functions as a sorting signal for the selective targeting of GPI-anchored proteins into the GEEC pathway.

Despite of these functional significances of GPI-anchored proteins from basic study to medical study, the studies on the physiological functions of GPI itself is little known. Budding yeast, *S. cerevisiae*, has several advantages to analyze the functions of the GPI and GPI-anchored proteins. First, GPI structure and biosynthetic pathway is clearly determined by biochemical methods (Figure 3). Second, the almost all genes on the GPI biosynthetic pathway in the endoplasmic reticulum (ER) are identified (Table I) (Kinoshita and Inoue, 2000; Eisenhaber *et al.*, 2003). Third, *S. cerevisiae* is easy to use both genetic and molecular biological methods. Finally, the comprehensive information, such as genomic data, protein profiles, and protein-protein interactions, has been collected on the yeast databases in order.

In this thesis, I tried to find out the physiological function of GPI moiety by studying the roles of genes involved in the GPI biosynthesis and modification in *S. cerevisiae*. In Chapter I, I revealed that the role of *GPI7*, which is required for the addition of side chain EtN-P to second Man on the GPI core structure, is important for the correct targeting of the GPI-anchored proteins in cell separation. In Chapter II, I elucidated that *BST1*, which is required for the inositol deacylation of GPI-anchored proteins, plays a crucial role for the quality control of GPI-anchored proteins.

GENERAL METHODS

Escherichia coli strain

For standard DNA propagation the strain DH5α (F^-, *f*80, *lac*ZDM15, D (*lac*ZYA-argF) U169, *hsd*R17 (rK^-,mK^+), *rec*A1, *end*A1, *deo*R, *thi*-1, *sup*E44, *gyr*A96, *rel*A1, l-) was used.

Yeast strains

Yeast strains used in this study are listed in Table II. W303-1A (*MAT***a** *ade2-1 his3-11 leu2-3,-112 trp1-1 ura3-1 can1-100*) was mainly used as wild-type cells (Sutton *et al.*, 1991).

Media

E. coli strains were grown in LB medium (1% Bacto-Tryptone (Difco, Detroit, Michigan, USA), 0.5% Bacto-Yeast extract (Difco), and 1% NaCl, pH 7.2) at 37˚C.

Yeast strains were cultivated in YPAD medium (2% glucose, 2% Bacto-Peptone (Difco), 1% Bacto-Yeast Extract, and 0.003% adenine-sulfate). For auxotrophic selection, Synthetic Dextrose (SD) medium (2% glucose, 0.67% Bacto-Yeast Nitrogen Base w/o amino acids (Difco)) was used. SD was supplemented with 20-400 μg/ml of amino acids, adenine-sulfate and uracil, when necessary. For tryptophan and uracil auxotrophic selection, SDCA medium (SD medium containing 0.5% Bacto-Casamino Acids (Difco) and 0.003% adenine-sulfate) was used. For spore formation, SPO medium (1% potassium acetate) was used. Yeast strains were cultivated at 30˚C.

Transformation of *E. coli* cells

Transformation of *E. coli* cells was done according to the method of Hanahan (Hanahan, 1983). One hundred μl of competent cells (purchased from Toyobo, Osaka, Japan) were gradually thawed and mixed gently with 5 μl of DNA solution. After incubation for 30 min on ice, cells were heat-shocked at 42˚C for 30 sec. Immediately 900 μl of SOC medium (2% Bacto-Tryptone, 0.5% Bacto-Yeast Extract, 10 mM NaCl, 2.5 mM KCl, 10 mM $MgSO_4$, 10 mM $MgCl_2$, and 20 mM glucose) was added. After incubation for 1 h at 37˚C in water bath, the culture medium was spread onto LB-Amp plate (LB medium containing 50 μg/ml ampicillin and 1.5% agar), allowed to cultivate overnight at 37˚C.

Preparation of plasmid DNA from *E. coli* cells

E. coli cells which contain plasmid DNA were cultured overnight in 3 ml of LB-Amp medium (LB medium containing 0.01% ampicillin). Plasmid DNA was extracted by QIAprep Spin Miniprep Kit (Qiagen, Hilden, Germany).

Transformation of *S. cerevisiae* cells

Transformation of *S. cerevisiae* cells as done according to the method of Gietz (Gietz *et al*., 1995). Yeast cells were incubated in 1 ml YPAD medium overnight at 30˚C with shaking. The preculture cells were diluted to 50 ml YPAD (~0.9 OD_{600}). The cells were grown for 5 h. Cells were harvested in the sterile plastic tubes at 3000 X *g* for 5 min and the pellet was collected. Then cells were suspended in 20 ml of sterile water and centrifuged again. The cell pellet was resuspended in 1 ml of 100 mM LiAc and

transferred to a 1.5 ml microtube. The suspension was centrifuged at top speed for 15 sec and the supernatant was removed with a micropipette. The cells were resuspended to a final volume of 500 μl. Then 50 μl of the competent cells was added to the transformation mixture (240 μl of 50% PEG 4000, 16 μl of 1 M LiAc, 5 μl of carrier DNA (10 mg/ml), 30 μl of sterile water, and 3 μl of plasmid DNA) and vortexed well. The suspension was incubated at 30˚C for 30 min and then heat-shocked at 42˚C for 20 min. The mixture was centrifuged and the supernatant was removed. The cell pellet was resuspended in 200 μl of sterile water and spread on a selective medium plate.

Recovery of plasmid DNA from transformed yeast cells

Yeast cells that were previously grown on 5 ml of selective medium were collected by centrifugation. Then 400 μl of yeast breaking buffer (0.1 M NaCl, 1 mM EDTA, 2% Triton X-100, and 1% SDS in 0.1 mM Tris-HCl, pH 8.0) was added. Acid washed glass beads (0.5 mm in diameter; Sigma, St. Louis, Missouri, USA) were filled into the microtube up to the meniscus. Two hundred μl of phenol/chloroform was added and vortexed for 3 min. The aqueous phase was recovered and transferred into a clean tube containing 800 μl of cold ethanol. DNA was precipitated by centrifugation, rinsed with cold 70% ethanol and resuspended in 50 μl of H_2O. About 5 μl of the DNA solution was used to transform *E. coli* cells.

Disruption of genes in yeast

Disruption of genes in yeast was performed with one step gene disruption method as described (Longtine *et al.*, 1998). PCR was performed using pFA6a-TRP1 and pFA6a-His3MX plasmids (Longtine *et al.*, 1998) as templates. Appropriate forward

target gene-specific primer with 5’-CGGATCCCCGGGTTAATTAA-3’ at the 3’ end and reverse target gene-specific primer with 5’-GAATTCGAGCTCGTTTAAAC-3’ at the 3’ end were used. The PCR product was purified with agarose gel extraction, and introduced to yeast host cells. The transformants were selected with appropriate auxotrophy, and checked the insertion site with yeast colony PCR using one primer that annealed within the transformation module and the second primer that annealed to the target gene locus outside the region altered.

Tetrad dissection

Mating

Yeast haploid strains of mating types of **a** and α were mixed and cultured on a YPAD plate for 2 days at room temperature.

Sporulation

Sporulation was carried out using SPO plate. Diploid strain grown on YPAD plate was picked up with sterilized toothpick and transferred to a SPO plate and incubated for 2 days at room temperature. Sporulation was confirmed microscopically.

Dissection

A diploid strain of *S. cerevisiae* was cultured on SPO plate for 2 days at room temperature for sporulation. The sporulrated cells were suspended in sterilized water. And small amounts of Zymolyase 100T were added into the suspension and incubated for 1 min at room temperature. Zymolyase digests cell wall of ascus. The suspension was spotted on YPAD plates, and dried up under a laminar flow cabinet. Tetrad

ascospore was dissected individually with micromanipulator under a microscope. The individual ascospore was cultured independently and assayed for auxotrophic markers and biological functions. The cell that had another genotype with a parent was obtained in this way.

Western blotting

Cells were grown in 5 ml of SD medium overnight, washed twice and resuspended with 100 μl of TEG buffer (50 mM Tris-HCl (pH 7.5), 100 mM NaCl, and 1 mM EDTA). Glass beads were added to the tube until the suspension being buried. The cells were broken by vortex with max speed for 10 min at 4˚C. Broken cells were centrifuged for 5 min at 600 X *g* to remove unbroken cells and cell wall, and the supernatant was centrifuged for 15 min at 13,000 X *g*. The membrane pellet was resuspended in 100 μl of TEG buffer.

For Western blotting, an equal volume of 2 x sample buffer was added to the sample. The samples were denatured during 95˚C for 5 min for soluble proteins or 1 h at 4˚C for membrane proteins and run on 7.5% or 5-20% SDS-polyacrylamide gels as described previously (Laemmli, 1970). After SDS-PAGE, the proteins on the polyacylamide gel was transferred to PVDF membrane with ATTO transfer system (ATTO, Tokyo, Japan) with constant current (2 mA/cm^2 membrane) for 1 h. The PVDF membrane was incubated in Buffer A (PBS (pH 7.5) with 5% skim milk and 0.1% Tween 20) for 1 h. Primary antibody was diluted by Buffer A and PVDF membrane was incubated in diluted primary antibody solution for 1 h at room temperature or overnight at 4˚C. After the incubation, the PVDF membrane was washed three times for 5 min with Buffer B (PBS (pH 7.5) with 0.3% Tween 20). Secondary antibody was diluted

with Buffer A and the membrane was incubated in secondary antibody solution for 1 h at room temperature. After washing three times for 10 min with Buffer B, the membrane was incubated with ECL-plus (Amersham Biosciences, Uppsala, Sweden) solution for 5 min, exposed and analyzed for the chemiluminescence with LAS 1000 plus (Fuji Film, Tokyo, Japan).

Fluorescence microscopy

All fluorescence images were observed using a model BX50 (Olympus, Tokyo, Japan) fluorescence microscope.

Measurement of cell viability

Viability of the cells was tested by staining method with methylene blue. Methylene blue solution (0.01% methylene blue, 2% sodium citrate) was mixed with an equal volume of cell culture, and stained cells were counted immediately with microscope**.**

CHAPTER I

GPI7 is essential for yeast cell separation

I-1. Summary

GPI7 is involved in adding ethanolaminephosphate to the second mannose in the biosynthesis of glycosylphosphatidylinositol (GPI) in *Saccharomyces cerevisiae*. I have isolated *gpi7* mutants, which have defects in cell separation and a daughter cell specific growth defect at the non-permissive temperature. *WSC1*, *RHO2*, *ROM2*, *GFA1* and *CDC5* genes were isolated as multicopy suppressors of *gpi7-2* mutant. Multicopy suppressors could suppress the growth defect of *gpi7* mutants, but not the cell separation defect. Loss of function mutations of genes involved in the Cbk1p-Ace2p pathway, which activates the expression of daughter-specific genes for cell separation after cytokinesis, bypassed the temperature-sensitive growth defect of *gpi7* mutants. Furthermore, deletion of *EGT2*, one of the genes controlled by Ace2p and encoding a GPI-anchored protein required for cell separation, ameliorated the temperature sensitivity of the *gpi7* mutant. In this mutant, Egt2p is displaced from the septal region to the cell cortex, indicating that *GPI7* plays an important role in cell separation *via* the GPI-based modification of daughter-specific proteins in *S. cerevisiae*.

I-2. Introduction

Glycosylphosphatidylinositol (GPI) anchoring is a post-translational modification conserved in many cell surface proteins of all eukaryotes. GPI anchors attach to certain proteins in the endoplasmic reticulum (ER) and determine their final localization. In mammalian polarized cells, the GPI anchor has been implicated in the potential recruitment of proteins to the apical domain (Brown *et al.*, 1989; Lisanti *et al.*, 1989). In yeast, GPI-anchored proteins are one of the major components of mannoproteins at the cell wall and play important roles in cell wall biogenesis and cell wall assembly (Kapteyn *et al.*, 1999). The yeast *Saccharomyces cerevisiae* has a cell wall composed of mannoproteins, glucan and chitin. The cell wall is a rigid structure that maintains cell morphology, however, it must be remodeled during the cell cycle, including bud emergence and the cell separation process.

The biosynthesis of the GPI anchor is essential for cell growth in yeast. Phosphatidylinositol (PI) is modified by the stepwise addition of sugars and ethanolaminephosphate (EtN-P), thus forming a complete precursor lipid in the ER. GPI transamidase complex recognizes a C-terminal signal in substrate proteins, cleaves a C-terminal peptide from the proprotein substrate and attaches a GPI moiety to the nascent carboxyl terminus, referred to as the ω-site (Kinoshita and Inoue, 2000). *GPI7/LAS21*, a gene involved in the GPI biosynthetic pathway, is required for the addition of a side chain EtN-P to the second mannose portion of the GPI core glycan structure (Figure 4) (Benachour *et al.*, 1999). *GPI7* is not essential for cell viability and GPI lacking a side chain EtN-P which is due to the loss of *GPI7* function is still transferred to proteins (Benachour *et al.*, 1999; Kinoshita and Inoue, 2000; Imhof *et al.*, 2004). Deletion of

GPI7 causes a growth defect at high temperature, hypersensitivity to calcofluor white and a decreased replacement of primary lipid moiety of GPI anchors by ceramide (Toh-e and Oguchi, 1998; Benachour *et al.*, 1999; Toh-e and Oguchi, 1999). Mutations in *GPI7* also affect cell wall anchorage in *S. cerevisiae* and *Candida albicans* (Richard *et al.*, 2002a). *GPI7* is involved in chlamydospore formation, budding patterns and cell shape in *C. albicans* (Richard *et al.*, 2002b) and invasive growth in the dimorphic yeast *Yarrowia lipolytica* (Richard *et al.*, 2001). However, how *GPI7* is involved in these phenomena is still unknown.

Cell separation is the last step of the cell division cycle in budding yeast. It is completed by the degradation of the septum, a specialized structure of the cell wall (Cabib *et al.*, 2001). A chitinase and some glucanases, which are expressed only in daughter cells, are transported to the bud neck and degrade the septum (Cabib *et al.*, 2001; Baladron *et al.*, 2002). These enzymes are under the control of a transcription factor, Ace2p, and Cbk1 kinase (Colman-Lerner *et al.*, 2001; Nelson *et al.*, 2003). In this report, I provide several lines of evidence that GPI biosynthesis, especially the addition of EtN-P to the glycan portion of the GPI anchor by Gpi7p, is involved in the control of cell separation *via* modification of daughter-specific cell wall assembly proteins. Furthermore, I propose a novel hypothesis that EtN-P of the GPI anchor is important for the correct targeting of the GPI-anchored proteins in yeast cell separation.

I-3. Materials and methods

Strains and media

Yeast strains used in this study are listed in Table II. YPAD and synthetic complete (SC) media were used as described previously (Sherman, 1991). SDCA contains 0.67% yeast nitrogen base without amino acids (Difco), 2% glucose, 0.5% casamino acids and 0.004% adenine sulfate. The disruption of genes in yeast was performed with a one-step gene disruption method as described previously (Longtine *et al.*, 1998).

Plasmids

Plasmids used in this study are listed in Table III.

Three tandem copies of the HA epitope were placed just before the stop codon of *GPI7* as follows: TOp1014 was kindly provided by Dr. Akio Toh-e (University of Tokyo), which carried the *GPI7* gene in YCUp4 (*CEN4*, *ARS1*, *URA3*). Using TOp1014 as a template, a *Nhe*I restriction site was introduced by PCR just before the stop codon of *GPI7*, and the PCR product was subcloned into the centromere plasmid pRS316 (Sikorski and Hieter, 1989) to generate pMF3, and sequenced for confirmation. The *Nhe*I-*Nhe*I cassette containing three copies of the HA epitope was prepared from pYT11 (Takita *et al.*, 1995), and inserted into the *Nhe*I site of pMF3 to generate pMF7 (pRS316-GPI7-HA). To create *gpi7* point mutations, I used a QuickChange Site-Directed Mutagenesis Kit (Stratagene).

The centromere plasmid pRS315-HA-EGT2, in which 3xHA tagged *EGT2* is expressed under its own promoter, was constructed as follows: a DNA fragment

containing the *EGT2* ORF, a 0.7-kb upstream region and a 0.5-kb downstream region was amplified by PCR and subcloned in pRS315 (Sikorski and Hieter, 1989) to generate pMF295. Using pMF295 as a template, the *Sma*I site was introduced into 78 nucleotides downstream from the start codon of *EGT2* by PCR. The PCR product was subcloned into pRS315 to generate pMF296, and sequenced for confirmation. The *Sma*I-*Sma*I cassette containing three copies of the HA epitope was inserted into the *Sma*I site of pMF296 to generate pMF297 (pRS315-HA-EGT2).

The centromere plasmid pRS315-HA-ENG1, in which 3xHA tagged *ENG1* is expressed under its own promoter, was constructed as follows: a DNA fragment containing the *ENG1* ORF, a 0.8-kb upstream region and a 0.4-kb downstream region was amplified by PCR and subcloned in pRS315 to generate pMF306. Using pMF306 as a template, the *Sma*I site was introduced 600 nucleotides downstream from the start codon of *ENG1* by PCR. The PCR product was subcloned into pRS315 to generate pMF309, and sequenced for confirmation. A *Sma*I-*Sma*I cassette containing three copies of the HA epitope was prepared, and inserted into the *Sma*I site of pMF309 to generate pMF310 (pRS315-HA-ENG1).

pRS315-HA-ENG1-EGT2, the 3xHA-tagged *ENG1-EGT2* chimeric gene expressed under the *ENG1* promoter, was constructed as follows: using pMF310 as a template, a *Hin*dIII restriction site was introduced by PCR just before the stop codon of *ENG1*, and the PCR product was subcloned into the centromere plasmid pRS315 to generate pMF355, and sequenced for confirmation. Using pMF295 as a template, a *Hin*dIII site was introduced 150 nucleotides upstream, and a *Xho*I site, 0.5-kb downstream from the stop codon of *EGT2* by PCR. The PCR product was subcloned into pMF355 to generate pMF357 (pRS315-HA-ENG1-EGT2), and sequenced for

confirmation.

Genetic screens

To obtain multicopy suppressors of *gpi7-2*, I transformed *gpi7*Δ cells carrying pRS316-gpi7-2-HA (*gpi7-2,* uracil marker) with a yeast genomic library (leucine marker). From about 15,000 transformants, 48 colonies that could grow at 35.7°C on SC–Leu–Ura plates were obtained. These colonies were grown on SC–Leu plates containing 0.1% 5- fluoroorotic acid to remove pRS316-gpi7-2-HA at 30°C. Then, the multicopy plasmids recovered from these cells were introduced again into *gpi7-2* cells. Of these colonies, 7 could grow at 35.7°C on SDCA. Restriction analysis or DNA sequencing was performed for the 7 plasmids. I obtained two kinds of plasmids. One plasmid contained *GPI7* itself. The others were derived from a locus different from each other. After subcloning, the suppressor genes in these plasmids were determined to be *WSC1*, *RHO2*, *ROM2*, *GFA1* and *CDC5*.

To screen for extragenic suppressors of *gpi7*Δ, a yeast genomic library mutagenized by an mTn-3xHA/GFP transposon kindly provided by Dr. Michael Snyder (Yale University) was used to transform MFY11 (*gpi7*Δ). A total of ~33,000 transformants were obtained on SC–Ura plates. The colonies were replica-plated on SC–Ura plates and cultured at 35.7°C to select mutants. The colonies that could survive at 35.7°C were streaked again on SC–Ura plates and cultured at 35.7°C to confirm the recovery of temperature sensitivity. Tagged transposon sites were identified by direct genomic sequencing as described previously (Horecka and Jigami, 2000).

[2-^{3}H]*myo*-inositol labeling of GPI intermediates

GPI intermediates were labeled with [2-^{3}H]*myo*-inositol (PerkinElmer) as described previously with some modifications (Benghezal *et al.*, 1995). Cells were grown in SDCA medium, and 2.5 X 10^{7} cells were resuspended in 600 μl of SD inositol-free medium containing 0.67% yeast nitrogen base without inositol and amino acid (Bio 101), 5% glucose, and nutrient supplements. They were divided into two tubes and preincubated for 20 min at 25°C or 35.7°C, and 0.25 MBq [2-^{3}H]*myo*-inositol was added. The cells were then incubated for 90 min at 25°C or 35.7°C, respectively. After the 90 min incubation, 10 mM (final concentration) of NaF and NaN3 were added to the reaction mixture to stop the reaction. The cells were washed with water. Lipids were extracted and desalted by butanol extraction as described previously (Sipos *et al.*, 1994). The lipid extracts were analyzed by ascending TLC using 0.2 mm-thick silica gel plates with a solvent system of chloroform/methanol/water (10: 10: 3). Radioactivity was detected using Molecular Imager FX (Bio-Rad).

Western blotting

The samples were denatured with sample buffer for 1 h at 4°C for membrane proteins and run on 7.5% SDS-polyacrylamide gels, as described previously (Laemmli, 1970). After SDS-PAGE, the proteins on the polyacylamide gels were transferred to PVDF membranes (Millipore). Gpi7-HAp was detected with the anti-HA monoclonal antibody 16B12 (Babco). Immunoreactive bands were visualized by staining with horseradish-conjugated goat anti-mouse IgG (Cell Signaling Technology) and chemiluminescence with ECL-plus (Amersham Biosciences).

Flow cytometry

Yeast cells grown on SC medium until 5 X 10^6 – 1 X 10^7 cells/ml with water bath shaker (Taitec) at a rate of 160 rpm were resuspended in 300 μl of 0.2 M Tris-HCl (pH 7.5), added to 700 μl of cold (–20°C) ethanol, and stored at –20°C. The cells were washed twice with 0.2 M Tris-HCl (pH 7.5) and sonicated with minimum output for 10 sec (Sonifier Cell Disruptor 350, Tomy). The cells were harvested and resuspended in RNase solution (1 mg/ml RNase A (Qiagen) in 0.2 M Tris-HCl (pH 7.5)) at 30°C for 3 – 4 h. The RNase-treated cells were harvested and resuspended in 100 μl of propidium iodide (PI) solution (0.1% sodium citrate, 0.058% NaCl, 0.1% NP-40, and 0.005% PI), put on ice for 15 min and added to 400 μl of 0.2 M Tris-HCl (pH 7.5). DNA contents were measured by FacsCalibur (Becton Dickinson). For cell synchronization, cells were arrested with α-factor (Peptide Institute, Inc.) for 3 h at 25°C, washed, and transferred into prewarmed YPAD medium at 35.7°C.

Fluorescence microscopy

All fluorescence images were observed using a fluorescence microscope, BX50 (Olympus). For calcofluor white staining, cells washed with water were sonicated for 10 sec as described above and calcofluor white solution (1 mg/ml calcofluor white (Sigma) in water) was added. The cells were then washed twice with water. For HA-Egt2p, HA-Eng1p and HA-Eng1-Egt2p localization, cells grown in SC medium were sonicated, incubated at 35.7°C for 4 h, fixed with 3.7% formaldehyde for 1 h at room temperature, and stained as described previously with some modifications (Abe *et al.*, 2003). Cells were washed with 250 μl of phosphate-buffered saline (PBS) with bovine serum albumin (BSA) (1 mg/ml) and rat anti-HA antibody 3F10 (Boehringer Mannheim) and

incubated at 4°C for 1 h. The cells were then washed twice in PBS and incubated in PBS buffer with BSA and Alexa 488-conjugated goat anti-rat IgG at 4°C for 1 h.

I-4. Results

Isolation and characterization of *gpi7-2* mutants

To understand the cellular functions of *GPI7*, I adopted two different genetic approaches: a multicopy suppressor analysis with a *gpi7* missense mutant and an extragenic suppressor analysis with a *gpi7* gene disrupted (*gpi7*Δ) mutant. Although several multicopy suppressors were isolated from *gpi7*Δ cells (Toh-e and Oguchi, 1998, 1999, 2002), no significant information was obtained to elucidate the biological function of *GPI7*. My purpose in this study is to obtain new suppressors from *gpi7* missense and *gpi7*Δ mutant cells, which may help to elucidate the biological functions of Gpi7p. To investigate the cellular function of *GPI7*, I tagged endogenous copy of *GPI7* with a sequence encoding the influenza hemagglutinin (HA) epitope (Figure 5). The fusion protein was functional, because the resulting strain showed a normal growth at both temperatures treated (25 and 37˚C) and no accumulation of GPI intermediate (Figure 6A and 6B). Fluorescence microscopy revealed that Gpi7-HA fusion protein was localized at the internal perinuclear membrane, probably the endoplasmic reticulum (Figure 6C). The localization of Gpi7-HAp is identical with that of other GPI synthetic enzymes.

Next, I have tried to isolate missense mutants of *GPI7* that show a deficiency in only a part of proposed several functions of Gpi7p (Toh-e and Oguchi, 1998; Benachour *et al.*, 1999; Toh-e and Oguchi, 1999; Richard *et al.*, 2002a; Toh-e and Oguchi, 2002; Imhof *et al.*, 2004), among site-directed mutagenic constructs. I replaced the positively or negatively charged amino acid(s) with alanine in a region that is conserved among the *GPI7* ORFs of *S. cerevisiae* (NP_012473), *C. albicans* (AAL83897), *Y. lipolytica*

(AAK52677), *Schizosaccharomyces pombe* (CAA91096), *Caenorhabditis elegans* (NP_495820), and *Homo sapiens* (BAC11227) (Figure 7). The mutation sites were as follows: R102A (*gpi7-1*), D153 and 154A (*gpi7-2*), D183A (*gpi7-3*), D212A (*gpi7-4*), D259A (*gpi7-5*), E461 and 462 and 463A (*gpi7-6*) and K802A (*gpi7-7*). One mutant, *gpi7-2*, in which the 153rd and 154th aspartic acids are replaced by two alanines (shown as "AA" in Figure 8A), showed temperature sensitivity at 35.7°C (Figure 8B). This mutational region was conserved among *GPI13* orthologues (Figure 8A), but not *MCD4* orthologues (data not shown). Both Gpi13p and Gpi7p transfer EtN-P to position 6 of the mannose, whereas Mcd4p transfers it to position 2 (Kinoshita and Inoue, 2000). Therefore, the mutation site in *gpi7-2* is conserved in the EtN-P transferases, which transfer EtN-P to position 6 of the mannose. The mutant cells recovered their cell growth on the medium with an osmotic stabilizer, 1 M sorbitol (Figure 8C), and were hypersensitive to calcofluor white (CFW) (Figure 8D), indicating that the mutant cells are defective in cell wall biogenesis or assembly. Western blotting analysis of HA-tagged Gpi7p revealed that the mutant Gpi7-2 proteins were of the same size as Gpi7-HA fusion protein (90 kDa) and were not significantly degraded in the cells by the point mutation (Figure 8E). Therefore, the temperature sensitivity of the *gpi7-2* strain might be due to the loss of the Gpi7p enzymatic activity and not due to the degradation of mutant Gpi7 proteins. Next I examined whether this mutant accumulates the GPI intermediate M4, which is specifically detected in *gpi7*Δ cells, at permissive and non-permissive temperatures (Benachour *et al.*, 1999). The lipid fraction from *gpi7-2* cells treated at the non-permissive temperature (35.7°C) showed M4 accumulation, while the M4 accumulation was decreased at the permissive temperature (25°C) (Figure 8F). These results indicate that the *gpi7-2* gene product partially functions in EtN-P transfer

activity at the permissive temperature, but loses its function at the non-permissive temperature. Therefore, I selected strain *gpi7-2* for further characterization.

I investigated the morphology of the *gpi7* mutant cells. Interestingly, *gpi7* mutants showed an abnormal cell arrangement after 4 h incubation at the restrictive temperature (35.7°C), while the morphology of the *gpi7* cells was normal at permissive temperature (25˚C) (data not shown). Approximately 30% of the *gpi7-2* cells showed a unique arrangement, in which the mother cell is attached to two daughter cells even after sonication (Figure 9B). This abnormal cell arrangement was still observed after 10 h incubation at 35.7°C. Judging from methylene blue staining, most of the *gpi7-2* cells were still viable after 10 h incubation at the non-permissive temperature (data not shown), suggesting that *gpi7-2* cells might arrest at this stage. The DNA content of propidium iodide-stained cells was analyzed by flow cytometry (Figure 9A and B). An abnormal peak, 3C DNA content, was observed in *gpi7-2* cells after 4 h incubation at 35.7°C (Figure 9B), while only the 1C and 2C DNA peaks were observed in wild-type cells. The 3C peak was also observed in *gpi7*Δ cells at the non-permissive temperature (data not shown). These 3C peaks tightly correlated to the abnormal cell arrangement observed in *gpi7* mutants at the restrictive temperature (Figure 9B). To confirm the three-cell arrangement observed in *gpi7* mutant cells more precisely, I examined the DNA content and cell morphology during the cell cycle progression using G1-synchronus cultures treated with α-factor. The synchronized wild-type and *gpi7-2* cells were released into YPAD medium at the non-permissive temperature, 35.7°C. The α-factor treated *gpi7-2* cells were not uniform completely, but showed 1C plus a few 2C peaks (Figure 9E), whereas wild-type cells were uniformly 1C (Figure 9C). Wild-type cells normally progressed through the cell cycle, regenerating G1 phase cells with 1C

DNA content at about 90 min after the release (Figure 9C and D). In contrast, *gpi7* mutant cells failed to regenerate a distinct 1C peak, and 3C DNA cells accumulated at about 180 min after the release (Figure 9E). The observation of cell morphology revealed that most of the *gpi7* mutant cells (more than 80% of total cells) showed a three-cell arrangement (Figure 9F).

Multicopy suppressors of *gpi7-2* mutant

Previous studies of *GPI7* showed that *PKC1*, *ECM33*, *PIR2* and *PSD1* acted as multicopy suppressors in strain *gpi7*Δ (Toh-e and Oguchi, 1998, 1999, 2002). Although several multicopy suppressors were isolated using the *gpi7*Δ mutant, new suppressors that suggest the biological function of *GPI7* may still be obtained from the *gpi7-2* missense mutant (Figure 10).

On screening for multicopy suppressors of *gpi7-2*, I identified five genes that could recover the growth of *gpi7-2* at 35.7°C. The suppressor genes were determined as *WSC1/SLG1*, *RHO2*, *ROM2*, *GFA1* and *CDC5* (Figure 11). *WSC1* encodes a plasma membrane protein required for maintenance of cell wall integrity and for stress response during vegetative growth (Ketela *et al.*, 1999). The *RHO2* gene product is a GTPase, a member of the *rho* family in the *ras* superfamily (Madden and Snyder, 1998). *ROM2* encodes a GDP-GTP exchange factor for Rho1p and Rho2p that can be activated by cell wall defects (Madden and Snyder, 1998). *GFA1* encodes a glutamine-fructose-6-phosphate aminotransferase, a key enzyme that catalyzes the first step in the pathways for chitin, GPI and *N*-glycosylation biosynthesis (Watzele and Tanner, 1989). *CDC5* encodes a serine/threonine protein kinase required for mitotic exit (Cheng *et al.*, 1998; Song and Lee, 2001). The presence of these multicopy suppressor genes suggests that

gpi7-2 may be defective in cell wall integrity and/or the cell cycle.

Microscopic observation and flow cytometric analysis of *gpi7* mutants carrying multicopy suppressors

The *gpi7* mutants showed an abnormal cell arrangement, with two daughter cells being attached to a mother cell at restrictive temperature (Fig. 9B). We further examined whether multicopy suppressors might recover the cell separation defect of the *gpi7-2* mutant. Interestingly, loose peaks higher than 3C peaks were observed in *gpi7-2* strains carrying multiple copies of *WSC1* (Figure 12C), *RHO2* (data not shown), *ROM2* (data not shown) and *GFA1* (Figure 12D), after 4 h incubation at 35.7°C. These cells displayed a unique phenotype, with more than three cells attached to each other without cell separation (Figure 12C and D).

Diffuse peaks containing more than 3C were also observed in *gpi7-2* strains carrying multiple copies of the *CDC5* gene (Figure 12E). These unusual peaks resulted from the overexpression of *CDC5* in *gpi7* mutants, because they were not observed in wild-type cells carrying multiple copies of *CDC5*, indicating the same profile as for the wild-type cells (Figure 13). The *gpi7-2* strain carrying multiple copies of *CDC5* proliferated without cell separation (Figure 12E), consistent with the appearance of loose peaks in the *gpi7-2* strain carrying multiple copies of *CDC5* in the flow cytometric analysis.

Genetic interaction between GPI biosynthesis and the Cbk1p pathway

I also used a transposon insertion mutagenesis method (Ross-Macdonald *et al.*, 1999) to identify mutations that can bypass the requirement of *GPI7* for cell growth

(Figure 14). From this screening, I obtained a mutant that could suppress the growth defect of *gpi7* deletion mutant cells at 35.7°C. Sequencing the DNA region adjacent to the transposon revealed that it is inserted into the carboxyl terminus of *CBK1* (Figure 15A). The insertion site was located 2040 base pairs downstream of the start codon of the 2268-base pair open reading frame of *CBK1* (Figure 15B). Since the predicted phosphorylation site Thr-743 in the conserved C-terminal region of Cbk1p is deleted (Figure 16A) (Tamaskovic *et al.*, 2003), it is likely that this transposon insertion results in a loss-of-function allele of *CBK1*. Cbk1p plays important roles in polarized growth and cell separation in *S. cerevisiae* (Racki *et al.*, 2000; Weiss *et al.*, 2002) (Figure 16B).

To investigate the genetic interaction between *GPI7* and *CBK1* more precisely, *CBK1* was disrupted in *gpi7*Δ mutants. The double mutation *gpi7*Δ *cbk1*Δ overcome the temperature-sensitive phenotype of *gpi7*Δ at 35.7°C (Figure 17). It is known that *CBK1* regulates cell separation *via* an Ace2p-dependent pathway and polarized growth *via* an Ace2p-independent pathway (Figure 16B) (Racki *et al.*, 2000; Bidlingmaier *et al.*, 2001). To examine whether the suppression of *gpi7*Δ cells by *cbk1*Δ disruption depends on *ACE2* or not, *ACE2* was disrupted in the *gpi7*Δ background. The *gpi7*Δ *ace2*Δ double mutant could grow as fast as the *gpi7*Δ *cbk1*Δ double mutant at 35.7°C (Figure 17), indicating that the disruption of the Cbk1p-Ace2p pathway bypasses the growth defect of the *gpi7* mutant cells. Ace2p activates a set of genes that are essential for mother-daughter cell separation, such as *CTS1* and *SCW11*, which encode proteins involved in degradation of the septum (Colman-Lerner *et al.*, 2001) (Figure 18A). It is reported that *EGT2*, which is also regulated by the Cbk1p-Ace2p pathway, encodes a GPI-anchored protein (Hamada *et al.*, 1998; Nelson *et al.*, 2003). *EGT2* is specifically expressed at the early G1 phase in daughter cells, and it has been proposed that Egt2p is a glucanase or a

regulator of glucanase (Kovacech *et al.*, 1996; Baladron *et al.*, 2002). The *egt2*Δ mutants were shown to have defects in cell separation (Kovacech *et al.*, 1996). These reports prompted us to investigate the relationship between *GPI7* and *EGT2*. Deletion of *EGT2* partially suppressed the growth defects of *gpi7* single mutants at the non-permissive temperature (Figure 18B). I also disrupted another glucanase encoded by *BGL2* to check the specificity of suppression. Bgl2p is a non-GPI type endoglucanase and the expression is not regulated by Ace2p (Mrsa *et al.*, 1993). Mutation in *BGL2* did not suppress the temperature sensitivity of *gpi7* cells (Figure 18B).

By microscopic observation, I found that the two daughter cells could not separate from the mother cell and the cell cycle was arrested in *gpi7* mutants (Figures 13B and 19). Since the Cbk1p-Ace2p pathway is involved in cell separation, the cell morphology was investigated in suppressor mutants. I found that *gpi7*Δ *cbk1*^{mTn} cells grow as clumps of round cells joined in regions that stained brightly with calcofluor white, a chitin-binding dye (Figure 19). This phenotype looks identical to the phenotype of *cbk1*Δ single mutant cells that show a severe cell separation defect (Racki *et al.*, 2000). The *gpi7*Δ *cbk1*Δ and *gpi7*Δ *ace2*Δ double mutants also showed serious defects in cell separation (Figure 19). The *gpi7*Δ *egt2*Δ double mutant cells showed defects in cell separation but the phenotype was less severe than that of the *gpi7*Δ *cbk1*Δ or *gpi7*Δ *ace2*Δ double mutant (Figure 19).

Localization of Egt2p in *gpi7* mutants

Daughter-specific proteins for cell separation are transported to the septum and degrade septum components from the daughter's side (Cabib *et al.*, 2001; Nelson *et al.*, 2003). To explain why a mutation in *EGT2* ovecomes the temperature sensitivity of *gpi7*

mutants, I investigated the localization of Egt2p. *EGT2* tagged with a sequence encoding HA after a signal peptide sequence (pRS315-HA-EGT2; Figure 20A) was introduced into *egt2*Δ cells. The HA-tagged protein was functional because no cell separation defect was observed in *egt2*Δ cells carrying pRS315-HA-EGT2, whereas *egt2*Δ cells carrying a control vector had such a defect (data not shown). Fluorescence microscopy revealed that HA-Egt2p specifically localized at the septum in wild-type cells (*egt2*Δ carrying pRS315-HA-EGT2, Figure 20B). However, in the *gpi7*Δ background, HA-Egt2p dispersed in the cell wall, sometimes concentrating in punctate and cortical structures (*gpi7*Δ *egt2*Δ carrying pRS315-HA-EGT2, Figure 20B). *ENG1*/*DSE4*, which is one of the daughter-specific genes regulated by Ace2p, encodes a secreted endo-glucanase (Baladron *et al.*, 2002). I also analyzed the distribution of Eng1p (Figure 20A). Eng1p was localized to the septum during cell separation (*eng1*Δ carrying pRS315-HA-ENG1, Figure 20C) (Baladron *et al.*, 2002). Even in the *gpi7* mutant cells (*gpi7*Δ *eng1*Δ carrying pRS315-HA-ENG1), Eng1p was localized at the septum (Figure 20C). These observations indicate that only the GPI-anchored proteins, such as Egt2p, are not transported to the septum correctly in *gpi7* mutants, resulting in the defect in cell separation.

Finally, I constructed a chimeric gene with *ENG1* and *EGT2* to examine the cellular localization of the product. The C-terminal region of Egt2p containing the GPI attachment signal sequence was fused to the C-terminal end of HA-Eng1p (named HA-Eng1-Egt2p; Figure 21A). As a control, localization of HA-Eng1p was observed in cells with the same background. HA-Eng1p was localized to the septum in both wild-type and *gpi7*Δ mutant cells (Figure 21B), which was consistent with the result in Figure 20C. In wild-type cells, HA-Eng1-Egt2p was localized at the septum (Figure 21C; WT

pRS315-HA-ENG1-EGT2). In contrast, the chimeric protein was not only localized at the septum but also displaced to the cell cortex in the *gpi7*Δ mutant (Figure 21C; *gpi7*Δ pRS315-HA-ENG1-EGT2). These results indicate that modification of the GPI anchor in the C-terminal region of Egt2p is responsible for its localization at the septum in wild-type cells and its displacement from the septum to the cell cortex in *gpi7* mutant cells.

I-5. Discussion

GPI7 encodes a transferase that adds a side chain EtN-P to the second mannose of the GPI core structure (Benachour *et al.*, 1999). However, the biological significance of this addition has remained unknown. In this report, I have demonstrated that the function of *GPI7* is required for the completion of cell separation. First, I found that *gpi7* mutants are abnormal in their cell morphology, showing defects in cell separation and daughter cell growth (Figures 9B and 19). Second, I isolated *WSC1*, *RHO2*, *ROM2*, *GFA1* and *CDC5* as multicopy suppressors of the *gpi7* mutants (Figure 11), suggesting that *gpi7* mutant cells may have defects in cell wall integrity and/or the cell cycle. I also showed that multicopy suppressors overcome the growth defect of *gpi7* mutants, but not the cell separation defect (Figure 12). Third, I found that mutations in the Cbk1p-Ace2p pathway bypass the temperature-sensitive growth of *gpi7* mutants (Figures 15A and 17). Finally, a GPI-anchored protein, Egt2p, that is required for cell separation, was not transported to the septum correctly in *gpi7* mutants (Figure 20). In summary, these results indicate that *GPI7* is involved in cell separation *via* targeting of daughter-specific GPI-anchored proteins.

In wild-type cells, cytokinesis occurs when cells exit mitosis together with actomyosin ring contraction and septum formation to accomplish a fission of mother and daughter cell cytoplasms (Bi *et al.*, 1998; Schmidt *et al.*, 2002). After cytokinesis, Cbk1p localizes at the bud neck and activates Ace2p. Ace2p up-regulates the expression of daughter-specific genes, such as *CTS1*, *SCW11*, *DSE1*, *DSE2*, *DSE3*, *ENG1* and *EGT2*. Notably, Egt2p is modified by a GPI anchor in the ER after protein synthesis (Hamada *et al.*, 1998). Daughter-specific cell wall proteins are transported to the bud

neck and degrade the components of the septum, such as β-1,3-glucan and chitin (Figure 18A). After that, wild-type cells are ready to proceed through phases G1 and S (Figure 24A). In the case of *gpi7* mutants, it is likely that Egt2p is not transported or localized to the bud neck correctly, resulting in a defect of cell separation (Figure 20B). Mislocalized Egt2p probably injures cell wall components, because it has glucanase activity (Figure 23). The weakened cell wall layer might give rise to cellular stress, arresting the cell cycle in the daughter cell at the G1 phase (Figures 23 and 24B). The mother cell could proceed to the next stage of the cell cycle, in spite of the arrest of the daughter cell. This might be the reason why *gpi7* mutants have defects in cell separation and daughter cell growth, showing a three-cell arrangement.

Roles of multicopy suppressors in *gpi7* mutants

Microscopic observation revealed that *gpi7* mutants carrying multicopy suppressors grew as clumps of round cells without completion of cell separation (Figure 11). Multicopy suppressors could suppress the growth defect of *gpi7* mutants, but not the cell separation defect (Figure 12). I have isolated two classes of suppressors. The first class of suppressors, such as *WSC1*, *RHO2*, *ROM2* and *GFA1*, facilitates the production of cell wall components, β-1,3-glucan and chitin. It is known that Wsc1p, Rho2p and Rom2p act in the same pathway and are activated by cellular stress such as cell wall damage (Schmidt *et al.*, 1997; Jacoby *et al.*, 1998) (Figure 22). Protein kinase C, Pkc1p, which was also isolated as a multicopy suppressor of *gpi7*Δ (Toh-e and Oguchi, 1998), is the downstream component of this pathway. *FKS1* and its homologue *FKS2*, *MNN1* and *CHS3*, which encode subunits of the β-1,3-glucan synthase complex, an α-1,3-mannosyltransferase for mannan synthesis and a chitin synthase, respectively,

have been shown to depend on this pathway for their full expression (Heinisch *et al.*, 1999). *GFA1* is also involved in chitin synthesis, because Gfa1p catalyzes the first step in the production of *N*-acetylglucosamine, which is a component of chitin. It has been reported that Gfa1p is the rate-limiting enzyme in chitin production (Lagorce *et al.*, 2002). Since each suppressor gene, *WSC1*, *RHO2*, *ROM2* and *GFA1*, promotes the production of cell wall components, the temperature-sensitive growth of *gpi7* cells that might be due to a defect in cell wall integrity could be overcome by supplementation of cell wall components (Figures 23 and 24C). In contrast, *CDC5*, the second class of suppressor, seems to be different from the others. Cdc5p is a yeast orthologue of polo-like kinase, a conserved protein kinase family found in many eukaryotic organisms from yeast to mammals. It plays multiple key roles in the coordination of mitosis (Cheng *et al.*, 1998; Cid *et al.*, 2002). *CDC5* was identified as a multicopy suppressor of various mutants related to progression of the M phase, such as *CDC15*, *CDC20*, *DBF2* and *TEM1* (Hardy and Pautz, 1996; Jaspersen *et al.*, 1998). *CDC5* was also obtained as a multicopy suppressor of an allele of *DBF4*, which arrests at the G1 phase of the cell cycle (Kitada *et al.*, 1993). Based on these studies, it is likely that the overproduction of *CDC5* overcomes the cell cycle arrest of the daughter cells in *gpi7* mutants (Figure 23).

Relationship between *GPI7* and Cbk1p-Ace2p pathway

I have also found that the mutation in *CBK1* overcomes the temperature-sensitive growth of *gpi7* mutants through extragenic suppressor screening (Figure 15A). The double mutation *gpi7*Δ *ace2*Δ suppressed the growth defect of *gpi7* mutant cells as did the mutation *gpi7*Δ *cbk1*Δ (Figure 17). Cbk1p is a protein kinase belonging to the nuclear Dbf2- related (NDR) family that is highly conserved from yeast to human

(Tamaskovic *et al.*, 2003). NDR family kinases are important regulators of cell morphogenesis and cell proliferation. In *S. cerevisiae*, Cbk1p is important for polarized growth, mating projection formation and cell separation (Bidlingmaier *et al.*, 2001). The *cbk1*Δ cells fail to separate after mitosis and grow in clumps (Racki *et al.*, 2000; Bidlingmaier *et al.*, 2001). Interestingly, both *gpi7*Δ *cbk1*Δ and *gpi7*Δ *ace2*Δ double mutants showed a severe defect in cell separation, which is similar to the phenotype of *cbk1*Δ and *ace2*Δ single mutant cells that grow as clumps joined at the septum (Figure 19).

It is likely that the suppression of the *gpi7* growth defect by the inactivation of Ace2p is due to the down-regulation of genes whose expression is regulated by Ace2p. Ace2p activates a set of daughter cell-specific genes that are essential for mother-daughter cell separation (Colman-Lerner *et al.*, 2001; Nelson *et al.*, 2003). These daughter-specific proteins are transported to the bud neck after cytokinesis and formation of the septum, and degrade the septum from the daughter cell's side (Cabib *et al.*, 2001; Colman-Lerner *et al.*, 2001; Baladron *et al.*, 2002). At least one gene required for cell separation, *EGT2*, encodes GPI-anchored proteins, presumed to be glucanases (Hamada *et al.*, 1998; Nelson *et al.*, 2003). In *gpi7* mutants, GPI-anchored proteins are modified by a GPI anchor lacking a second EtN-P, which are added by Gpi7p. Mutations in *EGT2* (*egt2*Δ) partially suppressed the temperature-sensitive growth defect of *gpi7* mutants, whereas mutation in *BGL2* (*bgl2*Δ), which encodes a non-GPI glucanase and is not regulated by Ace2p, could not suppress the defect at all (Figure 18B). Egt2p was not transported to the bud neck correctly in *gpi7* mutant cells (Figure 20B), suggesting that daughter-specific GPI-anchored proteins for cell separation cause cellular stress in *gpi7* mutants and affect the cell cycle (Figure 23). Although the *gpi7*

cbk1 and *gpi7 ace2* double mutants have a cell separation defect, daughter cells can grow because daughter-specific proteins, that are required for cell separation and may injure the cell wall if mislocalized, are not expressed (Figures 23 and 24D).

Eng1p was transported to the septum in both wild-type and *gpi7* mutant cells (Figures 20 and 21). Eng1p which was tagged with HA at the C-terminus was also reported to be transported correctly to the septum (Baladron *et al.*, 2002), indicating that the C-terminal tagging of Eng1p itself did not change its localization. I observed a displacement of Eng1-Egt2 chimeric protein to the cell cortex in *gpi7*Δ cells, but not in wild-type cells (Figure 21). Therefore, this mislocalization depends on GPI anchoring of Eng1p. These results suggest that there exist at least two different mechanisms for the localization of proteins to the septum region, i.e. GPI-dependent and GPI-independent mechanisms.

Specificity of cell separation control by *GPI7*

It is important to address whether the regulation of cell separation is general to any GPI biosynthetic genes or specific to the *GPI7* gene. Previous study indicated that *gpi1* mutant cells, which are defective in the first step of GPI biosynthesis, were large, round and budded with a separation defect at a semi-permissive temperature (Leidich and Orlean, 1996). The *gwt1-20* cells, which have a defect in inositol acylation of GPI, showed a swelling of whole cells, clump of cells and in some cases cell lysis (Umemura *et al.*, 2003). However, the defective phenotypes of *gpi1* and *gwt1-20* mutants are dissimilar to those of *gpi7* mutant cells. In *gpi7* mutants, GPI anchors are still transferred to proteins (Benachour *et al.*, 1999; Richard *et al.*, 2002a; Imhof *et al.*, 2004), whereas the transfer to proteins is defective in other mutants because the

biosynthesis of GPI is stopped at the intermediate stage (Hamburger *et al.*, 1995; Leidich and Orlean, 1996; Gaynor *et al.*, 1999; Taron *et al.*, 2000; Umemura *et al.*, 2003). In *gwt1-20* cells, Egt2p was not detected at the cell surface after incubation at the non-permissive temperature, consistent with the previous result that Egt2p is modified by the GPI anchor (Hamada *et al.*, 1998) (data not shown). Furthermore, mutation in *CBK1* or *ACE2* could not suppress the temperature sensitivity of *gwt1-20* (data not shown). Therefore, it is likely that the cell separation defect observed in *gpi7* mutants is not general among GPI biosynthesis, but that the addition of EtN-P to the side chain of the second mannose of the GPI glycan portion by Gpi7p is required for the completion of cell separation.

CHAPTER II

BST1 is required for the quality control of GPI-anchored proteins

II-1. Summary

Misfolded proteins are recognized in the endoplasmic reticulum (ER), transported back to the cytosol, and degraded by the proteasome. A number of proteins are processed and modified by a glycosylphosphatidylinositol (GPI) anchor in the ER, but the quality control mechanisms of GPI-anchored proteins remain unclear. Here, I report on the quality control mechanism of misfolded GPI-anchored proteins. I have constructed a mutant form of the β-1,3-glucanosyltransferase Gas1p (Gas1*p) as a model of misfolded GPI-anchored protein. Gas1*p was modified with a GPI anchor but retained in the ER and was degraded rapidly *via* the proteasome. Disruption of *BST1*, which encodes GPI inositol deacylase, caused a delay in the degradation of Gas1*p. This delay was due to an effect on the deacylation activity of Bst1p. Disruption of genes involved in GPI-anchored protein concentration and *N*-glycan processing caused different effects on the degradation of Gas1*p and a soluble misfolded protein, CPY*. Further, Gas1*p associated with both Bst1p and BiP/Kar2p, a molecular chaperone, *in vivo*. My data suggest that GPI inositol deacylation plays important roles in the quality control and ER-associated degradation of GPI-anchored proteins.

II-2. Introduction

Cells possess several quality control mechanisms for the maintenance of proper protein folding and function. Upon synthesis, membrane and secretory proteins are inserted into the lumen of the endoplasmic reticulum (ER), where they are folded and undergo oligomerization. There are a number of chaperones and enzymes in the ER required for proper protein folding (Ellgaard *et al*., 1999). Before exiting from the ER, proteins are monitored by a quality control system that ensures correct folding. Misfolded proteins that fail to pass the quality control checkpoint are transported back to the cytosol and degraded by an ER-associated degradation (ERAD) mechanism that involves the ubiquitin-proteasome pathway (Figure 25) (Kopito, 1997; Kostova and Wolf, 2003). *N*-linked oligosaccharide, one of the major post-translational modifications in the ER, is trimmed and processed by glucosidase I, glucosidase II, and mannosidase I (Jakob *et al.*, 1998; Helenius and Aebi, 2001). The processing of *N*-linked oligosaccharides plays important roles in the quality control of glycoprotein folding in the ER (Figure 26) (Helenius and Aebi, 2001, 2004).

A number of cell surface proteins are post-translationally modified in the ER with glycosylphosphatidylinositol (GPI). Mechanisms for quality control and degradation of GPI-anchored proteins are important in folding diseases, including prion diseases and transmissible spongiform encephalopathies, which are caused by a conformational modification of prion, a GPI-anchored protein (Prusiner, 1998). There have been several biochemical studies on both the degradation of mutated prions and the quality control of proteins with mutated GPI attachment signals (Field *et al.*, 1994; Oda *et al.*, 1996; Wainwright and Field, 1997; Jin *et al.*, 2000; Ito *et al.*, 2002; Ishida *et*

al., 2003). In contrast, the molecular mechanisms involved in the quality control and degradation of GPI-anchored proteins have not been elucidated.

The GPI anchor is synthesized in the ER by the stepwise addition of sugars and ethanolaminephosphate to phosphatidylinositol (Kinoshita and Inoue, 2000; Eisenhaber *et al.*, 2003). At an early step in the biosynthesis, the GPI inositol is acylated by Gwt1p (Umemura *et al.*, 2003) (Figure 27). The amounts of GPI-anchored proteins are greatly decreased in *gwt1* mutant cells, indicating that this acylation is critical for the attachment of GPI to proteins (Umemura *et al.*, 2003). Once the GPI anchor is attached to a protein, the inositol is usually deacylated in the ER (Figure 27) (Chen *et al.*, 1998). Recently, mammalian PGAP1 and the yeast orthologue, Bst1p, were identified as GPI inositol deacylases (Tanaka *et al.*, 2004). ER-to-Golgi transport of GPI-anchored proteins is defective in both PGAP1-deficient cells and *bst1* mutant cells, which shows that the inositol deacylation of GPI is important for the efficient transport of GPI-anchored proteins from the ER to the Golgi (Vashist *et al.*, 2001; Tanaka *et al.*, 2004).

Here, I investigated the degradation of GPI-anchored proteins in yeast. I constructed a mutant Gas1p (Gas1*p) as a model of misfolded GPI protein. Gas1*p was modified by GPI but retained in the ER. In addition, it was misfolded and rapidly degraded by the proteasome system. I found that the inositol deacylation of the misfolded GPI-anchored protein is required for its efficient degradation in the ER. My results further suggest that the GPI inositol deacylase is a key enzyme in initiating the degradation of misfolded GPI-anchored proteins. This is the first report addressing the molecular mechanisms of the quality control of GPI-anchored proteins.

II-3. **Materials and methods**

Strains and media

The yeast strains used in this study are listed in Table II. The disruption of genes in yeast was performed using a one-step gene disruption method as described previously (Longtine *et al*., 1998). YPAD and synthetic complete (SC) media are described elsewhere (Sherman, 1991). SDCA contains 0.67% yeast nitrogen base without amino acids (Difco, Detroit, MI), 2% glucose, 0.5% casamino acids, and 0.004% adenine sulfate.

Plasmids

The plasmids used in this study are listed in Table III.

Construction of *GAS1*: The promoter, coding, and terminator sequences of *GAS1* were cloned by amplification of genomic DNA using *PfuUltra* High-Fidelity DNA polymerase (Stratagene, La Jolla, CA) and the primers GAS1F (5'-AAAAGGATCCCGCCCATAATATTGTTACCA-3') and GAS1R (5'-AAAAACTAGTCCTTCTAGTGATGCTATGGC-3'). The amplified 2875-bp fragment was digested with *Bam*HI and *Spe*I and then purified. The purified fragment was ligated into pRS306 (Sikorski and Hieter, 1989) digested with the same enzymes to generate pMF600 (*GAS1*, *URA3*).

Construction of *HA-GAS1*: Using pMF600 as a template, *Mlu*I and *Nde*I sites were introduced 69 bp downstream from the start codon of *GAS1*, and the fragment was subcloned into pRS305 (Sikorski and Hieter, 1989) to generate pMF606. Three copies of the HA epitope were amplified, inserted into the *Mlu*I-*Nde*I site of pMF606 to

generate pMF607 (*HA-GAS1*, *LEU2*), and confirmed by sequencing. The DNA fragment containing monomeric red fluorescent protein (mRFP; kindly provided by Dr. Roger Tsien, University of California, San Diego), was also amplified, and inserted into the *Mlu*I-*Nde*I site of pMF606 to generate pMF608 (*mRFP-GAS1*, *LEU2*).

I substituted glycine 291 in Gas1p with arginine using a QuickChange site-directed mutagenesis kit (Stratagene) using pMF600, pMF607, or pMF608 as the template to generate pMF605 (*gas1**, *URA3*), pMF615 (*HA-gas1**, *LEU2*), and pMF617 (*mRFP-gas1**, *LEU2*), respectively. Plasmid pMF615 was digested with *Bam*HI and *Spe*I, and a fragment containing HA-tagged *gas1** was ligated into pRS306 to generate pMF616 (*HA-gas1**, *URA3*).

Construction of *SHG* and *SHg**: I substituted asparagine 528 in Gas1p with a stop codon using a QuickChange site-directed mutagenesis kit with pMF607 and pMF616 as the template to generate pMF874 (*SHG*, *LEU2*) and pMF876 (*SHg**, *URA3*), respectively.

Construction of YEp-BST1: *BST1* coding sequences were amplified from genomic DNA by PCR using primers BST1F (5'-AAAAGAGCTCGTTATGGGTATCAGGAGATTAG-3') and BST1R (5'-AAAATCTAGAACTGGGTTGTAGTTCTAATGTAT-3'). The amplified 3107-bp fragment was digested with *Sac*I and *Xba*I and then purified. The purified fragment was ligated into YEp351GAPII (Abe *et al*., 2003) digested with the same enzymes to generate pMF634 (YEp351-BST1). I substituted serine 236 in Bst1p with alanine using the QuickChange site-directed mutagenesis kit with YEp351-BST1 as a template to generate pMF636 (YEp351-BST1S236A).

Construction of YEp351-BST1-FLAG, YEp351-BST1S236A-FLAG,

YEp352-BST1-FLAG, and YEp352-BST1S236A-FLAG: Using YEp351-BST1 and YEp351-BST1S236A as templates, the DNA fragments containing the BST1 gene were amplified by PCR with primers BST1F and BST1-FLAG-R (5'-AAAATCTAGACTAGATATCATGATCCTTGTAATCACCGTCATGGTCTTTGTAGTCATGTATTGTTTCGAAAAATAG-3'). The amplified fragments were inserted into YEp351GAPII or YEp352GAPII (Abe *et al*., 2003) to generate pMF641 (YEp351-BST1-FLAG), pMF642 (YEp351-BST1S236A-FLAG), pMF643 (YEp352-BST1-FLAG), and pMF644 (YEp352-BST1S236A-FLAG), respectively.

Construction of GFP-HDEL: I constructed GFP-HDEL (pMO13; M. Okamoto, unpublished observations) as an ER marker. Briefly, GFP-HDEL, which contains the Kar2p signal-peptide sequence (the first 135 nucleotides of the *KAR2* gene) and the enhanced green fluorescent protein gene (BD Bioscience, San Jose, CA) modified to encode a C-terminal HDEL tetrapeptide, was amplified by PCR. The DNA fragments were cloned into the YCp50 (*CEN, URA3*) expression vector, which contains the *TDH3* (glyceraldehyde-3-phosphate dehydrogenase) promoter and actin terminator to generate pMO13.

Construction of YEp352-FLAG-KAR2: A DNA fragment encoding the Kar2p signal peptide was amplified with primers KAR2s-F (5'-AAAAGAGCTCCATACCATGTTTTTCAAC-3') and KAR2s-R (5'-AAAAGTCGACATCGATATCATCGGCACCTCTAAC-3') and inserted into YEp352GAPII to generate pMF833. The Kar2p-coding sequence after the signal peptide was amplified from genomic DNA using primers FLAG-KAR2-F (5'-AAAAATCGATTACAAGGACGACGATGACAAGGTAGAAAACTACGGAACTGTTATCG-3') and KAR2-R (5'-AAAAGTCGACCTACAATTCGTCGTGTTCG-3'). The

amplified 3107-bp fragment was digested with *Cla*I and *Sal*I and then purified. The purified fragment was ligated into pMF833 digested with the same enzymes to generate pMF834 (YEp352-FLAG-KAR2).

Construction of CPY*HA: An HA-tagged CPY* plasmid was constructed from YIp-CPY* (kindly provided by Dr. Tadashi Suzuki, Osaka University), which contains the open reading frame of mutant *prc1-1*. I inserted a *Spe*I site just before the stop codon of *PRC1* by QuickChange site-directed mutagenesis using YIp5-CPY* as a template to generate pMF845. Three copies of the HA epitope were amplified, inserted into the *Spe*I site of pMF845 to generate pMF846 (YIp5-CPY*HA), and confirmed by sequencing. Plasmid pMF846 was digested with *Eco*RI and *Hin*dIII, and the fragment containing HA-tagged *prc1-1* was ligated into pRS316 to generate pMF848 (pRS316-CPY*HA).

Construction of pRS315-SEC18: The promoter, coding, and terminator sequences of *SEC18* were amplified with primers SEC18F (5'-AAAAACTAGTAAAAGGTATGCTGGATGCTG-3') and SEC18R (5'-AAAACTCGAGTCACCTGGCAAAGCTTCTC-3'). The amplified 3377-bp fragment was digested with *Spe*I and *Xho*I and then purified. The purified fragment was ligated into pRS315 (Sikorski and Hieter, 1989) digested with the same enzymes to generate pMF880 (*SEC18*, *LEU2*).

Immunoblotting

Samples were denatured with SDS-sample buffer for 10 min at 37°C for membrane proteins and for 5 min at 95°C for soluble proteins and then separated by SDS-PAGE. For immunoblot analysis, 5 μl of sample was loaded in each lane. Gas1p

was detected with anti-Gas1 peptide polyclonal antibody (1:2000; kindly provided by Dr. Katsura Hata, Eisai Co., Tokyo, Japan) and horseradish peroxidase (HRP)-conjugated goat anti rabbit IgG (1:2000; Cell Signaling Technology, Beverly, MA). HA-Gas1p and CPY*HA were detected with anti-HA monoclonal antibody 16B12 (1:10,000; Babco, Richmond, CA) and HRP-conjugated goat anti-mouse IgG (1:10,000; Cell Signaling Technology). Dpm1p was detected with anti-Dpm1p monoclonal antibody (1:2000; Molecular Probes, Eugene, OR) and HRP-conjugated anti-mouse IgG (1:2000). Pgk1p was detected with anti-Pgk1p monoclonal antibody (1:10,000; Molecular Probes) and HRP-conjugated anti-mouse IgG (1:10,000). Glutathione S-transferase (GST)-tagged proteins were detected with HRP-conjugated anti-GST antibody (1:10,000; Amersham Biosciences, Uppsala, Sweden). FLAG-Kar2p and Bst1p-FLAG were detected with anti-FLAG monoclonal antibody M2 (1:5000; Sigma-Aldrich, St. Louis, MO) and HRP-conjugated goat anti-mouse IgG (1:5000). Immunoreactive bands were visualized by chemiluminescence with ECL-plus reagents (Amersham Biosciences).

Subcellular fractionation and glycosylation of Gas1*p

MFY163 cells were grown in YPAD medium to an OD_{600} of 1.0 to 2.0, and 5 X 10^8 cells were washed twice with TNE buffer (50 mM Tris-HCl, pH 7.5, 150 mM NaCl, 5 mM EDTA, 1 mM PMSF, and protease inhibitor cocktail [Roche, Basel, Switzerland]). One ml of TNE and the same volume of glass beads were added to the cells, and the cells were lysed with a FastPrep (Q-biogene, Morgan Irvine, CA). The lysate was centrifuged for 5 min at 300 X *g* to remove cell debris. The supernatant was further centrifuged for 15 min at 13,000 X *g*, yielding the P13 pellet and the S13

supernatant. The S13 supernatant was centrifuged for 1 h at 100,000 X *g*, yielding the P100 pellet and the S100 supernatant. The P13 and P100 fractions were washed twice with TNE and resuspended in 1 ml TNE. To detect HA-Gas1p in culture medium, proteins were precipitated with 10% trichloroacetic acid and then washed with cold acetone. To study the glycosylation, cell lysates were solubilized in the same volume of 2X SDS-sample buffer, and heated for 5 min at 95°C. Aliquots of the samples were treated with Endo H_f (New England Biolabs, Beverly, MA) for 3 h at 37°C.

Cycloheximide (CHX) chase analysis

CHX chase experiments were performed as described previously (Plemper *et al.*, 1998; Jakob *et al.*, 2001). Briefly, overnight cultures were inoculated into 5 ml of medium. Cells were grown to 2 X 10^7 cells/ml. After adding CHX (Nakalai Tesque, Kyoto, Japan) to a final concentration of 0.2 mg/ml, 1 X 10^7 cells were removed at specific time points, suspended in sodium azide solution (final concentration = 10 mg/ml), and frozen at –80°C. The preparation of samples and immunoblotting were performed as described above. The effect of the proteasome inhibitor was analyzed as described previously (Suzuki *et al*., 2000). Ten min before CHX was added, MG-132 (Merck, Darmstadt, Germany) was added to a final concentration of 50 μM from a freshly made 5 mM solution in dimethyl sulfoxide (DMSO). For control cells, the same amount of DMSO was added. For GST-tagged α-toxin affinity precipitation, 3 X 10^7 cells were collected at specific time points after adding CHX. Cells were broken using glass beads (*see* "Subcellular fractionation and glycosylation of Gas1*p"), and the cell lysate was adjusted to 1% SDS, boiled, and mixed with 1 ml of TNET (100 mM Tris-HCl, pH 8, 100 mM NaCl, 5 mM EDTA, and 1% Triton X-100). The lysate was

centrifuged at 13,000 X *g* for 15 min. The supernatant was incubated with 1 μg of GST-tagged α-toxin protein (kindly provided by Dr. Taroh Kinoshita and Dr. Yusuke Maeda, Osaka University) at 4°C for 30 min and then with 25 μl of glutathione-agarose beads (Sigma-Aldrich) at 4°C for 2 h. For SDS-PAGE, the beads were washed four times with TNET, resuspended in 30 μl of SDS-sample buffer, and boiled at 95°C for 5 min. Immunoblotting was performed as described above.

Inositol labeling and immunoprecipitation of HA-Gas1p

Cells (5 X 10^7) were washed three times and resuspended in 1 ml of SC–inositol medium. Cells were incubated at 30˚C for 30 min and then labeled with *myo*-[1,2-^{3}H]inositol (PerkinElmer, Wellesley, MA) for 3 h. The reaction was stopped by adding NaN_3/NaF solution to a final concentration of 10 mM. The suspension was washed with 10 mM NaN_3 and resuspended in 50 μl of TEPI (50 mM Tris-HCl, pH 7.5, 5 mM EDTA, and protease inhibitor cocktail). The cells were then broken with glass beads, and cell debris was removed (*see* "Subcellular fractionation and glycosylation of Gas1*p"). The cell lysate was adjusted to 1% SDS, boiled, and mixed with 1 ml of TNET. The lysate was centrifuged at 13,000 X *g* for 15 min. Then, the supernatant was incubated overnight at 4°C with 25 μl of anti-HA agarose beads (Roche). The agarose beads were washed four times with TNET and once with 20 mM Tris-HCl (pH 7.5), resuspended in 30 μl of SDS-sample buffer, and boiled at 95°C for 5 min. Samples were separated by SDS-PAGE and analyzed using a Molecular Imager FX (Bio-Rad, Hercules, CA).

Fluorescence microscopy

For the imaging of mRFP-Gas1 and mRFP-Gas1* proteins, cells grown to exponential phase were collected and washed with phosphate-buffered saline. Fluorescence images were observed using a BX50 fluorescence microscope (Olympus, Tokyo, Japan) and photographed with a microMax cooled CCD camera (Princeton Instruments, Trenton, NJ).

Immunoprecipitation

For detection of the Gas1p-Kar2p and Gas1p-Bst1p association, immunoprecipitation was performed as described previously with some modifications (Vallee and Riezman, 2005). Briefly, 100 OD_{600} of cells were washed twice with TNE buffer and disrupted with glass beads, after which cell debris and glass beads were removed by centrifugation (*see* "Subcellular fractionation and glycosylation of Gas1*p"). The supernatant was then centrifuged at 13,000 X *g* for 20 min at 4°C. The pellet was resuspended in TNE, and digitonin was added to a final concentration of 1%. The suspension was incubated for 1 h at 4°C with rotation, after which insoluble components were removed by centrifugation at 13,000 X *g* for 15 min at 4˚C. For immunoprecipitation of HA-tagged proteins, anti-HA IgG-agarose was incubated with the sample at 4°C for 3 h. For immunoprecipitation of FLAG-tagged proteins, anti-FLAG beads (Sigma-Aldrich) were incubated with the sample at 4°C for 3 h. The immunoprecipitated beads were washed three times with TNE containing 1% digitonin and eluted with SDS-sample buffer. Immunoblotting was performed as described above.

II-4. Results

Construction and characterization of misfolded Gas1 proteins

To understand the process by which misfolded GPI-anchored proteins are degraded, I constructed a model of misfolded GPI-anchored protein using the β-1,3-glucanosyltransferase Gas1p, one of the most abundant and well-characterized GPI-anchored proteins in *S. cerevisiae* (Conzelmann *et al.*, 1988; Popolo and Vai, 1999). Gas1p has also been used as a model to analyze the primary structural requirements for GPI anchoring (Nuoffer *et al.*, 1991; Nuoffer *et al.*, 1993) and the transport of GPI-anchored proteins from the ER to the Golgi apparatus (Riezman *et al.*, 1994; Muniz and Riezman, 2000; Watanabe *et al.*, 2002). *N*-linked ER-type Man_8 oligosaccharides, the *O*-linked Man_1 residues, and a GPI anchor are transferred to the primary translation product of Gas1p (65 kDa) in the ER, yielding an immature polypeptide of 105 kDa. Further elaboration of the oligosaccharide chains takes place through the Golgi, resulting in a mature 125-kDa form.

First, I tried to obtain a mutant Gas1p that causes misfolding. In yeast, a mutated carboxypeptidase Y (CPY*) has been used as a model for misfolding of soluble luminal glycoproteins, and the process of CPY* degradation and its effects of *N*-glycan processing have been investigated in detail (Knop *et al.*, 1996; Jakob *et al.*, 1998). Mutant CPY carries an arginine instead of a glycine residue at position 255 of prepro-CPY (Finger *et al.*, 1993). This mutated amino acid is located in a hydrophobic region in CPY. I speculated that the mutated CPY is misfolded because arginine, a hydrophilic and positive-charged amino acid, is placed in a hydrophobic region. Therefore, I adopted the same strategy to generate a misfolded form of Gas1p. I selected three

hydrophobic regions for site-directed mutagenesis of Gas1p, excluding the secretion signal sequence, the GPI attachment signal, and the glycosylation sites. From a hydropathy plot of Gas1p, each amino acid, alanine 116, valine 258, and glycine 291, was replaced with arginine. One of the three mutant proteins, G291R (designated Gas1*p; Figure 28A and B) could not rescue the slow growth phenotype of the *gas1*Δ strain (Figure 29A). Immunoblotting further revealed that, although the Golgi form of Gas1p (125 kDa) predominates in *gas1*Δ cells expressing wild-type *GAS1*, only a small amount of the ER form of Gas1p (105 kDa) was detected in *gas1*Δ cells expressing *gas1** (Figure 29B).

To determine what causes the difference in molecular size between Gas1p and Gas1*p, I compared their sizes before and after digestion with Endo H. This treatment decreased the apparent molecular weight of Gas1*p, indicating the presence of *N*-linked sugar chains (Figure 29C). The difference in the mobility between Endo H-treated Gas1p and Gas1*p could be due to the elongation of *O*-linked glycans of Gas1p but not Gas1*p in the Golgi. I further performed subcellular fractionation to investigate the subcellular localization of Gas1*p. The majority of Gas1*p was detected in the P13 fraction, which contains the ER membrane (Figure 29D). Gas1*p was detected not only in the membrane but also in the soluble fraction (S100) (Figure 29D). The molecular size of the major Gas1*p band was the same in the S100 and membrane fractions. This can be explained by the fact that the difference in the mobility of the non-GPI- and GPI-anchored forms of Gas1p is too small to be distinguished by SDS-PAGE (Nuoffer *et al.*, 1991). I also detected a minor 65-kDa band in the S100 fraction corresponding to Gas1p form without any sugar chains. This might be a deglycosylated form of Gas1*p.

Additional gene disruption is difficult in *gas1** cells because *gas1*Δ and *gas1**

cells grow slowly and because several genes involved in ER quality control (e.g., *GLS1* and *GLS2*) and GPI-anchored protein transport (e.g., *EMP24*) are synthetic lethal in the *gas1*Δ background (Tong *et al.*, 2004). Therefore, I constructed HA- and mRFP-tagged versions of Gas1p and Gas1*p to monitor their behaviors and localization. These proteins were generated by inserting the HA- or mRFP-tag in Gas1p after the cleavable N-terminal signal sequence (Figure 30A). Both HA-Gas1p and mRFP-Gas1p rescued the calcofluor white sensitivity of *gas1*Δ cells, indicating that the tagged proteins were functional (Figure 30B). In addition, immunoblotting revealed that HA-Gas1*p was in the ER form (Figure 30C). Also, mRFP-Gas1p was localized on the cell surface, whereas mRFP-Gas1*p was distributed in the intracellular compartment. Further analysis was difficult because of low fluorescence intensity in wild-type cells. These results indicate that the tagged Gas1*p behaves like Gas1*p.

Gas1* proteins are modified by GPI, but degraded via proteasome

To address whether misfolded Gas1*p is modified with GPI, I labeled the cells with [1,2-^{3}H] inositol and then specifically immunoprecipitated HA-Gas1*p with anti-HA-agarose (Figure 31A). I detected HA-Gas1p at the predicted position (Golgi form), whereas labeled HA-Gas1*p was detected as the ER form (Figure 31B). These results show that Gas1*p is modified with GPI.

Figures 29B and 30C indicate that there is less Gas1*p than wild-type Gas1p. Therefore, I next examined whether the lowered steady-state level of Gas1*p is due to a rapid degradation of misfolded protein. A CHX chase experiment (Plemper *et al.*, 1998; Jakob *et al.*, 2001) showed that Gas1*p was present initially as the ER form but rapidly decreased to an undetectable level, whereas wild-type Gas1p and the control ER marker,

Dpm1p, were stable even after protein synthesis was stopped by CHX (Figure 32A). In addition, in the CHX chase experiment, Gas1*p remained as the ER form but showed a gradually increased molecular weight. The reduced mobility of Gas1*p on SDS-PAGE was still apparent after Endo H treatment (Figure 32B), presumably due to the additional *O*-glycosylation (Nakatsukasa *et al.,* 2004). I checked for the presence of Gas1*p in culture medium to confirm that the disappearance of Gas1*p in the chase analysis was not due to protein secretion. Neither Gas1p nor Gas1*p were detected in the culture medium (Figure 33A), indicating that Gas1*p is lost due to intracellular degradation and not secretion.

I next investigated what kind of cellular degradation system is involved in the degradation of Gas1*p. First, I investigated the role of proteolysis in the vacuole in the degradation of Gas1*p. I found that the degradation of HA-Gas1*p was not affected in *pep4* mutant cells, which are defective in the vacuolar protease activity (Figure 33B), indicating that Gas1*p is not degraded in the vacuole. Next, I examined the involvement of the proteasome system using MG-132, a specific inhibitor of the proteasome (Suzuki *et al*., 2000). Gas1*p was dramatically stabilized by the addition of MG-132 (Figure 34A). In addition, the degradation of Gas1*p was significantly delayed in *rpn3-1* and *rpn12-1* proteasome mutant cells (Kominami *et al.*, 1995; Kominami *et al.*, 1997) (Figure 34B), strongly suggesting that it is degraded by ER-associated degradation (ERAD) and subsequent proteasome-mediated degradation.

ER-associated degradation pathway of Gas1* proteins

I further examined the role of ubiquitin ligases (E3) in the degradation of Gas1*p. I selected three kinds of E3 that are thought to be involved in ERAD pathway

(Figure 35), including the gene products of *HRD1*, which is involved in ERAD-luminal (ERAD-L) pathway (Ahner and Brodsky, 2004; Huyer *et al.*, 2004; Vashist and Ng, 2004; Nishikawa *et al.*, 2005); *DOA10*, which is involved in ERAD-cytosolic (ERAD-C) pathway; and *RSP5*, which is assumed to be involved in ERAD of misfolded protein when overproduced (Haynes *et al.*, 2002). Unexpectedly, the degradation of HA-Gas1*p was not stabilized in *hrd1*Δ and *doa10*Δ cells (Figure 36A and B). Furthermore, the degradation of Gas1*p without a HA-tag was unaffected in both the *hrd1*Δ and the *doa10*Δ cells (data not shown). Since it has reported that Hrd1p and Doa10p act redundantly (Swanson *et al.*, 2001), I checked the effect of Gas1*p degradation in *hrd1*Δ *doa10*Δ double mutant cells. As shown in Figure 36A, the degradation rate of HA-Gas1*p was not delayed even in *hrd1*Δ *doa10*Δ double mutant cells. I also confirmed that HA-Gas1*p was not affected in the different background of *hrd1*Δ *doa10*Δ double mutant cells (data not shown). I used the *rsp5-101* mutant cells to test the involvement of Rsp5p in the Gas1*p degradation (Yashiroda *et al.*, 1996). HA-Gas1*p was not stabilized in this mutant (Figures 36C and D). Rsp5p is involved in several functions including ERAD and ubiquitination for protein targeting to the Multivesicular bodies. Although the degradation of Gas1*p might be affected by some other *rsp5* alleles, no defects were observed in the degradation of Gas1*p at least in the *rsp5-101* mutant cells. Taken together, my results suggest that misfolded GPI-anchored proteins are not degraded by a known pathway, such as ERAD-L or ERAD-C, but rather by an unknown pathway, whereas the final stages of degradation may be mediated by the proteasome system as reported for misfolded soluble proteins and membrane proteins (Kostova and Wolf, 2003).

It has been reported that ERAD-L substrates are transported from the ER to

the Golgi and retrieved to the ER, whereas ERAD-C substrates are sorted for retention in the ER (Figure 35) (Vashist *et al.*, 2001; Ahner and Brodsky, 2004; Vashist and Ng, 2004). Gas1*p is synthesized and modified in the ER luminal side. I next investigated whether ER-to-Golgi transport is required for the degradation of Gas1*p, like ERAD-L substrates. I measured the HA-Gas1*p degradation in *sec18-1* mutant cells. Sec18p is required for vesicular fusion to the Golgi (Eakle *et al.*, 1988). I also used the HA-tagged misfolded CPY (CPY*HA), a model of misfolded glycoproteins in yeast, as a control (Ng *et al.*, 2000; Vashist *et al.*, 2001; Spear and Ng, 2003). The degradation of CPY*HA was delayed in *sec18-1* cells, as reported previously (Figure 37A and B). In *sec18-1* cells, the degradation of HA-Gas1*p was also delayed (Figure 37 C and D), confirming that it uses the same pathway as the ERAD-L substrates. Interestingly, even at the restrictive temperature, a mobility shift of HA-Gas1*p was still observed in *sec18-1* cells, suggesting that the shift is due to the reaction in the ER, but not in the Golgi. This mobility shift was not observed in other substrates (Vashist and Ng, 2004).

Degradation of Gas1* protein requires GPI inositol deacylation

The GPI moiety is transferred to proteins in the ER. The inositol in the complete GPI precursor is acylated. *GWT1* is required for the acylation of the GPI inositol (Umemura *et al.*, 2003). Once the GPI anchor is transferred to a protein, however, the acyl group is removed in the ER. Recently, it was shown that the deacylation of inositol in GPI is mediated by PGAP1 in mammalian cells and Bst1p in yeast (Figure 38) (Tanaka *et al.*, 2004). The maturation of GPI-anchored proteins is greatly delayed in both the PGAP1 mutant and *bst1* mutant, suggesting that the inositol deacylation of GPI is important for the efficient transport of GPI-anchored proteins

from the ER to the Golgi apparatus. *BST1* was first identified as a mutant that rescued the lethality of the *sec13* mutant (Elrod-Erickson and Kaiser, 1996). Interestingly, the *bst1*/*per17-1* mutant was also identified as a defect in the degradation of soluble misfolded proteins (Vashist *et al.*, 2001). On the basis of these reports, I speculated that the inositol deacylation of GPI by Bst1p mediates ER quality control of GPI-anchored proteins.

To determine whether *BST1* is involved in the degradation of GPI protein, I deleted the *BST1* gene in wild-type cells harboring the *HA-gas1** or the *gas1** constructs. CHX chase analysis in *bst1*-deleted cells (*bst1*Δ) revealed a 4-fold stabilization of both Gas1*p (Figure 39A) and HA-Gas1*p (Figure 39B). Notably, Gas1*p was modified with GPI (Figure 31). To verify that GPI-anchored Gas1*p is efficiently degraded in wild-type cells but not in *bst1*Δ cells, I performed CHX chase analysis followed by affinity precipitation with α-toxin, which binds to GPI (Gordon *et al.*, 1999; Hong *et al.*, 2002). After chase analysis, Gas1*p was precipitated with anti-HA or GST-tagged α-toxin and detected with anti-HA antibodies. Because Dpm1p, which is not a GPI-anchored protein, was not detected by precipitation with α-toxin and because equal amounts of GST-tagged α-toxin were precipitated in each lane using glutathione-agarose beads, the results reflect a true association of GPI-anchored proteins with GST-tagged α-toxin (Figure 40). Total Gas1*p immunoprecipitated with anti-HA behaved as in the standard CHX chase analysis (Figures 39 and 40). In wild-type cells, GPI-anchored Gas1*p was efficiently precipitated with α-toxin and gradually decreased during the chase time, indicating that Gas1*p is modified with GPI, after which it is degraded. In contrast, I observed a significant delay in Gas1*p degradation in *bst1*Δ cells (Figure 40). The remaining GPI-anchored Gas1*p in *bst1*Δ cells appeared to

reflect a delay in its degradation. These results suggest that the delay in degradation of Gas1*p in *bst1*Δ cells is due to the persistence of the inositol-acylated form of GPI-anchored Gas1*p caused by the defect in Bst1p function. Notably, in wild-type but not in *bst1*Δ cells, the amount of GPI-anchored Gas1*p transiently increased at 30 min and then gradually decreased during the chase period (Figure 40). It is likely that the transient accumulation of GPI-anchored Gas1*p in wild-type cells is due to the modification of Gas1*p with GPI, followed by the gradual degradation of GPI-anchored Gas1*p after deacylation of the inositol ring by Bst1p.

To determine whether Gas1*p stabilization in *bst1*Δ cells is specific to GPI-anchored proteins, I further constructed a soluble form of Gas1*p (SHg*) by adding a stop codon just before the signal sequence for GPI anchoring (Figure 41A). A soluble form of wild-type Gas1p (SHG) is efficiently secreted into the culture medium. In contrast, SHg* was not present in the medium but rather was inside the cell as an ER form (Figure 41B). These results strongly suggest that soluble Gas1*p is also misfolded. I also compared the rate of degradation of mutant Gas1*p (SHg*) between wild-type and *bst1*Δ cells. As shown in Figure 42A and B, I did not observe any differences in the degradation of SHg* between wild-type and *bst1*Δ cells, further supporting the idea that the degradation of misfolded non-GPI protein is independent of Bst1p function.

Both mammalian PGAP1 and yeast Bst1p possess a consensus motif for lipases (Figure 43A). This motif contains a serine residue that is thought to be part of the active site of deacylases. In fact, substitution of this putative catalytic serine residue of PGAP1 with alanine causes a loss of PGAP1 activity (Tanaka *et al.*, 2004). To confirm that the stabilization of Gas1*p is due to the deacylation activity of Bst1p rather than a defect in binding, I substituted the catalytic serine 236 with alanine (S236A). The

amounts of FLAG-tagged Bst1(S236A)p and FLAG-tagged Bst1p were similar, suggesting that Bst1(S236A)p is as stable as the wild-type Bst1p (Figure 43B). HA-Gas1*p was stabilized in *bst1*Δ cells containing a control vector, whereas *BST1* restored the degradation of Gas1*p in *bst1*Δ cells (Figure 44A and B). I also found that *bst1-S236A* did not restore the degradation of Gas1*p in *bst1*Δ cells (Figures 44A and B). These results indicate that the GPI inositol deacylase activity of Bst1p is important for the degradation of Gas1*p.

I also examined the localization of mRFP-tagged Gas1 and Gas1* proteins in *bst1*Δ cells. I found that mRFP-Gas1p is mainly localized in the plasma membrane, which is the native location of Gas1p (Figure 45A). In contrast, mRFP-Gas1*p was present not in the plasma membrane but rather in an intracellular compartment, probably in the ER membrane (Figure 45B). I next transformed the *bst1*Δ cells expressing mRFP-Gas1*p with GFP-HDEL as a marker of the ER (Monnat *et al*., 2000). I found that mRFP-Gas1*p colocalized with HDEL-GFP in the ER (Figure 45B). As I found in my initial experiments, the fluorescence of mRFP-Gas1*p in wild-type cells was too weak to detect. These results also indicate that the Gas1* protein, which was degraded through the ERAD pathway, accumulates in the ER in *bst1*Δ cells and that the degradation of Gas1*p is dependent on inositol deacylation of the GPI.

Degradation of Gas1* protein in mutants of GPI biosynthesis, concentration, and *N*-glycosylation

My results show that inositol deacylation of GPI is required for the ER quality control of misfolded GPI-anchored proteins (Figures 39 and 44). To identify other factors required for quality control in the ER, I performed CHX chase experiments of

Gas1*p in mutants defective in the biosynthesis of the GPI anchor, the concentration of GPI-anchored proteins, and the folding of *N*-glycosylated proteins. I also performed the same experiments in the mutants carrying CPY*HA to compare with the degradation of HA-Gas1*p.

First, I examined the effects of mutants involved in the biosynthesis of GPI on the degradation of Gas1*p. *GWT1* is required for inositol acylation early in the GPI biosynthetic pathway, which is the opposite reaction of Bst1p (Umemura *et al*., 2003). *GPI7* is involved in the addition of ethanolamine phosphate to the second mannose of GPI (Benachour *et al*., 1999; Fujita *et al*., 2004). I used a *gwt1-20* mutant that has a partial defect in inositol acylation activity at 30˚C, and a *gpi7*Δ mutant that shows a temperature-sensitive growth phenotype. HA-Gas1*p was not stabilized in these mutants (Figure 46A and C). Also, the degradation of CPY*HA was not delayed in any of the mutants (Figure 46B and D). The results are consistent with my finding that the degradation of SHg* is independent of Bst1p (Figure 42). It is not clear why the degradation of CPY* and KHN proteins are delayed in the *per17-1/bst1* mutant (Vashist *et al*., 2001), but, based on my finding that Bst1p deacylates inositol in GPI anchors, it is most likely that it is an indirect effect. The steady-state levels of CPY*HA seemed to be slightly higher in GPI biosynthetic mutants than in wild-type cells. Therefore, it is possible that the degradation of other proteins like CPY* is affected because pre-GPI proteins or immature GPI-anchored proteins are accumulated and degraded in the ER due to general defects in GPI anchor biosynthesis.

I next addressed whether mutations in the process of vesicular protein concentration of GPI-anchored proteins affect the degradation of GPI-anchored proteins. Members of the p24 family, such as *EMP24* and *ERV25*, have been shown to be

involved in the concentration of GPI-anchored proteins during vesicular transport (Muniz *et al*., 2000; Watanabe and Riezman, 2004). Deletion of p24 family genes activates the unfolded protein response (Belden and Barlowe, 2001). However, as reported previously (Caldwell *et al*., 2001), the degradation of CPY*HA was not affected when these genes are deleted (*emp24*Δ and *erv25*Δ; Figure 47B and D). In contrast, HA-Gas1*p was stabilized in *emp24*Δ, *erv25*Δ, and double *bst1*Δ *emp24*Δ mutants (Figure 47A and C). These results indicate that the processes of concentrating GPI-anchored proteins and degrading misfolded GPI-anchored proteins are closely related. Thus, the activation of the unfolded protein response in *emp24*Δ cells and *erv25*Δ cells (Belden and Barlowe, 2001) may be due to a defect in the degradation of GPI-anchored proteins.

Quality control of glycoproteins is well-characterized and involves the specific oligosaccharide structures $Glc_1Man_9GlcNAc_2$ and $Man_8GlcNAc_2$ (Helenius and Aebi, 2004). The Gas1 protein contains ten potential sites of *N*-glycosylation and is highly *O*-mannosylated (Popolo and Vai, 1999). I used *mns1*Δ and *htm1*Δ mutants to determine whether the quality control mechanisms of glycoproteins are involved in the degradation of misfolded GPI-anchored proteins. *MNS1* is required for the mannose trimming of an oligosaccharide (Camirand *et al*., 1991), and *HTM1* is involved in the recognition of the oligosaccharide portion of misfolded glycoproteins (Jakob *et al*., 2001). The degradation of misfolded glycoproteins was stabilized in these mutants. I also confirmed that the degradation of CPY* is delayed in *mns1*Δ, *htm1*Δ, and double *bst1*Δ *mns1*Δ mutants (Figure 48B and D). The degradation of Gas1*p was not stabilized in *mns1*Δ, whereas the deletion of *HTM1* slightly delayed the degradation of Gas1*p, although the stabilization was less efficient in these cells than in *bst1*Δ cells

(Figure 48A and C). Gas1*p was stabilized in double *bst1*Δ *mns1*Δ and *bst1*Δ *htm1*Δ mutants, but the efficiency of stabilization in these double mutants was similar to that in *bst1*Δ single-mutant cells (Figure 48A and C).

Misfolded Gas1 proteins associate with both the chaperone BiP/Kar2p and GPI inositol deacylase *in vivo*

If Gas1*p is misfolded, several chaperones should be associated with Gas1*p in the ER. A previous study showed that a precursor of GPI-anchored protein associates with the ER chaperone BiP but not with calnexin in mammalian cells (Oda *et al*., 1996). BiP also binds to mutant prion proteins (Jin *et al*., 2000). First, I examined whether Gas1*p could associate with yeast BiP (Kar2p) *in vivo*. For this purpose, I fused the FLAG epitope to Kar2p after the signal peptide in Kar2p and expressed the construct in yeast cells containing HA-Gas1p or HA-Gas1*p. Immunoprecipitation in 1% digitonin-solubilized extracts revealed that FLAG-Kar2p coprecipitated with a fraction of HA-Gas1*p but not with HA-Gas1p (Figure 49A, left panels). I examined the ability of anti-HA-agarose to coimmunoprecipitate FLAG-Kar2p with HA-Gas1p. I found that FLAG-Kar2p coprecipitated with HA-Gas1*p but not with HA-Gas1p (Figure 49A, right panels), suggesting that Gas1*p is misfolded and that Kar2p is involved in the folding of Gas1*p. Because FLAG-Kar2p was not detected by anti-HA immunoprecipitation in WT cells carrying FLAG-KAR2 (Figure 49A, right panels), the results reflect a true association of HA-Gas1*p with FLAG-Kar2p.

In these studies, I demonstrated that inositol deacylation of GPI is required for the degradation of Gas1*p (Figures 39 and 44). To determine whether Bst1p interacts with Gas1*p *in vivo*, I coexpressed Bst1p-FLAG with HA-Gas1p or HA-Gas1*p in

yeast cells. I immunoprecipitated Bst1p-FLAG from the microsomal fraction and examined for the presence of HA-Gas1p or HA-Gas1*p by immunoblot analysis. Figure 49B shows that wild-type Gas1p associates weakly with Bst1p, whereas there is a strong association of Gas1*p with Bst1p (Figure 49B, left panels). I also used anti-HA-agarose, to immunoprecipitate HA-Gas1p or HA-Gas1*p and then checked for associated Bst1p. I found that a small amount of Bst1p-FLAG coimmunoprecipitated with wild-type HA-Gas1p, whereas there was a substantial amount of Bst1p-FLAG that coprecipitated with HA-Gas1*p (Figure 49B, right panels), supporting the idea that Gas1*p associates with Bst1p. Because Bst1p has GPI inositol deacylase activity, it is possible that it associates with GPI-anchored proteins by binding to the GPI moiety. Finally, I examined whether Bst1(S236A)p, the lipase-inactive form of Bst1p, associates with Gas1*p. I found that Gas1*p associates with both wild-type Bst1p and Bst1(S236A)p *in vivo* (Figure 49C), supporting the idea that the stabilization of Gas1*p in S236A cells (Figure 44) is due to a loss in the GPI inositol deacylase activity rather than reduced binding of Gas1*p. These results suggest that Bst1p associates with misfolded GPI-anchored proteins and that deacylation activity is required for their degradation.

II-5. Discussion

Post-translational modification of proteins, including *N*-linked and *O*-linked glycosylation, that occur in the lumen of the ER, is involved in folding and ER quality control (Helenius and Aebi, 2004; Nakatsukasa *et al*., 2004). My current report is the first one indicating the molecular mechanisms of the quality control and degradation of GPI-anchored proteins, and I showed that the GPI anchor itself is involved in the quality control process. The first key finding was that a misfolded Gas1p, a model of misfolded GPI-anchored proteins, is GPI-anchored but retained in the ER and degraded *via* the proteasome pathway. I also found that deacylation of the inositol on GPI plays a crucial role in the degradation of GPI-anchored proteins.

Increases in the molecular weight of Gas1* proteins

In the CHX chase experiment, Gas1*p remained as the ER form but its molecular weight gradually increased. Immunoblot analysis showed that the steady-state forms of Gas1*p are broad (Figures 29B and 30C). The increases in the molecular weight of Gas1*p could not be due to reactions in the Golgi apparatus, such as outer chain elongation of *N*-glycans, because GPI-anchored Gas1*p was only present as the ER form (Figure 31) and because the mobility of Gas1*p increased during the chase experiment even after Endo H treatment (Figure 32) and the mobility shift of HA-Gas1*p was still observed in *sec18-1* mutant cells at the restrictive temperature (Figure 37). Rather, the increases in molecular weight seem to be due to a modification in the ER. I suspect that the mobility shift of Gas1*p during the chase period is caused by *O*-linked mannosylation because several aberrant proteins receive additional *O*-mannosyl

residues in the ER (Nakatsukasa *et al*., 2004). Gas1p has serine/threonine rich regions that are potential sites of *O*-mannosylation, and misfolded Gas1p might also receive additional *O*-mannosyl residues in the ER.

Effect of *N*-glycan processing on the degradation of Gas1* proteins

To investigate the involvement of *N*-glycans in the degradation of GPI-anchored proteins, I measured the degradation of Gas1*p in *mns1*Δ and *htm1*Δ cells. The deletion of *HTM1* slightly stabilized Gas1*p, whereas the deletion of *MNS1* had little effect (Figure 48). The effect of the *htm1* deletion on the delay of the Gas1*p degradation was weaker than that of the *bst1* deletion, suggesting that the degradation of Gas1*p is mainly affected by the GPI inositol deacylase activity. In yeast, GPI-anchored proteins are major components of the mannan layer in the cell wall. Almost all cell wall proteins and GPI-anchored proteins at the plasma membrane are highly *N*- and *O*-mannosylated (Orlean, 1997). Gas1p contains several modifications including ten potential *N*-glycosylation sites and a number of potential *O*-glycosylation sites. It might be difficult for Mns1p-Htm1p quality control systems to access highly glycosylated misfolded GPI-anchored proteins. Further analysis using a simpler system would be helpful, for example, a study of folding and degradation using a non-*N*-glycosylated GPI-anchored protein.

ER-associated degradation of Gas1* proteins

Recently, it was reported that a membrane protein and a soluble luminal protein in the ER were degraded by distinct cellular mechanisms (Taxis *et al.*, 2003; Huyer *et al.*, 2004; Vashist and Ng, 2004). In addition, two ER surveillance mechanisms

have been proposed: ERAD-L, which monitors the folded state of luminal domains; and ERAD-C, which monitors that of cytosolic domains (Figure 35) (Ahner and Brodsky, 2004; Vashist and Ng, 2004). Several specific factors have been identified for the ERAD-L and ERAD-C pathways. The proposed models could explain how misfolded proteins are degraded through the ERAD pathway, but there still are several exceptions to this pathway (Hampton, 2002; Schmitz and Herzog, 2004; Meusser *et al.*, 2005). In this study, I could not identify the E3 ubiquitin ligases that are involved in Gas1*p degradation. Although I investigated the effect of three kinds of E3 on Gas1*p degradation, neither ERAD-L nor ERAD-C had an apparent effect on the degradation of Gas1*p.

I suspect that the ERAD-L and ERAD-C pathways are not involved because of the unique properties of GPI-anchored proteins. First, GPI-anchored proteins are bound to the ER membrane by a lipid, which is different from membrane or soluble proteins. Second, GPI-anchored proteins are a component of lipid rafts, which are sphingolipid- and sterol-rich membrane microdomains, and Gas1p has been found to associate with a raft-like microdomain in the ER (Bagnat *et al.*, 2000). Third, GPI-anchored proteins are transported from the ER to the Golgi apparatus in distinct vesicles from those containing non-GPI proteins (Mayor and Riezman, 2004; Watanabe and Riezman, 2004). Apparently, specific components are required for sorting GPI-anchored proteins from other secretory proteins upon exit from the ER (Muniz *et al.*, 2000; Muniz and Riezman, 2000). These properties also suggest the presence of specific components that are required for the degradation of GPI-anchored proteins, wherein GPI anchoring might change the accessibility to chaperones and unique ubiquitin ligases might act on the GPI-anchored proteins. In fact, my results suggest that the inositol deacylation of

GPI by Bst1p plays an important role in this degradation pathway.

Folding of GPI-anchored proteins

It remains unclear when the folding of GPI-anchored proteins occurs. I demonstrated that Gas1*p is modified by the GPI anchor (Figure 31), suggesting that the unfolded protein precursor is transferred to the GPI anchor. GPI-protein precursors that fail to be processed and retain the C-terminal GPI signal peptide are accumulated and degraded through the ERAD pathway in mammalian cells (Wainwright and Field, 1997; Wilbourn *et al.*, 1998; Ali *et al.*, 2000). A precursor Gas1p that could not be modified by the GPI anchor is also retained in the ER (Nuoffer *et al.*, 1993; Doering and Schekman, 1996). In *Trypanosome brucei* GPI8-knock out (TbGPI8KO) cells, which lack a member of the GPI transamidase complex, GPI transamidase cannot process the trans-sialidase precursors by removing their GPI signals. TbGPI8KO cells have low trans-sialidase activity even in the cell lysate, and trans-sialidase is probably degraded in the ER (Nagamune *et al.*, 2004), suggesting that GPI signal cleavage of the precursor protein is important for the folding of GPI-proteins. These reports indicate that unanchored precursor GPI-proteins are not sufficient for complete folding of the protein, which appears to be carried out after the cleavage of GPI signals.

Bst1p is involved in the quality control of GPI-anchored proteins

Except in human erythrocytes, almost all GPI-anchored proteins are deacylated before their exit from the ER. In mammalian cells, a mammalian model GPI-anchored protein, DAF, was 56% deacylated in the ER within as little as 5 min (Chen *et al.*, 1998). Inositol deacylation of GPI is important for the efficient transport of GPI-

anchored proteins from the ER to the Golgi (Tanaka *et al*., 2004). I further demonstrated that the degradation of Gas1*p was significantly delayed in *bst1*Δ cells (Figure 39). The stabilization of Gas1*p in *bst1*Δ cells was due to the loss of GPI inositol deacylation activity (Figure 44). In addition, I found that Gas1*p associates with BiP and Bst1p *in vivo* (Figure 49). My results suggest that GPI inositol deacylation is further required for the efficient degradation of misfolded GPI-anchored proteins.

There are several numbers of ERAD substrates that exit from the ER and their efficient degradation requires ER-to-Golgi transport (Vashist *et al.*, 2001; Ahner and Brodsky, 2004; Vashist and Ng, 2004) (Figure 35). In this study, I showed Gas1*p is capable of exiting from the ER to a certain extent and this ER-to-Golgi transport is also important for the efficient degradation of Gas1*p (Figure 37). The degradation rate of SHg*, a misfolded non-GPI protein, was not changed between WT and *bst1*Δ cells (Figure 42), indicating that Bst1p affected only GPI-anchored proteins in exiting from the ER. One possibility for the degradation delay of Gas1*p in *bst1*Δ cells might be due to the delay of Gas1*p transport from the ER. The degradation of Gas1*p was also delayed in *emp24*Δ and *erv25*Δ cells (Figure 47). Emp24p and Erv25p are involved in the concentration of GPI-anchored proteins for the ER exit (Muniz *et al*., 2000; Watanabe and Riezman, 2004). These findings support the idea that a delay of Gas1*p transport from the ER affects its degradation in these mutant cells. My results also indicate that misfolded GPI-anchored proteins, as folded GPI-anchored proteins, would exit from the ER in certain vesicles that are distinct from those that contain many other secretory proteins (Mayor and Riezman, 2004; Watanabe and Riezman, 2004), because the degradation of CPY* was not affected in *emp24*Δ and *erv25*Δ cells.

It is an important issue whether Bst1p is indeed involved in the ER quality

control of GPI-anchored proteins. As shown in Figure 49B, Gas1*p was stably associated with Bst1p, whereas Gas1p was not so much. These results imply that Bst1p might wait for the correct folding of the GPI-anchored protein and deacylate the correctly folded proteins positively, but deacylate less efficiently the misfolded GPI-anchored proteins. Once GPI-anchored proteins are deacylated, they are rapidly sorted to exit from the ER (Figure 50) (Tanaka *et al.*, 2004). Therefore, inositol deacylation activity should be strictly regulated. Bst1p could receive information on the status of protein folding after the protein is anchored by GPI. Stable association between Gas1*p and Bst1p suggests that there are unknown molecules that participate in the sensing of the protein folding status of GPI-anchored proteins and then transmit this information to Bst1p before it deacylates GPI-anchored proteins. When the misfolded GPI-anchored proteins are expressed, chaperones such as BiP try to assist in their folding. If proteins could not form a proper folding within an appropriate period of time, Bst1p may function to transport them to the Golgi preventing the accumulation of aberrant proteins in the ER (Figure 50). The Bst1p function positions at the border between protein folding in the ER and ER exit for the GPI-anchored proteins. I suspect that the inositol deacylation of GPI-anchored proteins by Bst1p is involved in the ER quality control and acts as a gatekeeper that leads GPI-anchored proteins to the ER exit after receiving some information on their folding status (Figure 50).

GENERAL DISCUSSION

Overview of this thesis

In this thesis, I tried to figure out the physiological function of GPI moiety by studying the roles of genes involved in the GPI biosynthesis and modification in *S. cerevisiae*. I selected two genes involved in the GPI modification. In chapter I, I investigated the roles of a side chain EtN-P on the GPI core structure. *GPI7* is required for the addition of the side chain EtN-P to the second Man portion of the GPI core glycan structure. This is the last step reaction just before transferring GPI to protein. Although almost all genes involved in the GPI biosynthetic pathway are essential for cell growth in *S. cerevisiae*, *GPI7* is not essential for cell viability. The reason of viability of *gpi7*Δ cells is thought as follows: GPI moiety lacking a side chain EtN-P due to the loss of *GPI7* function is still transferred to proteins, and these GPI-anchored proteins are transported to the plasma membrane and cell wall. However, *gpi7* mutant cells showed several defective phenotypes. I revealed that one function of the side chain EtN-P added by Gpi7p is a correct targeting of GPI-anchored proteins in cell separation. In chapter II, I evaluated the function of acyl portion on inositol of GPI moiety. At an early step in the biosynthesis, the GPI inositol is acylated by Gwt1p (Umemura *et al*., 2003) (Figure 27). The amounts of GPI-anchored proteins are greatly decreased in *gwt1* mutant cells, indicating that this acylation is critical for the attachment of GPI to proteins (Umemura *et al*., 2003). Once the GPI anchor is attached to a protein, the inositol is usually deacylated by Bst1p in the ER (Figure 27) (Chen *et al*., 1998). I found that the inositol deacylation of the GPI-anchored protein is required for the quality control of them in the ER. My results further suggest that the GPI inositol deacylase is a

key enzyme in initiating the degradation of misfolded GPI-anchored proteins.

Roles of a side chain ethanolaminephosphate of GPI anchor added by Gpi7p

The *gpi7* mutants have defects in cell separation and daughter cell growth. It is likely that the mislocalization of daughter-specific GPI-anchored proteins causes a daughter-specific cell cycle arrest in *gpi7* mutants (Figures 20 and 21). Previous studies present several explanations for the cell separation defect and mislocalization of Egt2p in *gpi7* mutants. First, GPI-anchored proteins are components of lipid rafts, which are sphingolipid- and sterol-rich microdomains of the membrane. Polarization of sterol-rich domains to the shmoo tip was observed in mating pheromone-treated cells in *S. cerevisiae* (Bagnat and Simons, 2002). The mating efficiency decreased to 1/100 of the wild-type level when both mating partners were *gpi7*Δ strains (Toh-e and Oguchi, 1999). Lipid raft formation also contributes to the hyphal growth that is required for virulence in *C. albicans* (Martin and Konopka, 2004). Interestingly, *gpi7*Δ/*gpi7*Δ cells were defective in pseudohypal formation in *C. albicans* (Richard *et al.*, 2002b). Lipid rafts have been implicated in membrane trafficking and signaling in mammalian cells (Simons and Ikonen, 1997). In yeast, lipid raft formation is essential for the correct targeting of several proteins (Bagnat *et al.*, 2001; Bagnat and Simons, 2002; Umebayashi and Nakano, 2003). Ceramide remodeling on GPI-anchored proteins in the Golgi and plasma membrane was significantly reduced in *gpi7*Δ mutants (Benachour *et al.*, 1999). The lipid remodeling process might help GPI proteins to sort into membrane subdomains. It is possible that the addition of EtN-P to the GPI glycan portion by Gpi7p may be required for stability of lipid rafts, giving rise to the mislocalization of GPI proteins in *gpi7* mutants. Second, GPI-anchored proteins are transported from the ER to

the Golgi apparatus in distinct vesicles from those containing non-GPI proteins. Particular components are required for sorting GPI-anchored proteins from other secretory proteins upon exit from the ER (Muniz *et al.*, 2001; Morsomme *et al.*, 2003). The p24 family is thought to be components of cargo receptors for GPI-anchored proteins. Emp24p, a member of this family, is necessary for efficient packaging of Gas1p into ER-derived vesicles and can be directly cross-linked to Gas1p (Muniz *et al.*, 2000). Therefore, another possibility is that particular cargo receptor(s), such as the members of the p24 family, might recognize the EtN-P side chain of the GPI either to concentrate GPI-anchored proteins or to form a vesicle for correct targeting at the cell separation stage. Although these possibilities should be addressed further in future, to our knowledge this is the first report indicating that a complete GPI structure is essential for the correct targeting of GPI-anchored proteins.

Roles of inositol deacylation of GPI anchor by Bst1p

In the quality control of glycoproteins, *N*-glycans of the proteins play important roles for the folding and degradation. Mannose is trimmed from both correctly and aberrantly folded *N*-glycosylated proteins by ER-α1,2-mannosidase (Figure 26). *N*-glycans of correctly folded proteins are rapidly trimmed and processed to $Man_8GlcNAc_2$, and secretory proteins are transported from the ER to the Golgi (Jakob *et al.*, 1998). However, when a glycoprotein cannot acquire the correct conformation within an appropriate period of time, it is sorted to the ERAD pathway. The removal of one specific α-1,2-mannose residue by ER-α1,2-mannosidase may be the point at which a misfolded protein is routed to the degradation pathway (Figure 26) (Hosokawa *et al.*, 2001; Jakob *et al.*, 2001; Oda *et al.*, 2003). Almost all GPI-anchored proteins are

deacylated before their exit from the ER. Inositol deacylation of GPI is important for the efficient transport of GPI-anchored proteins from the ER to the Golgi (Tanaka *et al.*, 2004). Our results suggest that GPI inositol deacylation is further required for the efficient degradation of misfolded GPI-anchored proteins.

Bst1p is required for both the efficient degradation of misfolded GPI-anchored proteins and the efficient ER-to-Golgi transport of correctly folded GPI-anchored proteins. Gas1*p was stably associated with Bst1p, whereas Gas1p was not so much. These results imply that Bst1p might wait for the correct folding of the GPI-anchored protein and deacylate the correctly folded proteins positively, but deacylate less efficiently the misfolded GPI-anchored proteins. Once GPI-anchored proteins are deacylated, they are rapidly sorted to exit from the ER (Tanaka *et al.*, 2004). Therefore, inositol deacylation activity should be strictly regulated. Bst1p removes the acyl portion of the GPI after it is transferred to the protein and must not deacylate GPI intermediates during the biosynthesis of GPI. Bst1p should receive information on the status of protein folding after the protein is anchored by GPI. Stable association between Gas1*p and Bst1p also suggests that there are unknown molecules that participate in the sensing of the protein folding status of GPI-anchored proteins and then transmit this information to Bst1p before it deacylates GPI-anchored proteins. The folding status of GPI-anchored proteins might be recognized by GPI-specific lectins or chaperones. Gas1*p associates with BiP/Kar2p, which is a member of the Hsp70 family of chaperones. Hsp40 family proteins act as cochaperones and enhance the ATPase activity of Hsp70, and there are several Hsp40 members in the ER, one of which could cooperate with BiP to transmit the folding status of GPI-anchored proteins to Bst1p. When the misfolded GPI-anchored proteins are expressed, chaperones such as BiP try to assist in their folding. If proteins

could not form a proper folding within an appropriate period of time, Bst1p may function to prevent the accumulation of aberrant proteins in the ER. The Bst1p function positions at the border between protein folding in the ER and ER exit for the GPI-anchored proteins. Inositol deacylation of GPI-anchored proteins by Bst1p is involved in the ER quality control and acts as a gatekeeper that leads GPI-anchored proteins to the ER exit after receiving some information on their folding status (Figure 50).

Contribution of this thesis to GPI anchor research

GPI anchors are complex structures, but biological significance of GPI anchor is an outstanding issue. In this thesis, I demonstrated that GPI anchoring, a post-translational modification, plays important roles for the determination of life and fate for GPI-anchored proteins. These findings contribute to several research aspects of the GPI anchor research. In the Gpi7p field, these discoveries may serve as apical sorting or transport of GPI-anchored proteins. The side chain EtN-P of GPI anchor may be also involved in the mating and hyphal growth that is required for virulence, because *gpi7* mutant cells are defective in mating efficiency and pseudohypal formation (Toh-e and Oguchi, 1999; Richard *et al.*, 2002b). It is possible that the addition of EtN-P to the GPI glycan portion by Gpi7p is required for the targeting of several GPI-anchored proteins for mating or hyphal growth, giving rise to the mislocalization of them in *gpi7* mutant cells. In mammalian polarized cells, GPI-anchored proteins are sorted and transported to the apical domain. Mammalian GPI7 proteins are not essential for cell surface expression of GPI-anchored proteins (Shishioh *et al.*, 2005), but may be involved in processes such as remodeling of GPI or targeted transport of GPI-anchored proteins.

In the Bst1p field, my results indicate that inositol deacylation is required for

the quality control of GPI-anchored proteins. Investigation of quality control of GPI-anchored proteins contributes to elucidate mechanisms of folding disease, particularly prion diseases including Creuzfeldt-Jakob disease, Gerstmann-Straussler-Scheinker disease, and fatal familial insomnia, and hypophosphatasia. The cellular prion protein PrP^{c} is a GPI-anchored protein that plays a key role in the transmissible spongiform encephalopathies. PrP^{c} is converted into a pathological conformer, PrP^{sc}, the scrapie isoform of the prion protein. The infectious mode usually involves the transformation of wild-type PrP^{c} into PrP^{sc}. Familial prion diseases are linked to pathogenic mutations in PrP. Several misfolding mutants of PrP^{c} are degraded through the ERAD-proteasome pathway. Hypophosphatasia is a genetic disease characterized by reduced levels of TNSALP in serum and tissue. TNSALP is also a GPI-anchored protein. Mutated forms of TNSALP are recognized as ERAD substrates and are degraded by proteasome. Both prion diseases and hypophosphatasia are caused by the abnormality of protein folding. My results are the first finding that inositol deacylation of GPI anchor by Bst1p is involved in the quality control of GPI-anchored proteins. Molecular mechanisms of the quality control and degradation of GPI-anchored proteins are still unknown. My findings could be adapted to the quality control systems of GPI-anchored proteins in mammalian cells. Down regulation of PGAP1, which is the mammalian functional homolog of Bst1p, might show the degradation delay of misfolded GPI-anchored proteins. Elucidation of quality control and degradation systems of GPI-anchored proteins using yeast genetic methods will lead to the clinical approach for the folding disease caused by the abnormality of GPI-anchored proteins.

Perspectives

As described above, I have revealed several novel aspects on the roles of GPI anchor in yeast, particularly functions of a side chain EtN-P on second mannose and acyl portion on inositol, in this thesis. However, the following points still remained to be figured out in the future.

I revealed one of the important functions of EtN-P on the GPI anchor is the correct targeting of GPI-anchored proteins for cell separation. However, a detailed molecular mechanism for the targeting of GPI-anchored proteins, such as Egt2p, is unknown. First, are there cargo receptors to transport GPI-anchored proteins to the septum specifically? Second, is the lipid moiety of Egt2p remodeled to ceramide, and is the remodeling process essential for the targeting of Egt2p to the septum? Third, can GPI-anchored proteins exist on the lipid rafts in *gpi7*Δ cells? In *gpi7*Δ cells, several defects have been reported (Toh-e and Oguchi, 1999; Richard *et al.*, 2002b). Are these defects caused by mislocalization of GPI-anchored proteins due to disruption of *GPI7* gene?

I uncovered one aspect of the quality control and degradation pathway for GPI-anchored proteins in this study, although the process remains unknown. I developed Gas1*p, which enables the study of the degradation of GPI-anchored proteins and therefore provides a unique and useful addition to the existing models of misfolded soluble glycoproteins and membrane proteins. The degradation of Gas1*p undergoes the same pathway with ERAD-L substrates in some respects (*e.g.*, ER-to-Golgi transport), but passes different route from ERAD-L and ERAD-C substrates in other points (*e.g.*, Bst1p-dependency and effect of ubiquitin ligases). However, several questions remain. For example, which components are involved in the degradation of

misfolded GPI-anchored proteins? Are common factors or specific factors employed in the degradation of GPI-anchored proteins, soluble glycoproteins, and membrane proteins? What factor distinguishes between folded and misfolded GPI-anchored proteins? When does Bst1p deacylate the misfolded GPI-anchored proteins? Although these questions remain to be answered, the analysis of molecules that interact with Gas1*p may reveal how the ER quality control machinery for GPI-anchored proteins is linked to proteasome-mediated degradation.

ACKNOWLEDGEMENTS

I would like to express my sincere gratitude to Dr. Yoshifumi Jigami, Director of Research Center for Glycoscience, National Institute of Advanced Industrial Science and Technology (AIST), for his kind guidance and encouragement throughout the course of this investigation.

I am indebted to my committee members Dr. Hideko Urushihara, Dr. Hiroshi Kamada, Dr. Osamu Numata, and Dr. Yoshimasa Tanaka, Graduate School of Life and Environmental Sciences, the University of Tsukuba. I appreciate the major time and effort they all contributed to improve this thesis.

I would like to acknowledge the continuing guidance, encouragement, and helpful discussions of Dr. Takehiko Yoko-o, Research Center for Glycoscience, AIST.

I wish to express my gratitude to Dr. Yoh-ichi Shimma, Dr. Yasunori Chiba, Dr. Xiao-Dong Gao, Dr. Ken-ichi Nakayama, and Ms. Michiyo Okamoto at Glycobiosynthesis Team, Research Center for Glycoscience, AIST, for their experimental guidance and valuable discussions.

I am very grateful to Dr. Peter Orlean, University of Illinois at Urbana-Champaign, and to Dr. Taroh Kinoshita, Osaka University, for critical reading of my manusctipts and helpful suggestion, to Dr. Yasushi Kamisaka, Lipid Engineering Group, Institute for Biological Resources and Functions, AIST, for basic knowledge and technique of lipid analysis, to Dr. Akio Toh-e, University of Tokyo, for TOp1014 plasmid, *las21-1*, *las21-2*, *rpn12-1*, and *rpn3-1* strains, to Dr. Michael Snyder, Yale University, for yeast genomic library mutagenized by an mTn-3xHA/GFP transposon, to Dr. Kappei Tsukahara, Eisai Co., for YEp352GAPII-ROM2 plasmid, to Dr. Yusuke

Maeda, Osaka University, for providing GST-tagged α-toxin protein, to Dr. Tadashi Suzuki, Osaka University, for providing the YIp-CPY* plasmid, to Dr. Roger Tsien, University of California, San Diego, for providing the mRFP plasmid, to Dr. Katsura Hata, Eisai Co., for providing the anti-Gas1 peptide polyclonal antibody, to Dr. Yoshiko Kikuchi, University of Tokyo, for providing the *rsp5-101* strains, and to Dr. Mark Hochstrasser, Yale University, for providing the *hrd1*Δ *doa10*Δ strains.

I also express my appreciation to Dr. Takuji Oka, Ms. Mariko Umemura, Dr. Toru Sumita, Mr. Toshihiko Kitajima, Dr. Yuko Chigira, and Ms. Minako Takashiba, at AIST, Mr. Hiroto Hirayama, at the University of Tsukuba, and other all members in the Glycobiosynthesis Team, Research Center for Glycoscience, AIST, for their useful discussions and every kind of helps.

Finally, I would like to thank my parents, my brother, my grandfather, and grandmothers, for their continuous encouragement and support to my research. Without their understanding and help, I could not go through my graduate career. I would like to say to them biggest, THANK YOU!

REFERENCES

Abe, H., Shimma, Y., and Jigami, Y. (2003). In vitro oligosaccharide synthesis using intact yeast cells that display glycosyltransferases at the cell surface through cell wall-anchored protein Pir. Glycobiology *13*, 87-95.

Ahner, A., and Brodsky, J.L. (2004). Checkpoints in ER-associated degradation: excuse me, which way to the proteasome? Trends Cell Biol *14*, 474-478.

Ali, B.R., Claxton, S., and Field, M.C. (2000). Export of a misprocessed GPI-anchored protein from the endoplasmic reticulum in vitro in an ATP- and cytosol-dependent manner. FEBS Lett *483*, 32-36.

Bagnat, M., Chang, A., and Simons, K. (2001). Plasma membrane proton ATPase Pma1p requires raft association for surface delivery in yeast. Mol Biol Cell *12*, 4129-4138.

Bagnat, M., Keranen, S., Shevchenko, A., Shevchenko, A., and Simons, K. (2000). Lipid rafts function in biosynthetic delivery of proteins to the cell surface in yeast. Proc Natl Acad Sci U S A *97*, 3254-3259.

Bagnat, M., and Simons, K. (2002). Cell surface polarization during yeast mating. Proc Natl Acad Sci U S A *99*, 14183-14188.

Baladron, V., Ufano, S., Duenas, E., Martin-Cuadrado, A.B., del Rey, F., and Vazquez de Aldana, C.R. (2002). Eng1p, an endo-1,3-beta-glucanase localized at the daughter side of the septum, is involved in cell separation in *Saccharomyces cerevisiae*. Eukaryot Cell *1*, 774-786.

Barz, W.P., and Walter, P. (1999). Two endoplasmic reticulum (ER) membrane proteins that facilitate ER-to-Golgi transport of glycosylphosphatidylinositol-anchored proteins. Mol Biol Cell *10*, 1043-1059.

Belden, W.J., and Barlowe, C. (2001). Deletion of yeast p24 genes activates the unfolded protein response. Mol Biol Cell *12*, 957-969.

Benachour, A., Sipos, G., Flury, I., Reggiori, F., Canivenc-Gansel, E., Vionnet, C., Conzelmann, A., and Benghezal, M. (1999). Deletion of GPI7, a yeast gene required for addition of a side chain to the glycosylphosphatidylinositol (GPI) core structure, affects GPI protein transport, remodeling, and cell wall integrity. J Biol Chem *274*, 15251-15261.

Benghezal, M., Lipke, P.N., and Conzelmann, A. (1995). Identification of six complementation classes involved in the biosynthesis of glycosylphosphatidylinositol anchors in *Saccharomyces cerevisiae*. J Cell Biol *130*, 1333-1344.

Bi, E., Maddox, P., Lew, D.J., Salmon, E.D., McMillan, J.N., Yeh, E., and Pringle, J.R. (1998). Involvement of an actomyosin contractile ring in *Saccharomyces cerevisiae* cytokinesis. J Cell Biol *142*, 1301-1312.

Bidlingmaier, S., Weiss, E.L., Seidel, C., Drubin, D.G., and Snyder, M. (2001). The Cbk1p pathway is important for polarized cell growth and cell separation in *Saccharomyces cerevisiae*. Mol Cell Biol *21*, 2449-2462.

Brown, D.A., Crise, B., and Rose, J.K. (1989). Mechanism of membrane anchoring affects polarized expression of two proteins in MDCK cells. Science *245*, 1499-1501.

Brown, D.A., and Rose, J.K. (1992). Sorting of GPI-anchored proteins to glycolipid-enriched membrane subdomains during transport to the apical cell surface. Cell *68*, 533-544.

Cabib, E., Roh, D.H., Schmidt, M., Crotti, L.B., and Varma, A. (2001). The yeast cell wall and septum as paradigms of cell growth and morphogenesis. J Biol Chem *276*, 19679-19682.

Caldwell, S.R., Hill, K.J., and Cooper, A.A. (2001). Degradation of endoplasmic

reticulum (ER) quality control substrates requires transport between the ER and Golgi. J Biol Chem *276*, 23296-23303.

Camirand, A., Heysen, A., Grondin, B., and Herscovics, A. (1991). Glycoprotein biosynthesis in *Saccharomyces cerevisiae*. Isolation and characterization of the gene encoding a specific processing alpha-mannosidase. J Biol Chem *266*, 15120-15127.

Chen, R., Walter, E.I., Parker, G., Lapurga, J.P., Millan, J.L., Ikehara, Y., Udenfriend, S., and Medof, M.E. (1998). Mammalian glycophosphatidylinositol anchor transfer to proteins and posttransfer deacylation. Proc Natl Acad Sci U S A *95*, 9512-9517.

Cheng, L., Hunke, L., and Hardy, C.F. (1998). Cell cycle regulation of the *Saccharomyces cerevisiae* polo-like kinase cdc5p. Mol Cell Biol *18*, 7360-7370.

Cid, V.J., Jimenez, J., Molina, M., Sanchez, M., Nombela, C., and Thorner, J.W. (2002). Orchestrating the cell cycle in yeast: sequential localization of key mitotic regulators at the spindle pole and the bud neck. Microbiology *148*, 2647-2659.

Colman-Lerner, A., Chin, T.E., and Brent, R. (2001). Yeast Cbk1 and Mob2 activate daughter-specific genetic programs to induce asymmetric cell fates. Cell *107*, 739-750.

Conzelmann, A., Riezman, H., Desponds, C., and Bron, C. (1988). A major 125-kd membrane glycoprotein of *Saccharomyces cerevisiae* is attached to the lipid bilayer through an inositol-containing phospholipid. EMBO J *7*, 2233-2240.

Doering, T.L., and Schekman, R. (1996). GPI anchor attachment is required for Gas1p transport from the endoplasmic reticulum in COP II vesicles. EMBO J *15*, 182-191.

Eakle, K.A., Bernstein, M., and Emr, S.D. (1988). Characterization of a component of the yeast secretion machinery: identification of the SEC18 gene product. Mol Cell Biol *8*, 4098-4109.

Eisenhaber, B., Maurer-Stroh, S., Novatchkova, M., Schneider, G., and Eisenhaber, F.

(2003). Enzymes and auxiliary factors for GPI lipid anchor biosynthesis and post-translational transfer to proteins. Bioessays *25*, 367-385.

Ellgaard, L., Molinari, M., and Helenius, A. (1999). Setting the standards: quality control in the secretory pathway. Science *286*, 1882-1888.

Elrod-Erickson, M.J., and Kaiser, C.A. (1996). Genes that control the fidelity of endoplasmic reticulum to Golgi transport identified as suppressors of vesicle budding mutations. Mol Biol Cell *7*, 1043-1058.

Field, M.C., Moran, P., Li, W., Keller, G.A., and Caras, I.W. (1994). Retention and degradation of proteins containing an uncleaved glycosylphosphatidylinositol signal. J Biol Chem *269*, 10830-10837.

Finger, A., Knop, M., and Wolf, D.H. (1993). Analysis of two mutated vacuolar proteins reveals a degradation pathway in the endoplasmic reticulum or a related compartment of yeast. Eur J Biochem *218*, 565-574.

Fivaz, M., Vilbois, F., Thurnheer, S., Pasquali, C., Abrami, L., Bickel, P.E., Parton, R.G., and van der Goot, F.G. (2002). Differential sorting and fate of endocytosed GPI-anchored proteins. EMBO J *21*, 3989-4000.

Fujita, M., Yoko-o, T., Okamoto, M., and Jigami, Y. (2004). GPI7 involved in glycosylphosphatidylinositol biosynthesis is essential for yeast cell separation. J Biol Chem *279*, 51869-51879.

Gaynor, E.C., Mondesert, G., Grimme, S.J., Reed, S.I., Orlean, P., and Emr, S.D. (1999). MCD4 encodes a conserved endoplasmic reticulum membrane protein essential for glycosylphosphatidylinositol anchor synthesis in yeast. Mol Biol Cell *10*, 627-648.

Gietz, R.D., Schiestl, R.H., Willems, A.R., and Woods, R.A. (1995). Studies on the transformation of intact yeast cells by the LiAc/SS-DNA/PEG procedure. Yeast *11*, 355-360.

Gordon, V.M., Nelson, K.L., Buckley, J.T., Stevens, V.L., Tweten, R.K., Elwood, P.C., and Leppla, S.H. (1999). Clostridium septicum alpha toxin uses glycosylphosphatidylinositol-anchored protein receptors. J Biol Chem *274*, 27274-27280.

Hamada, K., Fukuchi, S., Arisawa, M., Baba, M., and Kitada, K. (1998). Screening for glycosylphosphatidylinositol (GPI)-dependent cell wall proteins in *Saccharomyces cerevisiae*. Mol Gen Genet *258*, 53-59.

Hamburger, D., Egerton, M., and Riezman, H. (1995). Yeast Gaa1p is required for attachment of a completed GPI anchor onto proteins. J Cell Biol *129*, 629-639.

Hampton, R.Y. (2002). ER-associated degradation in protein quality control and cellular regulation. Curr Opin Cell Biol *14*, 476-482.

Han, K.K., and Martinage, A. (1992). Post-translational chemical modification(s) of proteins. Int J Biochem *24*, 19-28.

Hanahan, D. (1983). Studies on transformation of *Escherichia coli* with plasmids. J Mol Biol *166*, 557-580.

Hardy, C.F., and Pautz, A. (1996). A novel role for Cdc5p in DNA replication. Mol Cell Biol *16*, 6775-6782.

Haynes, C.M., Caldwell, S., and Cooper, A.A. (2002). An HRD/DER-independent ER quality control mechanism involves Rsp5p-dependent ubiquitination and ER-Golgi transport. J Cell Biol *158*, 91-101.

Heinisch, J.J., Lorberg, A., Schmitz, H.P., and Jacoby, J.J. (1999). The protein kinase C-mediated MAP kinase pathway involved in the maintenance of cellular integrity in *Saccharomyces cerevisiae*. Mol Microbiol *32*, 671-680.

Helenius, A., and Aebi, M. (2001). Intracellular functions of N-linked glycans. Science *291*, 2364-2369.

Helenius, A., and Aebi, M. (2004). Roles of N-linked glycans in the endoplasmic reticulum. Annu Rev Biochem *73*, 1019-1049.

Hirose, S., Mohney, R.P., Mutka, S.C., Ravi, L., Singleton, D.R., Perry, G., Tartakoff, A.M., and Medof, M.E. (1992). Derivation and characterization of glycoinositol-phospholipid anchor-defective human K562 cell clones. J Biol Chem *267*, 5272-5278.

Hong, Y., Ohishi, K., Inoue, N., Kang, J.Y., Shime, H., Horiguchi, Y., van der Goot, F.G., Sugimoto, N., and Kinoshita, T. (2002). Requirement of N-glycan on GPI-anchored proteins for efficient binding of aerolysin but not *Clostridium septicum* alpha-toxin. EMBO J *21*, 5047-5056.

Horecka, J., and Jigami, Y. (2000). Identifying tagged transposon insertion sites in yeast by direct genomic sequencing. Yeast *16*, 967-970.

Hosokawa, N., Wada, I., Hasegawa, K., Yorihuzi, T., Tremblay, L.O., Herscovics, A., and Nagata, K. (2001). A novel ER alpha-mannosidase-like protein accelerates ER-associated degradation. EMBO Rep *2*, 415-422.

Huyer, G., Piluek, W.F., Fansler, Z., Kreft, S.G., Hochstrasser, M., Brodsky, J.L., and Michaelis, S. (2004). Distinct machinery is required in *Saccharomyces cerevisiae* for the endoplasmic reticulum-associated degradation of a multispanning membrane protein and a soluble luminal protein. J Biol Chem *279*, 38369-38378.

Hyman, R. (1988). Somatic genetic analysis of the expression of cell surface molecules. Trends Genet *4*, 5-8.

Ilgoutz, S.C., Zawadzki, J.L., Ralton, J.E., and McConville, M.J. (1999). Evidence that free GPI glycolipids are essential for growth of Leishmania mexicana. EMBO J *18*, 2746-2755.

Imhof, I., Flury, I., Vionnet, C., Roubaty, C., Egger, D., and Conzelmann, A. (2004). Glycosylphosphatidylinositol (GPI) proteins of *Saccharomyces cerevisiae* contain ethanolamine phosphate groups on the alpha1,4-linked mannose of the GPI anchor. J Biol Chem *279*, 19614-19627.

Ishida, Y., Komaru, K., Ito, M., Amaya, Y., Kohno, S., and Oda, K. (2003). Tissue-nonspecific alkaline phosphatase with an Asp(289)-->Val mutation fails to reach the cell surface and undergoes proteasome-mediated degradation. J Biochem (Tokyo) *134*, 63-70.

Ito, M., Amizuka, N., Ozawa, H., and Oda, K. (2002). Retention at the cis-Golgi and delayed degradation of tissue-non-specific alkaline phosphatase with an Asn153-->Asp substitution, a cause of perinatal hypophosphatasia. Biochem J *361*, 473-480.

Jacoby, J.J., Nilius, S.M., and Heinisch, J.J. (1998). A screen for upstream components of the yeast protein kinase C signal transduction pathway identifies the product of the SLG1 gene. Mol Gen Genet *258*, 148-155.

Jakob, C.A., Bodmer, D., Spirig, U., Battig, P., Marcil, A., Dignard, D., Bergeron, J.J., Thomas, D.Y., and Aebi, M. (2001). Htm1p, a mannosidase-like protein, is involved in glycoprotein degradation in yeast. EMBO Rep *2*, 423-430.

Jakob, C.A., Burda, P., Roth, J., and Aebi, M. (1998). Degradation of misfolded endoplasmic reticulum glycoproteins in *Saccharomyces cerevisiae* is determined by a specific oligosaccharide structure. J Cell Biol *142*, 1223-1233.

Jaspersen, S.L., Charles, J.F., Tinker-Kulberg, R.L., and Morgan, D.O. (1998). A late mitotic regulatory network controlling cyclin destruction in *Saccharomyces cerevisiae*. Mol Biol Cell *9*, 2803-2817.

Jin, T., Gu, Y., Zanusso, G., Sy, M., Kumar, A., Cohen, M., Gambetti, P., and Singh, N. (2000). The chaperone protein BiP binds to a mutant prion protein and mediates its

degradation by the proteasome. J Biol Chem *275*, 38699-38704.

Kapteyn, J.C., Van Den Ende, H., and Klis, F.M. (1999). The contribution of cell wall proteins to the organization of the yeast cell wall. Biochim Biophys Acta *1426*, 373-383.

Kawasaki, T. (2003). [Glycobiology basics: glycoproteins]. Tanpakushitsu Kakusan Koso *48*, 910-915.

Ketela, T., Green, R., and Bussey, H. (1999). *Saccharomyces cerevisiae* mid2p is a potential cell wall stress sensor and upstream activator of the PKC1-MPK1 cell integrity pathway. J Bacteriol *181*, 3330-3340.

Kinoshita, T., and Inoue, N. (2000). Dissecting and manipulating the pathway for glycosylphos-phatidylinositol-anchor biosynthesis. Curr Opin Chem Biol *4*, 632-638.

Kitada, K., Johnson, A.L., Johnston, L.H., and Sugino, A. (1993). A multicopy suppressor gene of the *Saccharomyces cerevisiae* G1 cell cycle mutant gene dbf4 encodes a protein kinase and is identified as CDC5. Mol Cell Biol *13*, 4445-4457.

Knop, M., Hauser, N., and Wolf, D.H. (1996). N-Glycosylation affects endoplasmic reticulum degradation of a mutated derivative of carboxypeptidase yscY in yeast. Yeast *12*, 1229-1238.

Kominami, K., DeMartino, G.N., Moomaw, C.R., Slaughter, C.A., Shimbara, N., Fujimuro, M., Yokosawa, H., Hisamatsu, H., Tanahashi, N., Shimizu, Y., Tanaka, K., and Toh-e, A. (1995). Nin1p, a regulatory subunit of the 26S proteasome, is necessary for activation of Cdc28p kinase of *Saccharomyces cerevisiae*. EMBO J *14*, 3105-3115.

Kominami, K., Okura, N., Kawamura, M., DeMartino, G.N., Slaughter, C.A., Shimbara, N., Chung, C.H., Fujimuro, M., Yokosawa, H., Shimizu, Y., Tanahashi, N., Tanaka, K., and Toh-e, A. (1997). Yeast counterparts of subunits S5a and p58 (S3) of the human 26S proteasome are encoded by two multicopy suppressors of nin1-1. Mol Biol Cell *8*, 171-187.

Kopito, R.R. (1997). ER quality control: the cytoplasmic connection. Cell *88*, 427-430.
Kostova, Z., and Wolf, D.H. (2003). For whom the bell tolls: protein quality control of the endoplasmic reticulum and the ubiquitin-proteasome connection. EMBO J *22*, 2309-2317.

Kovacech, B., Nasmyth, K., and Schuster, T. (1996). EGT2 gene transcription is induced predominantly by Swi5 in early G1. Mol Cell Biol *16*, 3264-3274.

Laemmli, U.K. (1970). Cleavage of structural proteins during the assembly of the head of bacteriophage T4. Nature *227*, 680-685.

Lagorce, A., Le Berre-Anton, V., Aguilar-Uscanga, B., Martin-Yken, H., Dagkessamanskaia, A., and Francois, J. (2002). Involvement of GFA1, which encodes glutamine-fructose-6-phosphate amidotransferase, in the activation of the chitin synthesis pathway in response to cell-wall defects in *Saccharomyces cerevisiae*. Eur J Biochem *269*, 1697-1707.

Leidich, S.D., Drapp, D.A., and Orlean, P. (1994). A conditionally lethal yeast mutant blocked at the first step in glycosyl phosphatidylinositol anchor synthesis. J Biol Chem *269*, 10193-10196.

Leidich, S.D., and Orlean, P. (1996). Gpi1, a *Saccharomyces cerevisiae* protein that participates in the first step in glycosylphosphatidylinositol anchor synthesis. J Biol Chem *271*, 27829-27837.

Lisanti, M.P., Caras, I.W., Davitz, M.A., and Rodriguez-Boulan, E. (1989). A glycophospholipid membrane anchor acts as an apical targeting signal in polarized epithelial cells. J Cell Biol *109*, 2145-2156.

Longtine, M.S., McKenzie, A., 3rd, Demarini, D.J., Shah, N.G., Wach, A., Brachat, A., Philippsen, P., and Pringle, J.R. (1998). Additional modules for versatile and economical PCR-based gene deletion and modification in *Saccharomyces cerevisiae*.

Yeast *14*, 953-961.

Madden, K., and Snyder, M. (1998). Cell polarity and morphogenesis in budding yeast. Annu Rev Microbiol *52*, 687-744.

Martin, S.W., and Konopka, J.B. (2004). Lipid raft polarization contributes to hyphal growth in *Candida albicans*. Eukaryot Cell *3*, 675-684.

Mayor, S., and Riezman, H. (2004). Sorting GPI-anchored proteins. Nat Rev Mol Cell Biol *5*, 110-120.

Meusser, B., Hirsch, C., Jarosch, E., and Sommer, T. (2005). ERAD: the long road to destruction. Nat Cell Biol *7*, 766-772.

Monnat, J., Neuhaus, E.M., Pop, M.S., Ferrari, D.M., Kramer, B., and Soldati, T. (2000). Identification of a novel saturable endoplasmic reticulum localization mechanism mediated by the C-terminus of a *Dictyostelium* protein disulfide isomerase. Mol Biol Cell *11*, 3469-3484.

Mornet, E. (2000). Hypophosphatasia: the mutations in the tissue-nonspecific alkaline phosphatase gene. Hum Mutat *15*, 309-315.

Morsomme, P., Prescianotto-Baschong, C., and Riezman, H. (2003). The ER v-SNAREs are required for GPI-anchored protein sorting from other secretory proteins upon exit from the ER. J Cell Biol *162*, 403-412.

Mrsa, V., Klebl, F., and Tanner, W. (1993). Purification and characterization of the *Saccharomyces cerevisiae* BGL2 gene product, a cell wall endo-beta-1,3-glucanase. J Bacteriol *175*, 2102-2106.

Muniz, M., Morsomme, P., and Riezman, H. (2001). Protein sorting upon exit from the endoplasmic reticulum. Cell *104*, 313-320.

Muniz, M., Nuoffer, C., Hauri, H.P., and Riezman, H. (2000). The Emp24 complex recruits a specific cargo molecule into endoplasmic reticulum-derived vesicles. J Cell Biol *148*, 925-930.

Muniz, M., and Riezman, H. (2000). Intracellular transport of GPI-anchored proteins. EMBO J *19*, 10-15.

Nagamune, K., Acosta-Serrano, A., Uemura, H., Brun, R., Kunz-Renggli, C., Maeda, Y., Ferguson, M.A., and Kinoshita, T. (2004). Surface sialic acids taken from the host allow trypanosome survival in tsetse fly vectors. J Exp Med *199*, 1445-1450.

Nagamune, K., and Kinoshita, T. (2002). [GPI biosynthetic pathway as a target for antiprotozoan drugs]. Tanpakushitsu Kakusan Koso *47*, 30-36.

Nagamune, K., Nozaki, T., Maeda, Y., Ohishi, K., Fukuma, T., Hara, T., Schwarz, R.T., Sutterlin, C., Brun, R., Riezman, H., and Kinoshita, T. (2000). Critical roles of glycosylphosphatidylinositol for *Trypanosoma brucei*. Proc Natl Acad Sci U S A *97*, 10336-10341.

Nakatsukasa, K., Okada, S., Umebayashi, K., Fukuda, R., Nishikawa, S., and Endo, T. (2004). Roles of O-mannosylation of aberrant proteins in reduction of the load for endoplasmic reticulum chaperones in yeast. J Biol Chem *279*, 49762-49772.

Nelson, B., Kurischko, C., Horecka, J., Mody, M., Nair, P., Pratt, L., Zougman, A., McBroom, L.D., Hughes, T.R., Boone, C., and Luca, F.C. (2003). RAM: a conserved signaling network that regulates Ace2p transcriptional activity and polarized morphogenesis. Mol Biol Cell *14*, 3782-3803.

Ng, D.T., Spear, E.D., and Walter, P. (2000). The unfolded protein response regulates multiple aspects of secretory and membrane protein biogenesis and endoplasmic reticulum quality control. J Cell Biol *150*, 77-88.

Nishikawa, S., Brodsky, J.L., and Nakatsukasa, K. (2005). Roles of molecular

chaperones in endoplasmic reticulum (ER) quality control and ER-associated degradation (ERAD). J Biochem (Tokyo) *137*, 551-555.

Nuoffer, C., Horvath, A., and Riezman, H. (1993). Analysis of the sequence requirements for glycosylphosphatidylinositol anchoring of *Saccharomyces cerevisiae* Gas1 protein. J Biol Chem *268*, 10558-10563.

Nuoffer, C., Jeno, P., Conzelmann, A., and Riezman, H. (1991). Determinants for glycophospholipid anchoring of the *Saccharomyces cerevisiae* GAS1 protein to the plasma membrane. Mol Cell Biol *11*, 27-37.

Oda, K., Wada, I., Takami, N., Fujiwara, T., Misumi, Y., and Ikehara, Y. (1996). Bip/GRP78 but not calnexin associates with a precursor of glycosylphosphatidylinositol-anchored protein. Biochem J *316 (Pt 2)*, 623-630.

Oda, Y., Hosokawa, N., Wada, I., and Nagata, K. (2003). EDEM as an acceptor of terminally misfolded glycoproteins released from calnexin. Science *299*, 1394-1397.

Orlean, P. (1997). Biogenesis of yeast wall and surface components: The Molecular and Cellular Biology of the Yeast Saccharomyces. Cell Cycle and Biology. Cold Spring Harbor Laboratory Press, 229–362.

Plemper, R.K., Egner, R., Kuchler, K., and Wolf, D.H. (1998). Endoplasmic reticulum degradation of a mutated ATP-binding cassette transporter Pdr5 proceeds in a concerted action of Sec61 and the proteasome. J Biol Chem *273*, 32848-32856.

Popolo, L., and Vai, M. (1999). The Gas1 glycoprotein, a putative wall polymer cross-linker. Biochim Biophys Acta *1426*, 385-400.

Prusiner, S.B. (1998). Prions. Proc Natl Acad Sci U S A *95*, 13363-13383.

Racki, W.J., Becam, A.M., Nasr, F., and Herbert, C.J. (2000). Cbk1p, a protein similar to the human myotonic dystrophy kinase, is essential for normal morphogenesis in

Saccharomyces cerevisiae. EMBO J *19*, 4524-4532.

Reggiori, F., Canivenc-Gansel, E., and Conzelmann, A. (1997). Lipid remodeling leads to the introduction and exchange of defined ceramides on GPI proteins in the ER and Golgi of *Saccharomyces cerevisiae*. EMBO J *16*, 3506-3518.

Richard, M., De Groot, P., Courtin, O., Poulain, D., Klis, F., and Gaillardin, C. (2002a). GPI7 affects cell-wall protein anchorage in *Saccharomyces cerevisiae* and *Candida albicans*. Microbiology *148*, 2125-2133.

Richard, M., Ibata-Ombetta, S., Dromer, F., Bordon-Pallier, F., Jouault, T., and Gaillardin, C. (2002b). Complete glycosylphosphatidylinositol anchors are required in Candida albicans for full morphogenesis, virulence and resistance to macrophages. Mol Microbiol *44*, 841-853.

Richard, M., Quijano, R.R., Bezzate, S., Bordon-Pallier, F., and Gaillardin, C. (2001). Tagging morphogenetic genes by insertional mutagenesis in the yeast *Yarrowia lipolytica*. J Bacteriol *183*, 3098-3107.

Riezman, H., Horvath, A., Manning-Krieg, U., and Movva, R. (1994). Intracellular transport of GPI-anchored proteins by yeast. Braz J Med Biol Res *27*, 323-326.

Ross-Macdonald, P., Sheehan, A., Friddle, C., Roeder, G.S., and Snyder, M. (1999). Transposon mutagenesis for the analysis of protein production, function, and localization. Methods Enzymol *303*, 512-532.

Schmidt, A., Bickle, M., Beck, T., and Hall, M.N. (1997). The yeast phosphatidylinositol kinase homolog TOR2 activates RHO1 and RHO2 via the exchange factor ROM2. Cell *88*, 531-542.

Schmidt, M., Bowers, B., Varma, A., Roh, D.H., and Cabib, E. (2002). In budding yeast, contraction of the actomyosin ring and formation of the primary septum at cytokinesis depend on each other. J Cell Sci *115*, 293-302.

Schmitz, A., and Herzog, V. (2004). Endoplasmic reticulum-associated degradation: exceptions to the rule. Eur J Cell Biol *83*, 501-509.

Sherman, F. (1991). Getting started with yeast. Methods Enzymol *194*, 3-21.

Shishioh, N., Hong, Y., Ohishi, K., Ashida, H., Maeda, Y., and Kinoshita, T. (2005). GPI7 is the second partner of PIG-F and involved in modification of glycosylphosphatidylinositol. J Biol Chem *280*, 9728-9734.

Sikorski, R.S., and Hieter, P. (1989). A system of shuttle vectors and yeast host strains designed for efficient manipulation of DNA in *Saccharomyces cerevisiae*. Genetics *122*, 19-27.

Simons, K., and Ikonen, E. (1997). Functional rafts in cell membranes. Nature *387*, 569-572.

Sipos, G., Puoti, A., and Conzelmann, A. (1994). Glycosylphosphatidylinositol membrane anchors in *Saccharomyces cerevisiae*: absence of ceramides from complete precursor glycolipids. EMBO J *13*, 2789-2796.

Song, S., and Lee, K.S. (2001). A novel function of *Saccharomyces cerevisiae* CDC5 in cytokinesis. J Cell Biol *152*, 451-469.

Spear, E.D., and Ng, D.T. (2003). Stress tolerance of misfolded carboxypeptidase Y requires maintenance of protein trafficking and degradative pathways. Mol Biol Cell *14*, 2756-2767.

Sutton, A., Immanuel, D., and Arndt, K.T. (1991). The SIT4 protein phosphatase functions in late G1 for progression into S phase. Mol Cell Biol *11*, 2133-2148.

Suzuki, T., Park, H., Hollingsworth, N.M., Sternglanz, R., and Lennarz, W.J. (2000). PNG1, a yeast gene encoding a highly conserved peptide:N-glycanase. J Cell Biol *149*,

1039-1052.

Swanson, R., Locher, M., and Hochstrasser, M. (2001). A conserved ubiquitin ligase of the nuclear envelope/endoplasmic reticulum that functions in both ER-associated and Matalpha2 repressor degradation. Genes Dev *15*, 2660-2674.

Takeda, J., Miyata, T., Kawagoe, K., Iida, Y., Endo, Y., Fujita, T., Takahashi, M., Kitani, T., and Kinoshita, T. (1993). Deficiency of the GPI anchor caused by a somatic mutation of the PIG-A gene in paroxysmal nocturnal hemoglobinuria. Cell *73*, 703-711.

Takita, Y., Ohya, Y., and Anraku, Y. (1995). The CLS2 gene encodes a protein with multiple membrane-spanning domains that is important Ca2+ tolerance in yeast. Mol Gen Genet *246*, 269-281.

Tamaskovic, R., Bichsel, S.J., and Hemmings, B.A. (2003). NDR family of AGC kinases--essential regulators of the cell cycle and morphogenesis. FEBS Lett *546*, 73-80.

Tanaka, S., Maeda, Y., Tashima, Y., and Kinoshita, T. (2004). Inositol deacylation of glycosylphosphatidylinositol-anchored proteins is mediated by mammalian PGAP1 and yeast Bst1p. J Biol Chem *279*, 14256-14263.

Taniguchi, N. (2003). [Importance of sugar chain functions and their characterization]. Tanpakushitsu Kakusan Koso *48*, 901-909.

Taron, C.H., Wiedman, J.M., Grimme, S.J., and Orlean, P. (2000). Glycosylphosphatidylinositol biosynthesis defects in Gpi11p- and Gpi13p-deficient yeast suggest a branched pathway and implicate gpi13p in phosphoethanolamine transfer to the third mannose. Mol Biol Cell *11*, 1611-1630.

Taxis, C., Hitt, R., Park, S.H., Deak, P.M., Kostova, Z., and Wolf, D.H. (2003). Use of modular substrates demonstrates mechanistic diversity and reveals differences in chaperone requirement of ERAD. J Biol Chem *278*, 35903-35913.

Toh-e, A., and Oguchi, T. (1998). Isolation and characterization of the yeast las21 mutants, which are sensitive to a local anestheticum, tetracaine. Genes Genet Syst *73*, 365-375.

Toh-e, A., and Oguchi, T. (1999). Las21 participates in extracellular/cell surface phenomena in *Saccharomyces cerevisiae*. Genes Genet Syst *74*, 241-256.

Toh-e, A., and Oguchi, T. (2002). Genetic characterization of genes encoding enzymes catalyzing addition of phospho-ethanolamine to the glycosylphosphatidylinositol anchor in *Saccharomyces cerevisiae*. Genes Genet Syst *77*, 309-322.

Tong, A.H., Lesage, G., Bader, G.D., Ding, H., Xu, H., Xin, X., Young, J., Berriz, G.F., Brost, R.L., Chang, M., Chen, Y., Cheng, X., Chua, G., Friesen, H., Goldberg, D.S., Haynes, J., Humphries, C., He, G., Hussein, S., Ke, L., Krogan, N., Li, Z., Levinson, J.N., Lu, H., Menard, P., Munyana, C., Parsons, A.B., Ryan, O., Tonikian, R., Roberts, T., Sdicu, A.M., Shapiro, J., Sheikh, B., Suter, B., Wong, S.L., Zhang, L.V., Zhu, H., Burd, C.G., Munro, S., Sander, C., Rine, J., Greenblatt, J., Peter, M., Bretscher, A., Bell, G., Roth, F.P., Brown, G.W., Andrews, B., Bussey, H., and Boone, C. (2004). Global mapping of the yeast genetic interaction network. Science *303*, 808-813.

Umebayashi, K., and Nakano, A. (2003). Ergosterol is required for targeting of tryptophan permease to the yeast plasma membrane. J Cell Biol *161*, 1117-1131.

Umemura, M., Okamoto, M., Nakayama, K., Sagane, K., Tsukahara, K., Hata, K., and Jigami, Y. (2003). GWT1 gene is required for inositol acylation of glycosylphosphatidylinositol anchors in yeast. J Biol Chem *278*, 23639-23647.

Vallee, B., and Riezman, H. (2005). Lip1p: a novel subunit of acyl-CoA ceramide synthase. EMBO J *24*, 730-741.

Vashist, S., Kim, W., Belden, W.J., Spear, E.D., Barlowe, C., and Ng, D.T. (2001). Distinct retrieval and retention mechanisms are required for the quality control of

endoplasmic reticulum protein folding. J Cell Biol *155*, 355-368.

Vashist, S., and Ng, D.T. (2004). Misfolded proteins are sorted by a sequential checkpoint mechanism of ER quality control. J Cell Biol *165*, 41-52.

Wainwright, L.J., and Field, M.C. (1997). Quality control of glycosylphosphatidylinositol anchor attachment in mammalian cells: a biochemical study. Biochem J *321 (Pt 3)*, 655-664.

Watanabe, R., Funato, K., Venkataraman, K., Futerman, A.H., and Riezman, H. (2002). Sphingolipids are required for the stable membrane association of glycosylphosphatidylinositol-anchored proteins in yeast. J Biol Chem *277*, 49538-49544.

Watanabe, R., and Riezman, H. (2004). Differential ER exit in yeast and mammalian cells. Curr Opin Cell Biol *16*, 350-355.

Watzele, G., and Tanner, W. (1989). Cloning of the glutamine:fructose-6-phosphate amidotransferase gene from yeast. Pheromonal regulation of its transcription. J Biol Chem *264*, 8753-8758.

Weiss, E.L., Kurischko, C., Zhang, C., Shokat, K., Drubin, D.G., and Luca, F.C. (2002). The *Saccharomyces cerevisiae* Mob2p-Cbk1p kinase complex promotes polarized growth and acts with the mitotic exit network to facilitate daughter cell-specific localization of Ace2p transcription factor. J Cell Biol *158*, 885-900.

Wilbourn, B., Nesbeth, D.N., Wainwright, L.J., and Field, M.C. (1998). Proteasome and thiol involvement in quality control of glycosylphosphatidylinositol anchor addition. Biochem J *332 (Pt 1)*, 111-118.

Yashiroda, H., Oguchi, T., Yasuda, Y., Toh-e, A., and Kikuchi, Y. (1996). Bul1, a new protein that binds to the Rsp5 ubiquitin ligase in *Saccharomyces cerevisiae*. Mol Cell Biol *16*, 3255-3263.

FIGURES AND TABLES

Figure 1	Molecular architecture of yeast cell surface
Figure 2	Presumed structure of the yeast glycosylphosphatidylinositol (GPI)-anchored protein
Figure 3	GPI biosynthetic pathway in yeast
Figure 4	Enzymatic activity of Gpi7p
Figure 5	Plasmid construction of the HA tagged *GPI7*
Figure 6	Characterization of *GPI7-HA*
Figure 7	*GPI7* protein sequence alignment and sites of the point mutations
Figure 8	*gpi7-2* mutant is temperature-sensitive and accumulates M4 intermediate
Figure 9	The *gpi7-2* mutant cells show a cell separation defect and accumulated three-cell arrangement
Figure 10	Principle of multicopy suppressors
Figure 11	Multicopy suppressors of *gpi7-2* missense mutant
Figure 12	Cell morphology, nuclear staining and flow cytometric analysis of *gpi7-2* strain and strains with multicopy suppressors
Figure 13	Flow cytometric analysis of *gpi7-2* and *gpi7-2* carrying YEp-CDC5
Figure 14	Principle of extragenic suppressors of *gpi7* mutant
Figure 15	Carboxyl terminal truncation of *CBK1* bypasses the growth defect of *gpi7*Δ
Figure 16	Structure and function of Cbk1p
Figure 17	Disruption of Cbk1p-Ace2p pathway overcomes the growth defect of *gpi7*Δ cells

Figure 18 Disruption of *EGT2* ameliorated the growth defect of *gpi7*Δ cells

Figure 19 Disruption of Cbk1-Ace2p pathway cancels the temperature-sensitve phenotype, but not cell separation defect of *gpi7*Δ mutant

Figure 20 Egt2p is displaced from the septal region to the cell cortex in *gpi7*Δ mutant cells

Figure 21 Chimeric protein, Eng1-Egt2p, is partially displaced to the cell cortex in *gpi7*Δ mutant cells

Figure 22 Illustration of Wsc1p-Pkc1p pathways

Figure 23 Summary of the regulation of cell separation by *GPI7*

Figure 24 Mechanisms for abnormal cellular morphologies

Figure 25 Protein folding and quality control in the ER

Figure 26 Involvement of *N*-glycosylation in the ER quality control

Figure 27 Inositol acylation and deacylation of the GPI moiety during the biosynthesis of GPI in yeast

Figure 28 Construction of misfolded Gas1p

Figure 29 Characterization of Gas1*p

Figure 30 Construction of HA- or mRFP-tagged Gas1p and Gas1*p

Figure 31 Gas1*p is modified by GPI anchor

Figure 32 Gas1*p is unstable and rapidly degraded

Figure 33 Gas1*p is not secreted into the medium and is not degraded in the vacuole

Figure 34 Gas1*p is a substrate for ER-associated degradation via the proteasome

Figure 35 Two distinct ERAD pathways function according too the location of the misfolded domain

Figure 36 Effects of E3 ubiquitin ligases in the degradation of Gas1*p

Figure 37 Effects of ER-to-Golgi transport in the degradation of Gas1*p

Figure 38 Enzymatic activity and topology of Bst1p

Figure 39 Deletion of *BST1* stabilizes the degradation of misfolded Gas1p

Figure 40 Gas1*p receives a GPI anchor before its degradation

Figure 41 Construction and characterization of soluble forms of Gas1p (SHG) and Gas1*p (SHg*)

Figure 42 Degradation of a soluble form of Gas1*p is independent of Bst1p function

Figure 43 Construction of lipase-dead mutant Bst1p

Figrue 44 GPI-inositol deacylase activity is important for the efficient degradation of misfolded Gas1p

Figure 45 Localization of mRFP-Gas1p and mRFP-Gas1*p in *bst1*Δ cells

Figure 46 Effects of mutations in GPI biosynthesis on the degradation of Gas1*p and CPY*

Figure 47 Effects of mutations in cargo receptors for GPI-anchored proteins on the degradation of Gas1*p and CPY*

Figure 48 Effects of mutations in *N*-glycan processing on the degradation of Gas1*p and CPY*

Figure 49 BiP/Kar2p and Bst1p associate with Gas1*p *in vivo*

Figure 50 Model for the quality control of GPI-anchored proteins by Bst1p

Table I GPI biosynthetic genes

Table II Yeast strains used in this study

Table III Plasmid used in this study

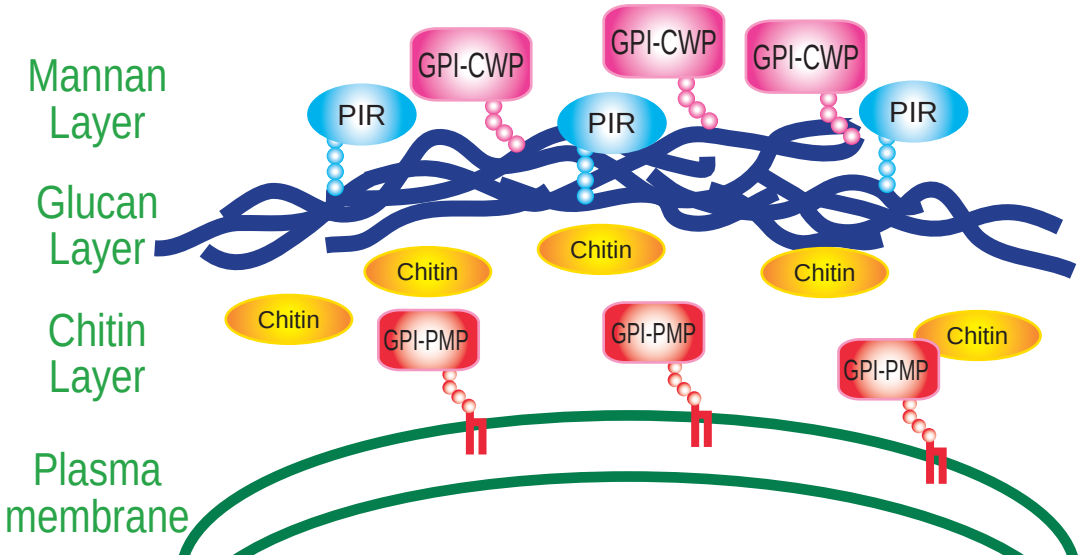

Figure 1. Molecular architecture of yeast cell surface

The internal skeletal layer consists of β-1,3-glucan macromolecule that forms a three-dimensional network surrounding the entire cell. Highly mannosylated cell wall proteins, such as GPI-anchored protein and Pir family proteins, are covalently bound directory to β-1,3-glucan or indirectly through interconnecting β-1,6-glucan, and form mannan-layer at the most external area of the cell wall. Most of GPI-anchored proteins are processed at the plasma membrane and linked to β-1,6-glucan of the cell wall, some of them retain on the plasma membrane.

Abbreviations- PMP, plasma membrane protein; CWP, cell wall protein; GPI, glycosylphosphatidylinositol; Pir, protein with internal repeats

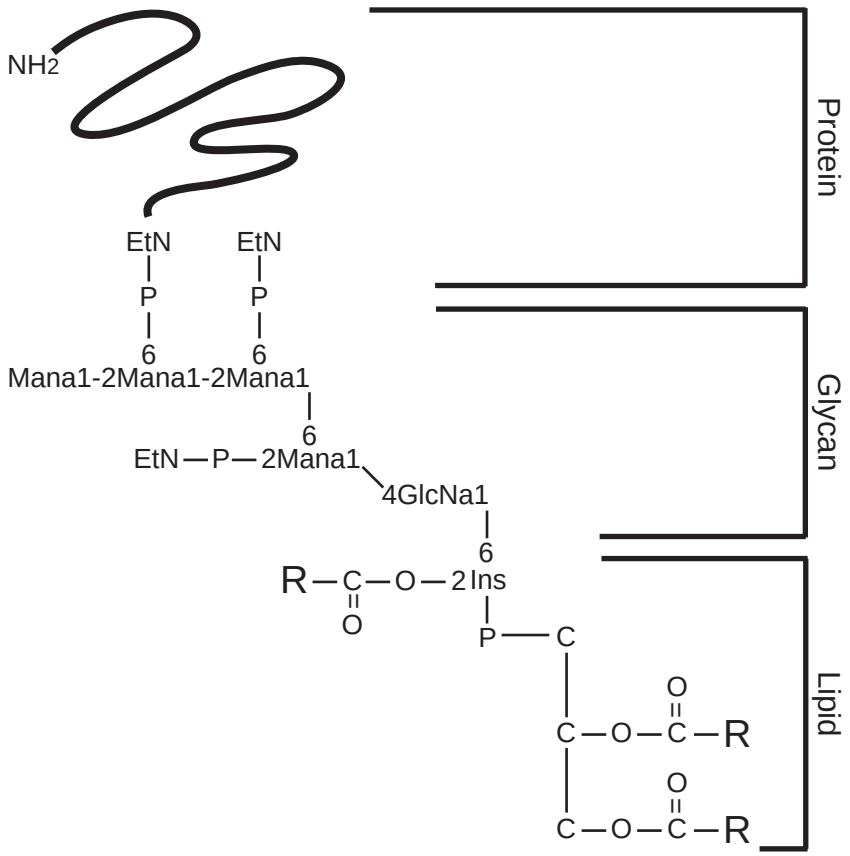

Figure 2. Presumed structure of the yeast glycosylphosphatidylinositol (GPI) anchored protein

GPI anchored protein consists of lipid, glycan and protein parts. Man, GlcN, Ins, EtN indicate mannose, glucosamine, inositol and ethanolamine, respectively. a and numbers between Man and Man designate the linkage patterns. R, alkyl; P, phosphate.

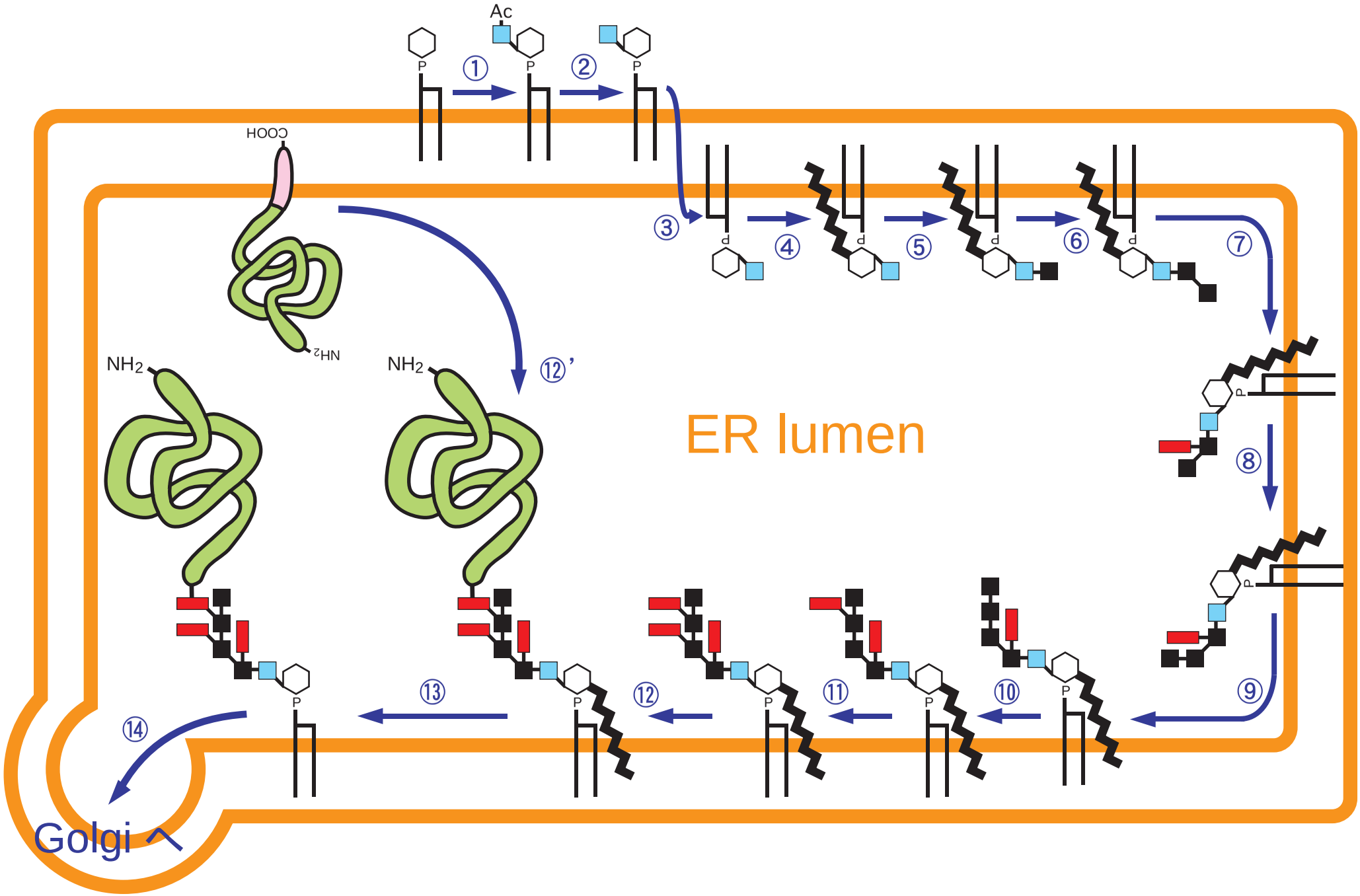
Ac
P
①
②
HOOC
NH2
③
④
⑤
⑥
⑦
⑧
⑨
⑩
⑪
⑫
⑫'
⑬
⑭
ER lumen
Golgi へ

Figure 3. GPI biosynthetic pathway in yeast

GPI biosynthesis is performed in the ER. The biosynthetic pathway consists of at least 12 reaction steps. More than 20 genes are involved in this pathway. The first step of GPI-anchor biosynthesis is mediated by GPI-N-acetylglucosaminyltransferase complex. The second step is mediated by N-acetylglucosaminylphosphatidylinositol de-*N*-acetylase. *myo*-inositol of glucosaminylphosphatidylinositol (GlcN-PI) translocates from cytoplasmic side to the lumenal side by an unidentified flippase at step 3. Step 4 is the acylation of the GlcN-PI at position 2. The first mannose is then transferred from mannosyl dolichol-phosphate (Dol-P-Man) to position 4 of GlcN at step 5. The second mannose is transferred from Dol-P-Man to position 6 of the first mannose in Man-GlcN-acyl-PI (step 6). The first mannose is modified by ethanolaminephosphate (EtN-P) at step 7. The third mannose is transferred from Dol-P-Man to position 2 of the second mannose by an α-1,2-mannosyltransferase (step 8). The fourth mannose is transferred from Dol-P-Man to position 2 of the third mannose in yeast (step 9). The EtN-P that links GPI to proteins is transferred from phosphatidylethanolamine to position 6 of the third mannose (step 10). The second mannose can be modified by side chain EtN-P at position 6 (step 11). Finally, pre-assembled GPI is transferred to proteins bearing a carboxyl-terminal GPI-attachment signal sequence by GPI transamidase complex (step 12). After GPI attachment to protein, GPI-anchored protein is deacylated (step13) and transported to the Golgi (step14).

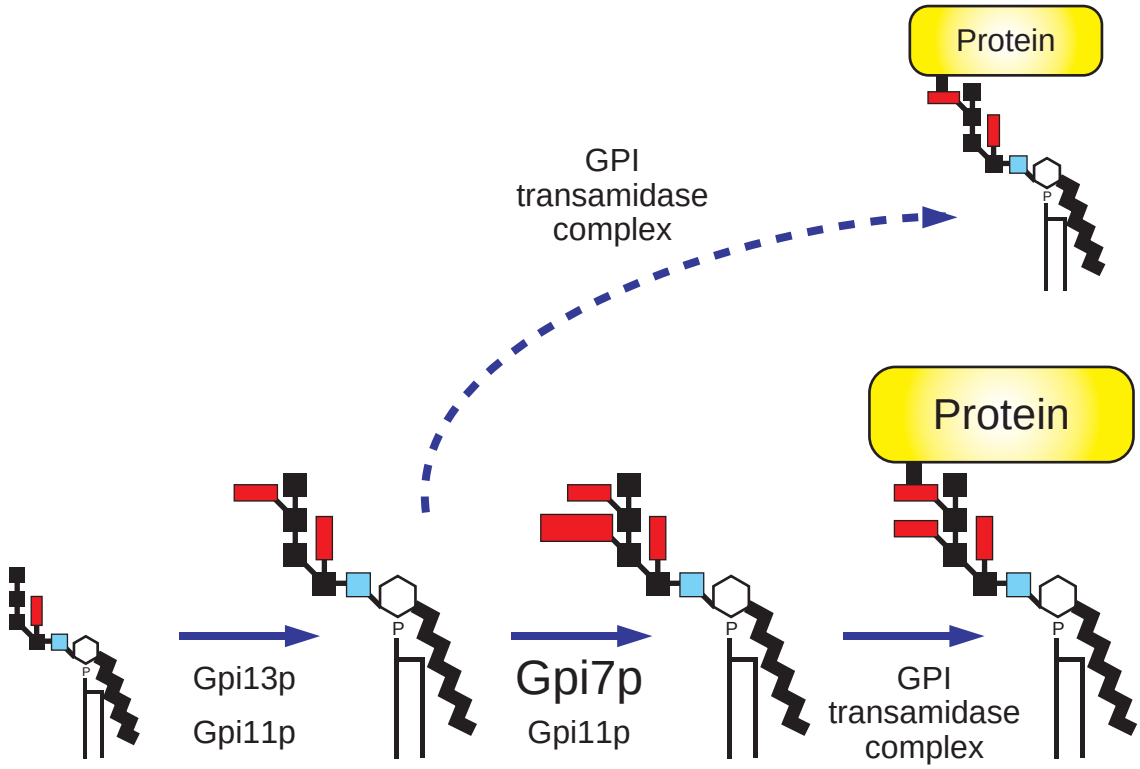

Figure 4. Enzymatic activity of Gpi7p

Gpi7p adds a side chain EtN-P onto the second mannose of the GPI core structure. This is the adjacent reaction before GPI transfer to proteins, whereas both substrate and product of Gpi7p reaction are potentially direct precursors of protein-bound anchors. Gpi11p is a regulator for both Gpi13p and Gpi7p.

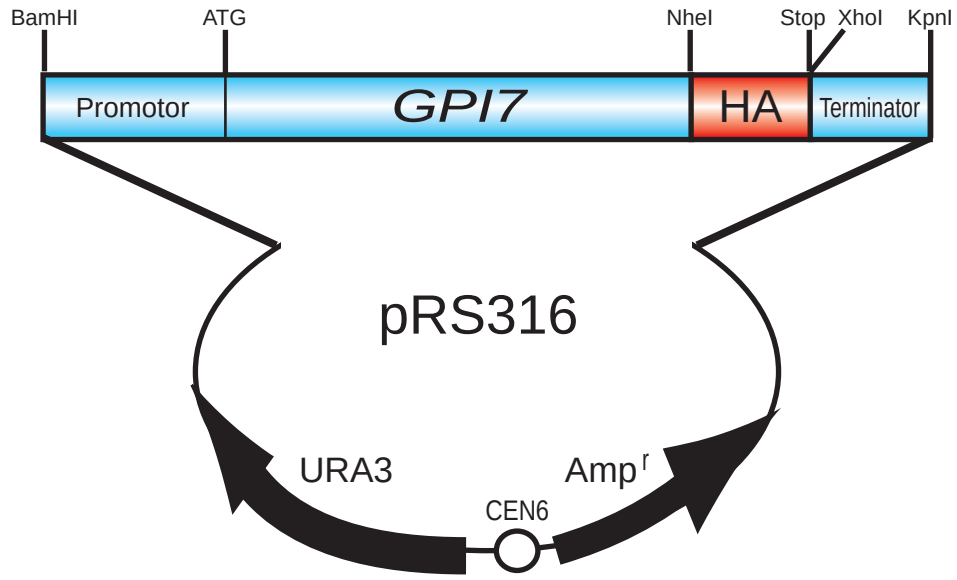

Figure 5. Plasmid construction of the HA tagged *GPI7*

Three tandem copies of the HA epitope were placed just before the stop codon of *GPI7* as described in Materials and methods.

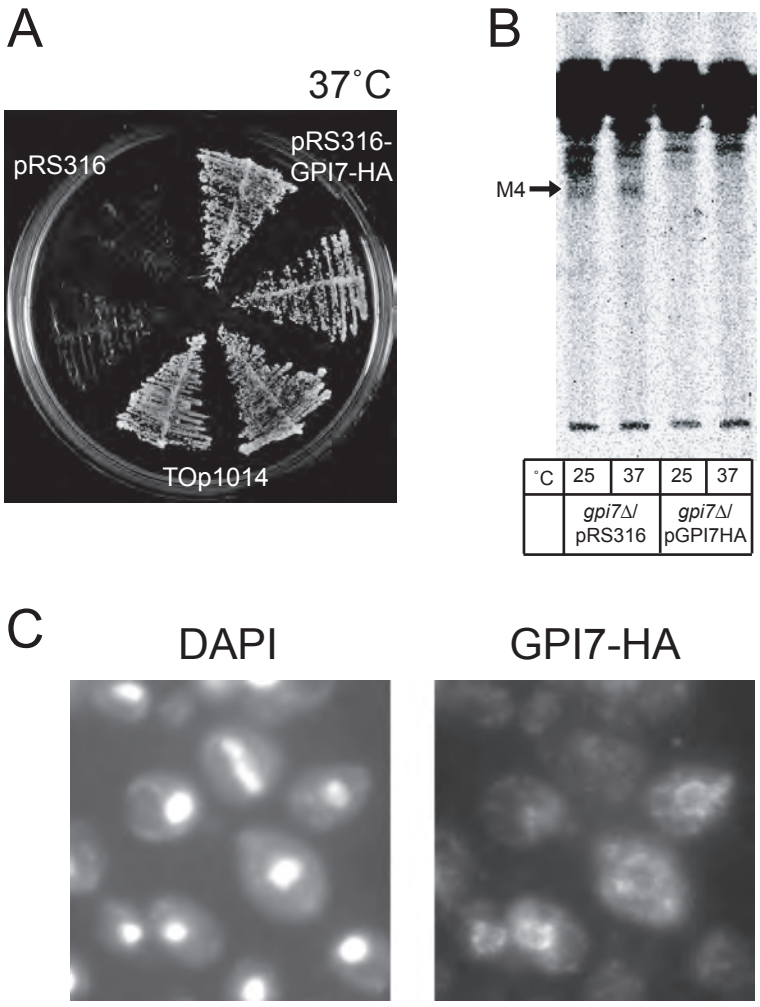

Figure 6. Characterization of *GPI7-HA*

A. MFY11 (*gpi7*Δ) cells carrying the indicated plasmids were grown on a SDCA plate for 3 days at 37˚C. B. Expotentially growing cells were radiolabeled at 25 or 37˚C with [^{3}H]Ins (2 mCi/OD_{600}), and desalted lipid extracts were analyzed by TLC (chloroform : methanol : water = 10 : 10 : 3). The same amount of radioactivity was spotted in each lane. M4 is the GPI intermediate containing Mana1,2-(EtN-P-6)Mana1,2-Mana1,6-(EtN-P-2)Mana1,4-GlcNa1,6Ins-PO_4-lipid. C. MFY11 cells carrying pRS316-GPI7-HA (low copy) were grown to mid-log phase, fixed, treated with zymolyase 100T (Seikagaku Kogyo), and stained with anti-HA antibodies (HA.11; Babco) to visualize Gpi7p by indirect immunofluorescence.

GPI7 homologues ClustalW

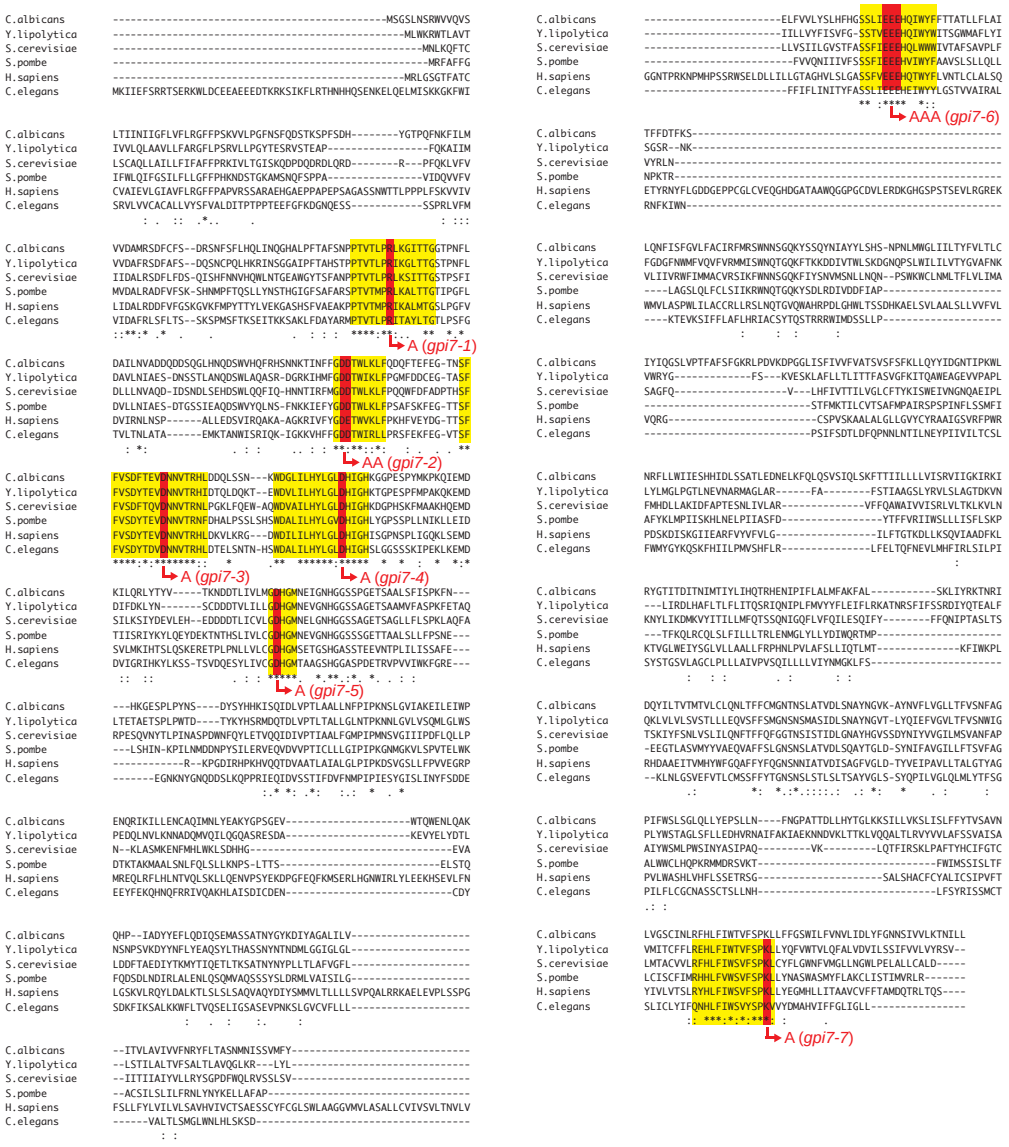

Figure 7. *GPI7* protein sequence alignment and sites of the point mutations

Alignment of *GPI7* proteins from *Saccharomyces cerevisiae* (Accession NP_012473), *Candida albicans* (AAL83897), *Yarrowia lipolytica* (AAK52677), *Schizosaccharomyces pombe* (CAA91096), *Caenorhabditis elegans* (NP_495820), and *Homo sapiens* (BAC11227), using the CLUSTALW Multiple Sequence Alignment Program. Seven highly conserved regions are in yellow boxes. Red lines are point mutation regions in which alanine is substituted for original amino acid(s).

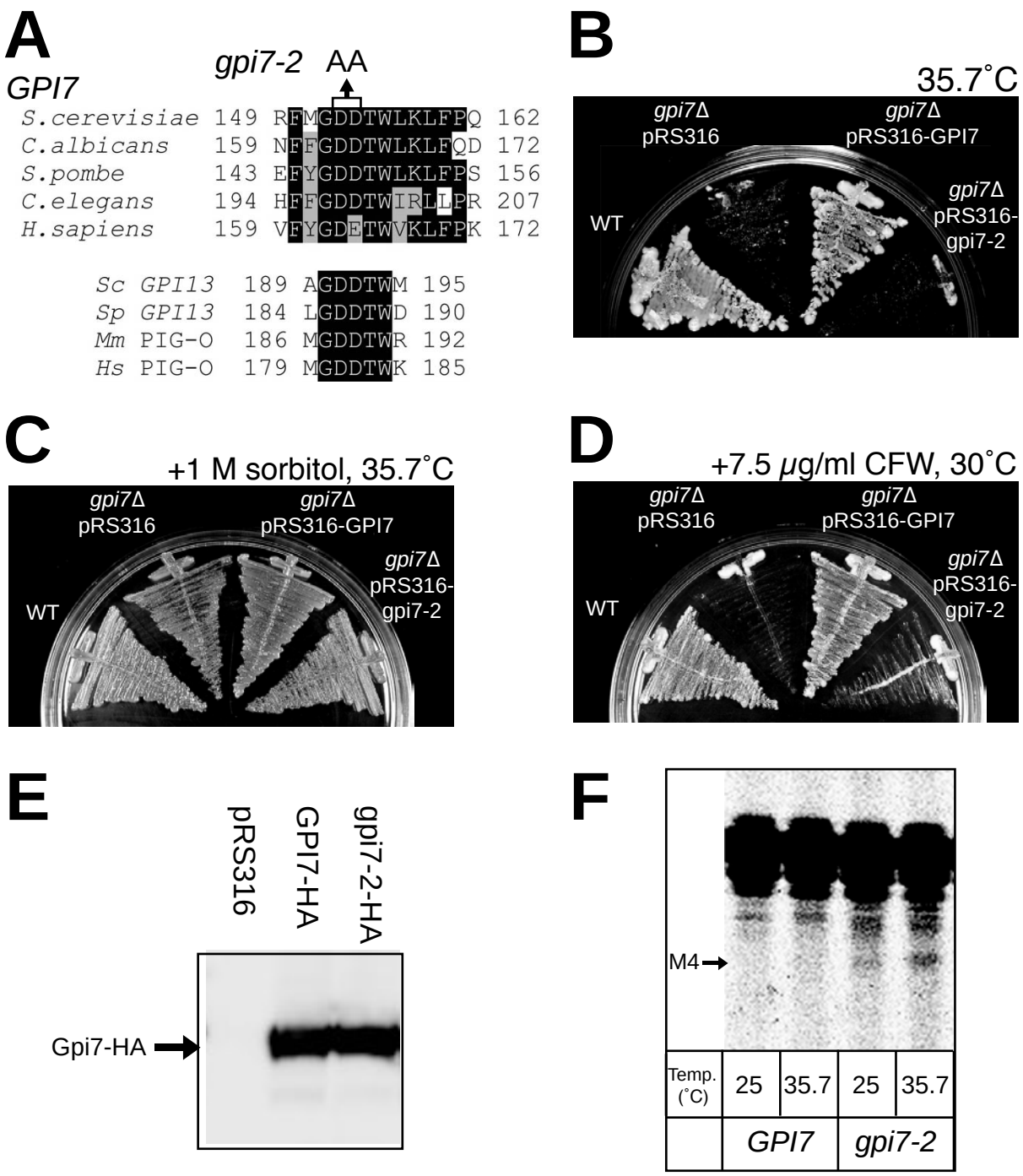

Figure 8. *gpi7-2* mutant is temperature-sensitive and accumulates M4 intermediate

(A) Alignment of a conserved region in the amino acid sequences of *GPI7* (upper) and *GPI13* (lower) orthologues. In *S. cerevisiae gpi7-2*, two alanines (A) are substituted for aspartic acids (D) at positions 153 and 154. (B)(C)(D) Wild-type (WT) and *gpi7*Δ cells carrying pRS316, pRS316-GPI7-HA or pRS316-gpi7-2-HA were grown on YPAD (B), YPAD containing 1 M sorbitol (C) and YPAD containing 7.5 μg/ml calcofluor white (D) at the indicated temperature for 3 days. (E) *gpi7*Δ cells carrying pRS316, pRS316-GPI7-HA or pRS316-gpi7-2-HA were grown in SDCA medium at 30˚C. Cells were broken and P13 fractions were isolated and subjected to immunoblotting with anti-HA mouse antibodies and anti-mouse HRP. (F) Exponentially growing cells were radiolabeled at 25˚C or 35.7˚C with [^{3}H] inositol (0.1 MBq/1 x 107 cells), and desalted lipid extracts were analyzed by TLC (solvent system; chloroform: methanol: water = 10: 10: 3). The same amount of radioactivity was spotted in each lane. M4 indicates a GPI intermediate accumulated in *gpi7-2*, consisting of Manα1,2-(EtN-P)Manα1,2-Manα1,6-(EtN-P)Manα1,4-GlcNα1,6Ins-PO$_4$-lipid.

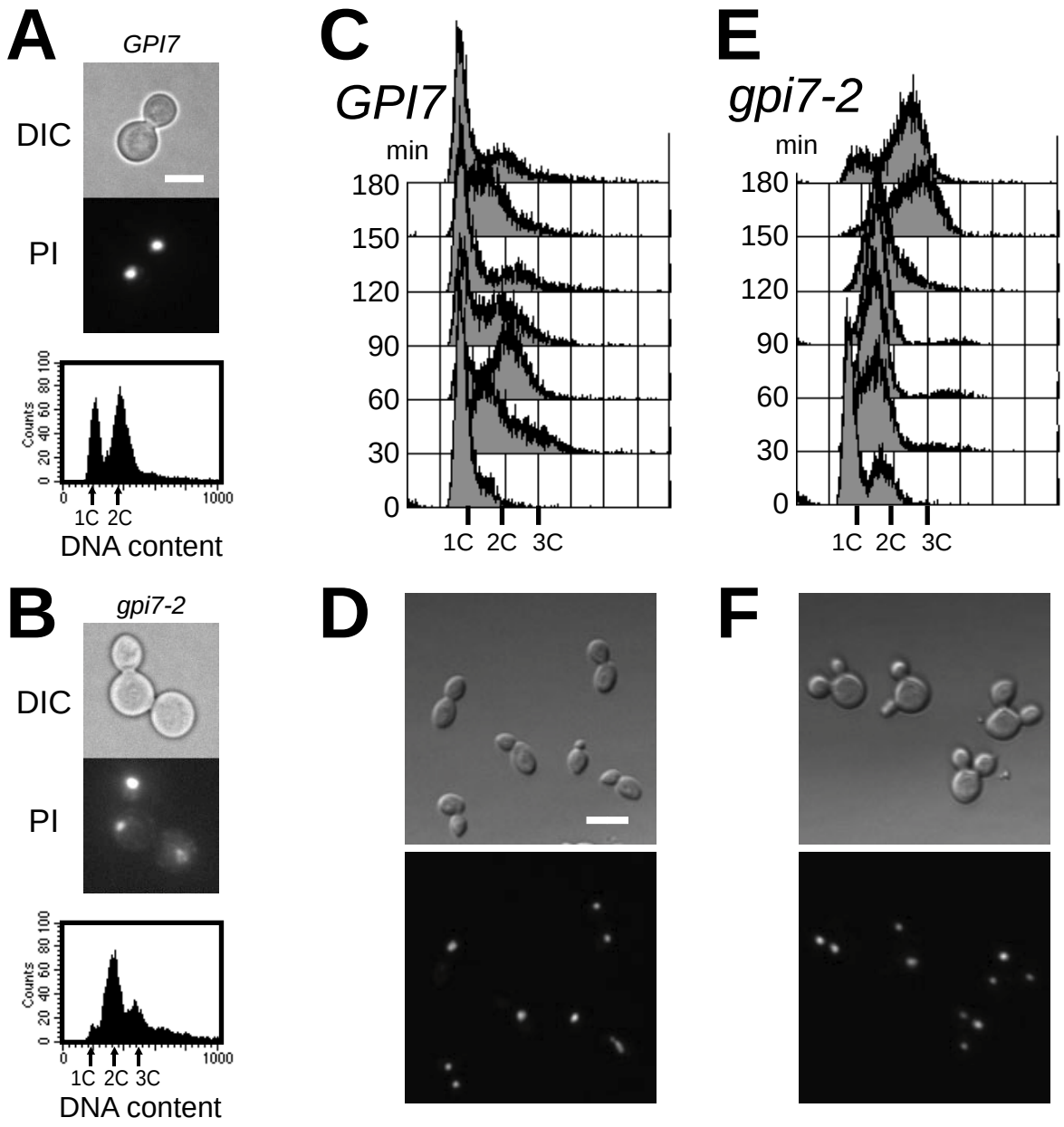

Figure 9. The *gpi7-2* mutant cells show a cell separation defect and accumulated three-cell arrangement

(A)(B) Cell morphology (DIC), propidium iodide (PI) fluorescence image and flow cytometric analysis of propidium iodide (PI)-stained wild-type (A) and *gpi7-2* mutant (B) cells after 4 h of incubation at 35.7˚C. 1C, 2C, and 3C indicate the peak of the relative DNA content in the flow cytometric analysis. Bar, 5 μm. (C)(D)(E)(F) DNA content during cell cycle progression in wild-type (C) and *gpi7-2* (E) cells. Growing wild-type or *gpi7-2* cells at an early log phase were synchronized with α-factor in G1, resuspended in YPAD, and incubated at 35.7˚C. Samples were taken at the indicated time points. Cell morphology (upper) and PI fluorescence image (lower) of wild-type (D) and *gpi7-2* cells (F) after 180 min of incubation at 35.7˚C are shown. Bar, 10 μm.

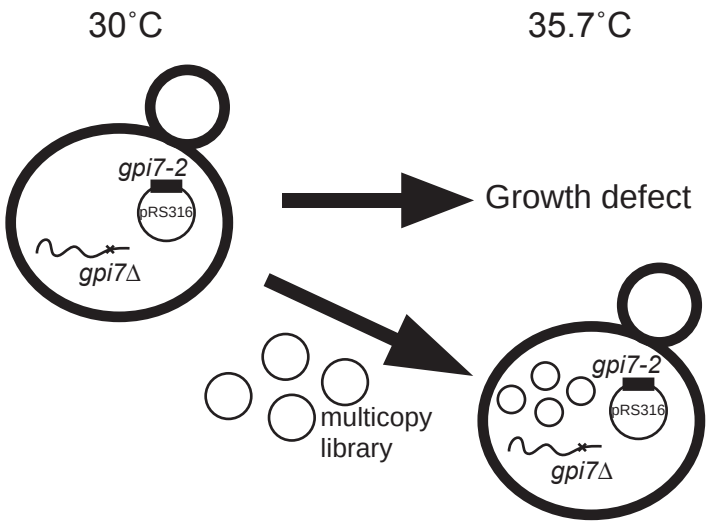

Figure 10. Principle of multicopy suppressors

Under normal condition, *gpi7-2* cells can grow at 30˚C but not grow at 35.7˚C. I introduced multicopy genomic library into *gpi7-2* cells and incubated at 35.7˚C to screen multicopy suppressor genes.

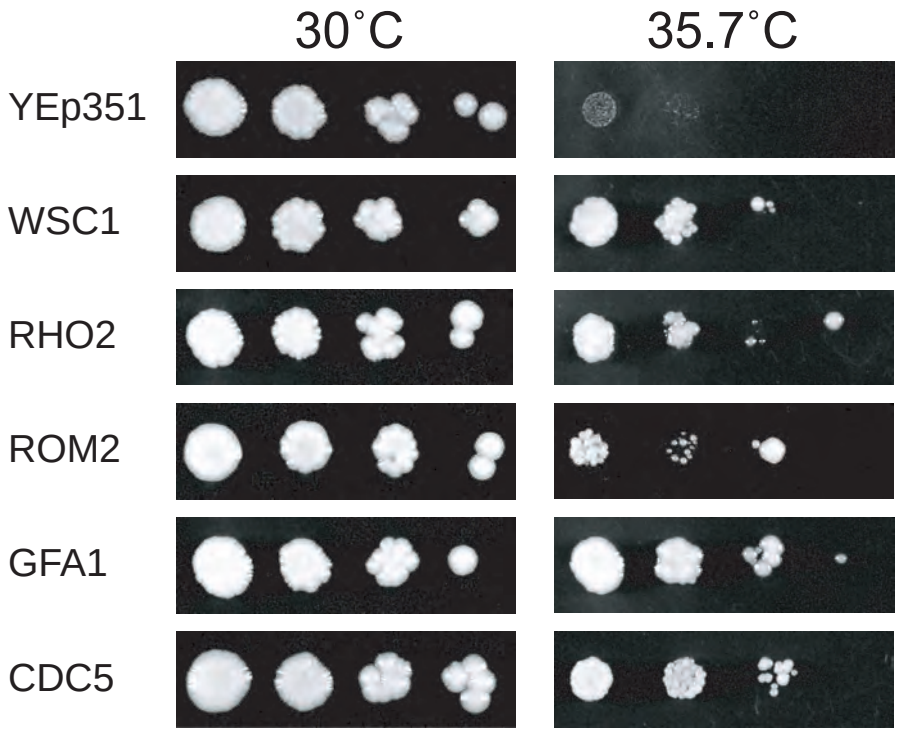

Figure 11. Multicopy suppressors of *gpi7-2* missense mutant

The plasmids that suppress the temperature sensitivity of *gpi7-2* were subcloned and sequenced. The suppressor genes in these plasmids were determined as *WSC1, RHO2, ROM2, GFA1* and *CDC5*, respectively. MFY36 (*gpi7-2*) cells carrying the indicated plasmids were grown in SD (–Trp, –Ura and –Leu) medium. Cell were washed and adjusted at the density of 10^7 cells/ml. Five microliter aliguots of 10 fold serial dilutions were spotted on YPAD plates and incubated at 30˚C or 35.7˚C.

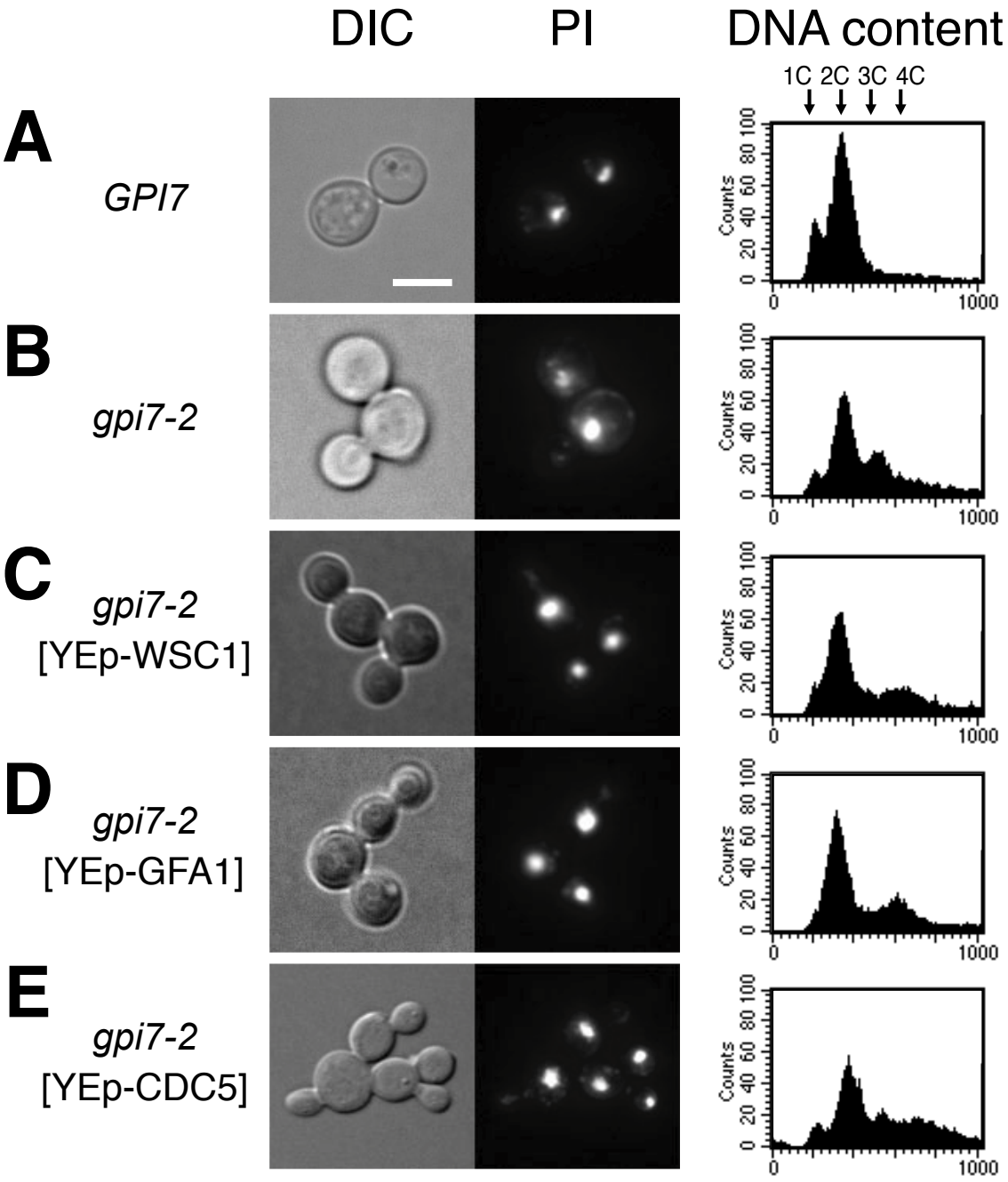

Figure 12. Cell morphology, nuclear staining and flow cytometric analysis of *gpi7-2* strain and strains with multicopy suppressors

Indicated cells were cultured on SD medium at 25˚C overnight. Then cells were incubated at 35.7˚C for 4 h, harvested, and fixed. The fixed cells were treated with RNase and stained with propidium iodide (PI). Each 1C, 2C, and 3C indicates the peak of the DNA content at flow cytometric analysis. DIC, differential interference contrasts.

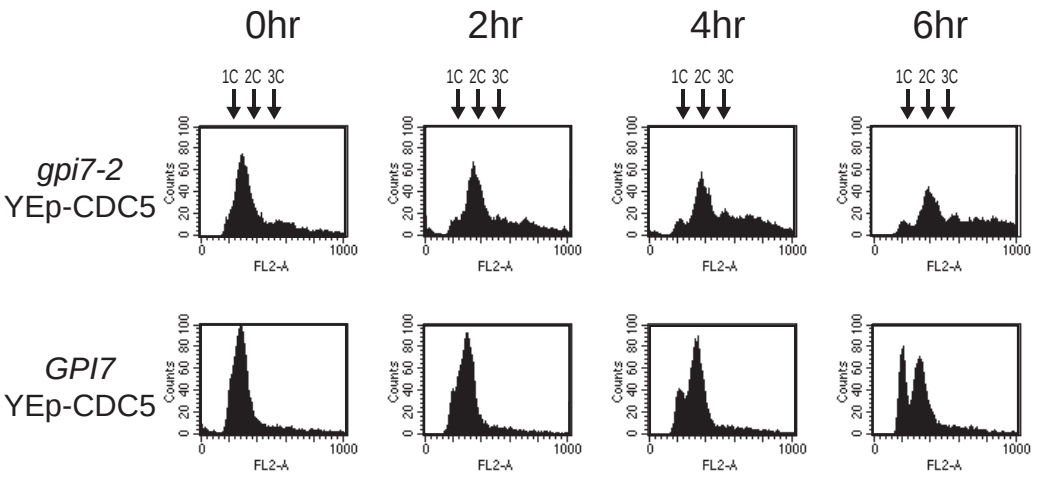

Figure 13. Flow cytometric analysis of wild-type and *gpi7-2* carrying YEp-CDC5

Cells were cultured on SD medium at 25˚C overnight, then were incubated at 35.7˚C for different periods. Samples were taken at the indicated time points. 1C, 2C, and 3C indicates the peak of the DNA content. *GPI7*, wild type *GPI7*; YEp-CDC5, YEp351-CDC5

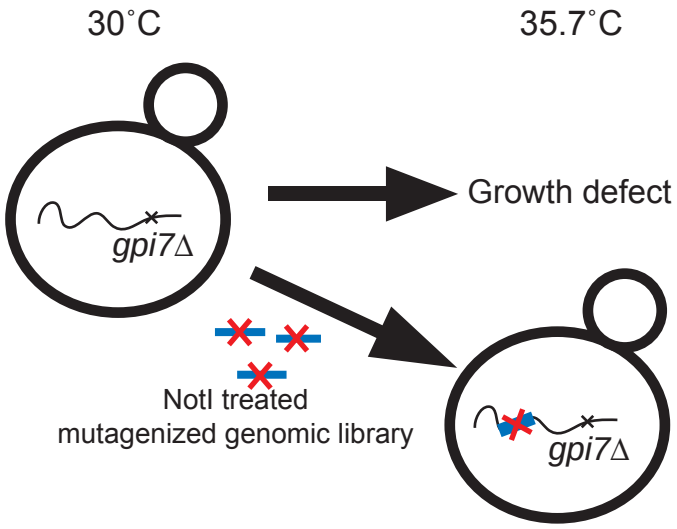

Figure 14. Principle of extragenic suppressors of *gpi7* mutant

Under normal condition, *gpi7*Δ cells can grow at 30˚C but not grow at 35.7˚C. I introduced pools of mTn-3xHA/GFP-mutagenized genomic library cut with NotI into *gpi7*Δ and incubated at 35.7˚C to screen suppressor genes. After 3 days, colonies that could grow at 35.7˚C contained bypass mutations of growth defect on *gpi7*Δ background.

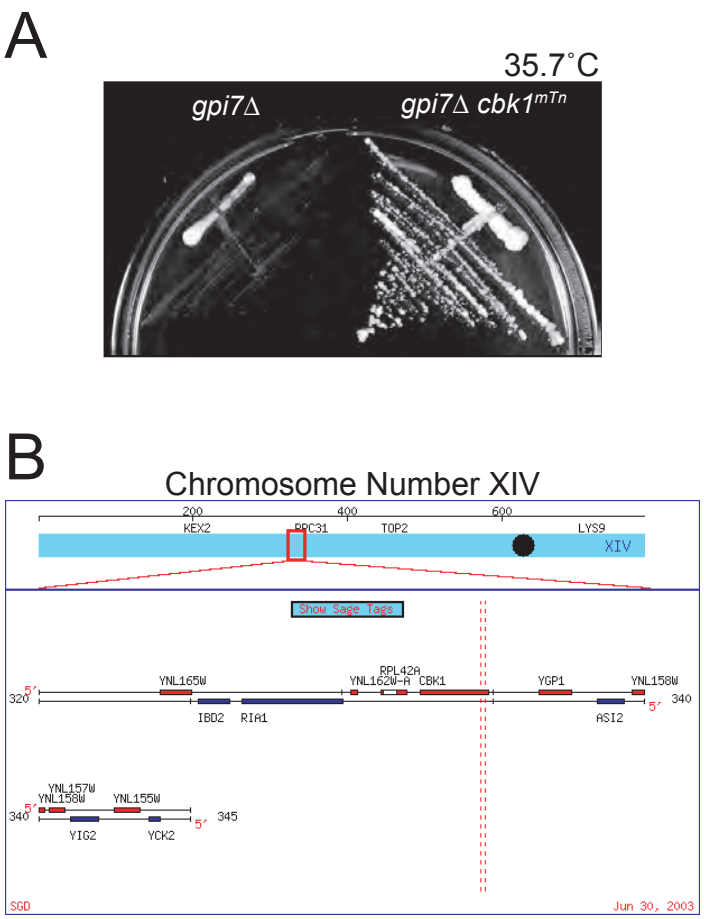

Figure 15. Carboxyl terminal truncation of *CBK1* bypasses the growth defect of *gpi7*Δ

A. *cbk1*^{mTn} suppresses the growth defect of *gpi7*Δ. The *gpi7*Δ and *gpi7*Δ *cbk1*^{mTn} cells were streaked on a YPAD plate and incubated at 35.7˚C for 40 h. B. mTn-3xHA/GFP is inserted at the carboxyl terminal of *YNL161W* (*CBK1*) in chromosome XIV of the yeast genome. Broken lines indicate the insertion area to the genome.

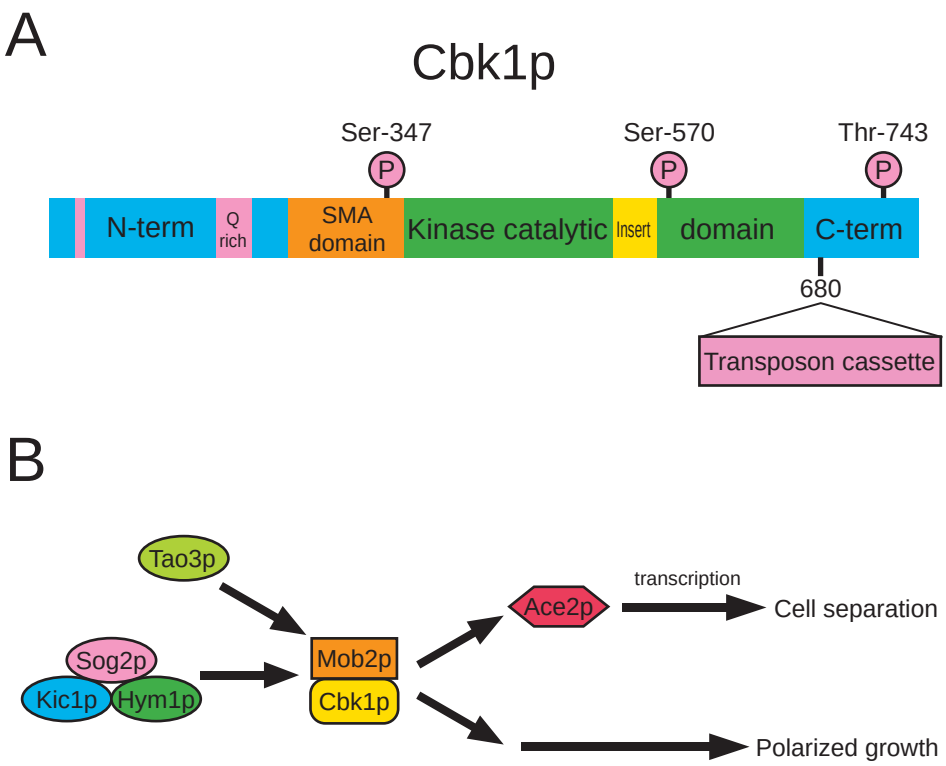

Figure 16. Structure and function of Cbk1p

A. The domain structure of Cbk1p is shown. It has (i) the N-terminal extention containing glutamine (Q) rich regions, (ii) regulatory SMA domain containing the S100B- and Mob1- binding region with the autophosphorylation residue Ser-347, (iii) the catalytic domain spliced by a several amino acid insert and containing the activation segment residue Ser-570 and (iv) the C-terminal extension comprising the regulatory hydrophobic motif with the residue Thr-743. mTn-3xHA/GFP transposon cassette was inserted after the residue of Thr-679. B. A model for regulation of Ace2p activity and cellular morphogenesis (RAM) network in yeast is modified from Nelson et al. (2003). Cbk1p kinase activity is dependent on all the known RAM proteins. Cbk1p functions in two distinct cell morphogenesis pathways: an Ace2p-independent pathway that is required for apical growth and mating projection formation and an Ace2p-dependent pathway that is required for cell separation.

Figure 17. Disruption of the Cbk1p-Ace2p pathway overcomes the growth defect of *gpi7*Δ cells

Both *cbk1*Δ and *ace2*Δ suppress the growth defect of *gpi7*Δ cells. *gpi7*Δ*, gpi7*Δ *cbk1*Δ, and *gpi7*Δ *ace2*Δ cells were streaked on a YPAD plate and incubated at 35.7˚C for 2 days.

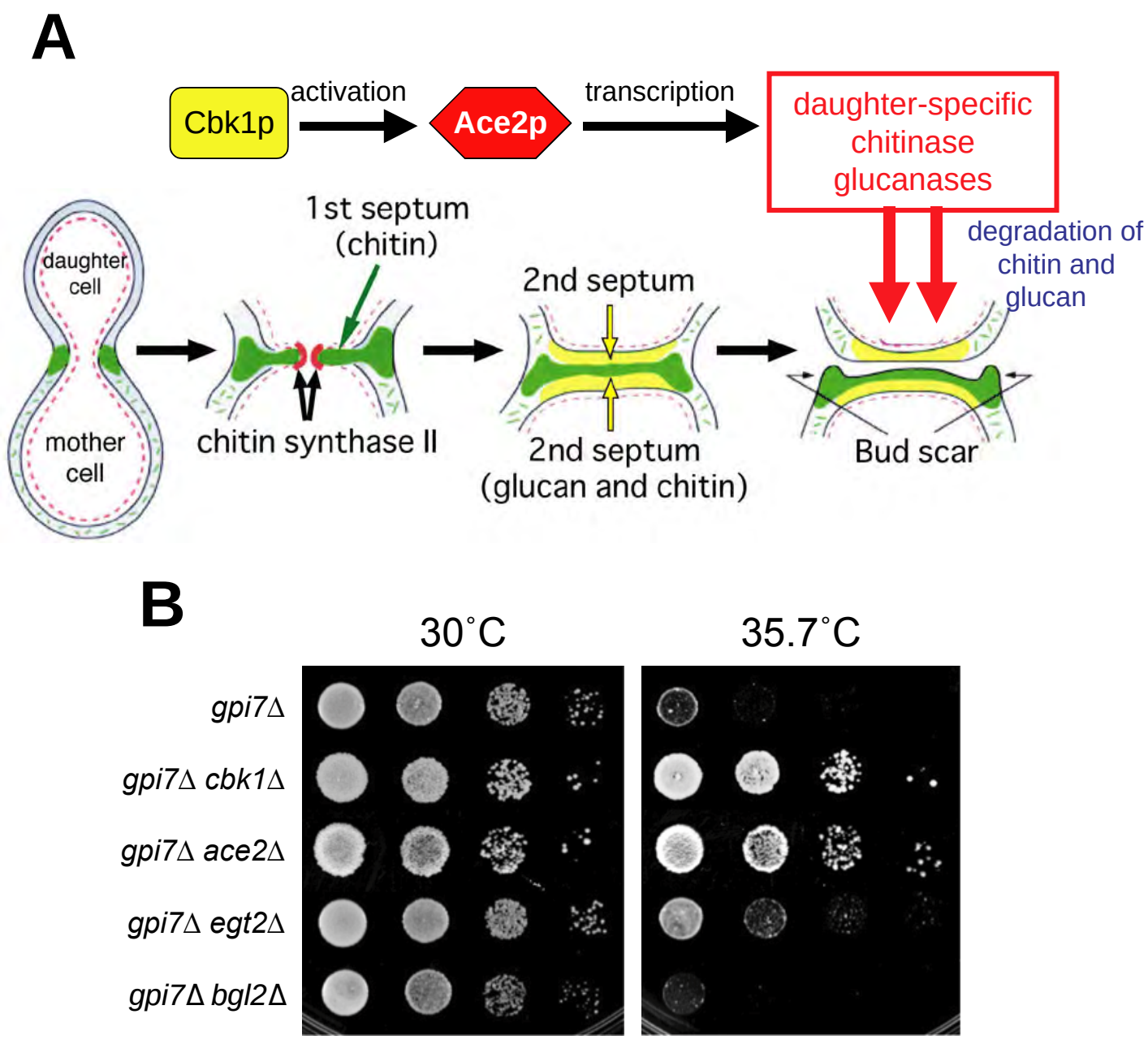

Figure 18. Disruption of *EGT2* ameliorated the growth defect of *gpi7*Δ cells

(A) Septum formation and cell separation process.This figure was cited and modified from previous report (Cabib et al. *J.Biol.Chem.* (2001) 276, 19679-19682). (B) Both *cbk1*Δ and *ace2*Δ suppress the growth defect of *gpi7*Δ, whereas *egt2*Δ partially suppresses the growth defect of *gpi7*Δ. The *gpi7*Δ, *gpi7*Δ *cbk1*Δ, *gpi7*Δ *ace2*Δ, *gpi7*Δ *egt2*Δ and *gpi7*Δ *bgl2*Δ cells were spotted onto YPAD plates and incubated at the indicated temperatures for 2 days.

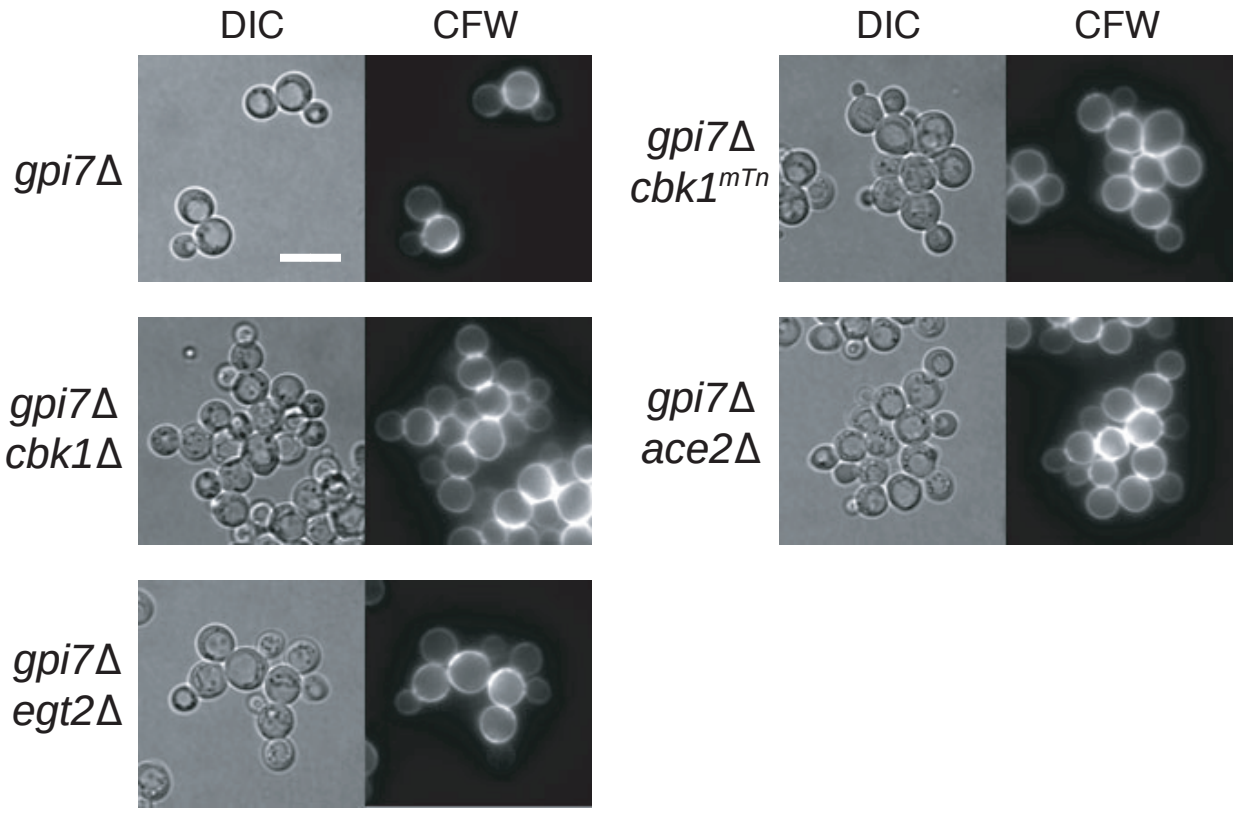

Figure 19. Disruption of Cbk1p-Ace2p pathway cancels the temperature-sensitive phenotype, but not cell separation defect of *gpi7*△ mutant

Cells were incubated in SD medium at 25˚C for 12 h, then incubated at 35.7˚C for 4 h. Cells were stained with calcoflour white (CFW), and observed with fluorescence microscopy (right panels), highlighting mother/daughter junctions and cell shape. Differential interference contrasts (DIC) are shown on the left. Bar, 10μm.

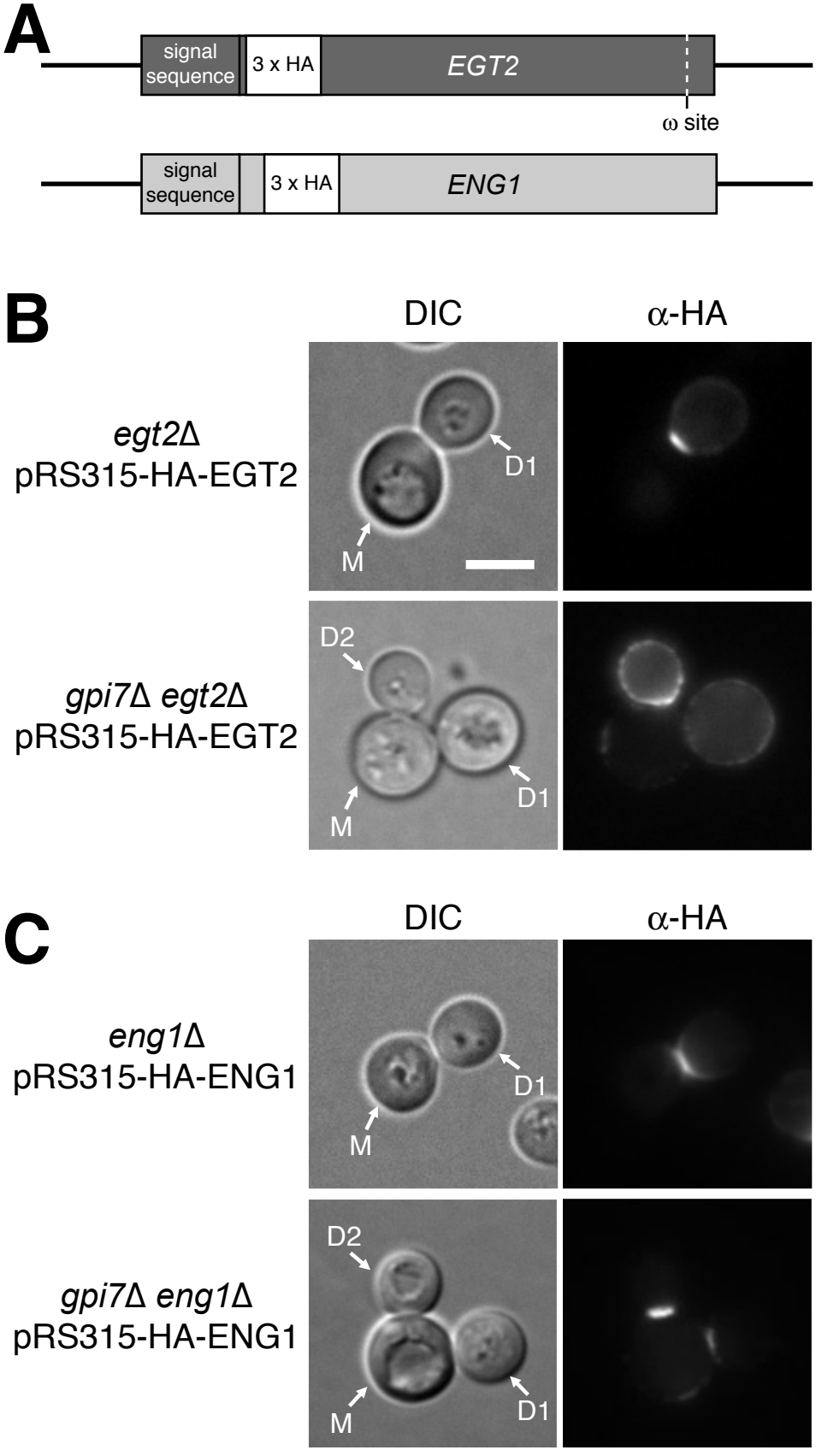
A
signal sequence
3 x HA
EGT2
ω site
signal sequence
3 x HA
ENG1
B
DIC
α-HA
egt2Δ
pRS315-HA-EGT2
D1
M
gpi7Δ egt2Δ
pRS315-HA-EGT2
D2
D1
M
C
DIC
α-HA
eng1Δ
pRS315-HA-ENG1
D1
M
gpi7Δ eng1Δ
pRS315-HA-ENG1
D2
D1
M

Figure 20. Egt2p is displaced from the septal region to the cell cortex in *gpi7*Δ mutant cells

(**A**) Construction of 3xHA-tagged *EGT2* and *ENG1* genes. The 3xHA tag was inserted after a sequence corresponding to the signal sequence (78 bp or 600 bp from the start codon in the *EGT2* or *ENG1* ORF, respectively). It has the promoter and terminator of *EGT2* or *ENG1*, respectively. (**B**) HA-Egt2p was visualized by indirect immunofluorescence assay in wild-type (*egt2*Δ pRS315-HA-EGT2) and *gpi7*Δ (*gpi7*Δ *egt2*Δ pRS315-HA-EGT2) cells. M, D1 and D2 indicate mother cell, 1st daughter cell and 2nd daughter cell, respectively. DIC, differential interference contrasts. Bar, 5 μm. (**C**) HA-Eng1p was visualized by indirect immunofluorescence assay in wild-type (*eng1*Δ pRS315-HA-ENG1) and *gpi7*Δ (*gpi7*Δ *eng1*Δ pRS315-HA-ENG1) cells.

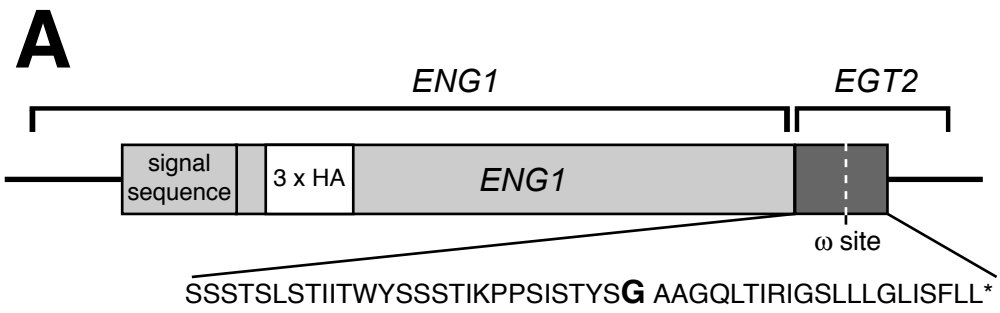
A
ENG1
EGT2
signal sequence
3 x HA
ENG1
ω site
SSSTSLSTIITWYSSSTIKPPSISTYSG AAGQLTIRIGSLLLGLISFLL*

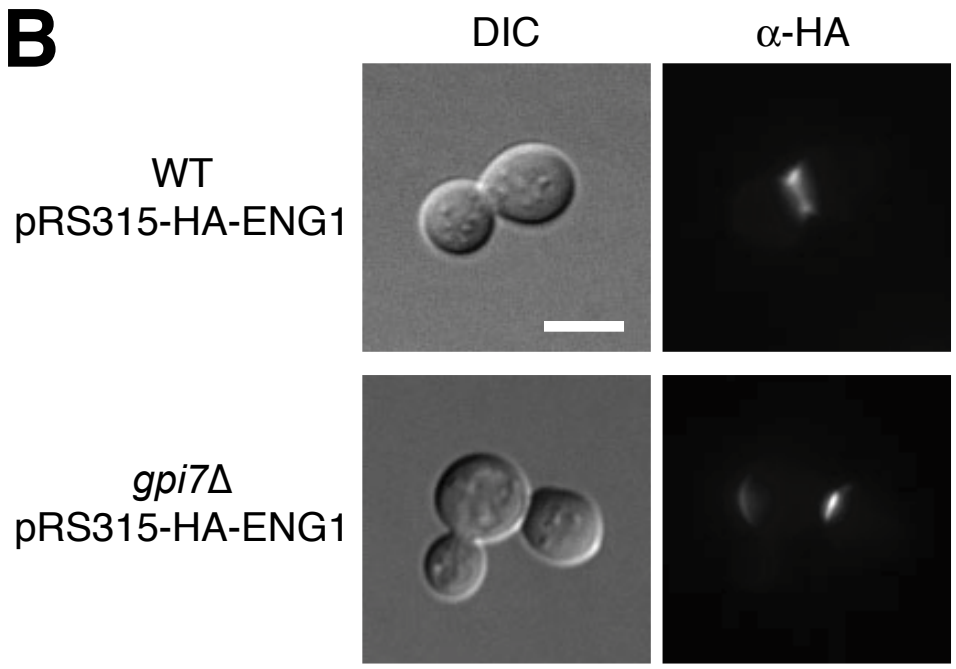
B
DIC
α-HA
WT
pRS315-HA-ENG1
gpi7Δ
pRS315-HA-ENG1

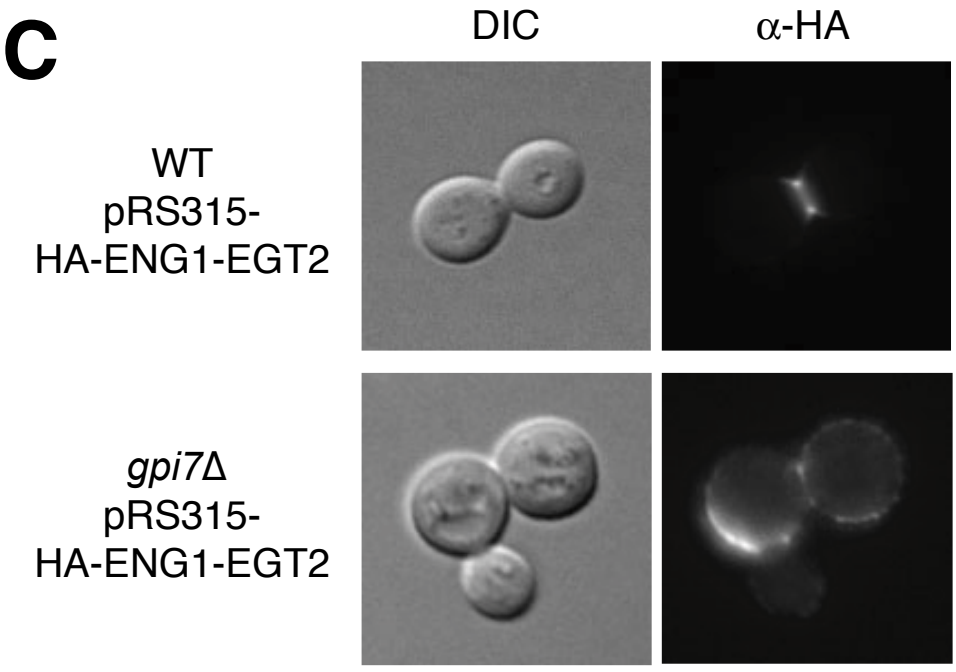
C
DIC
α-HA
WT
pRS315-
HA-ENG1-EGT2
gpi7Δ
pRS315-
HA-ENG1-EGT2

Figure 21. Chimeric protein, Eng1-Egt2p, is partially displaced to the cell cortex in *gpi7*Δ mutant cells

(**A**) Construction of a 3xHA-tagged ENG1-EGT2 chimeric gene. A fragment corresponding to the C terminal 49 amino acids and 482 bp of the terminator region of *EGT2* was fused to the C-terminal end of *ENG1*. It has the promoter of *ENG1*. The potential GPI-attachment site (ω-site) of Egt2p is marked in *bold*. Star(*), stop codon. (**B**) HA-Eng1p was visualized by indirect immunofluorescence assay in wild-type (WT pRS315-HA-ENG1) and *gpi7*Δ (*gpi7*Δ pRS315-HA-ENG1) cells. DIC, differential interference contrasts. Bar, 5 μm. (**C**) HA-Eng1-Egt2p was visualized by indirect immunofluorescence assay in wild-type (WT pRS315-HA-ENG1-EGT2) and *gpi7*Δ (*gpi7*Δ pRS315-HA-ENG1-EGT2) cells.

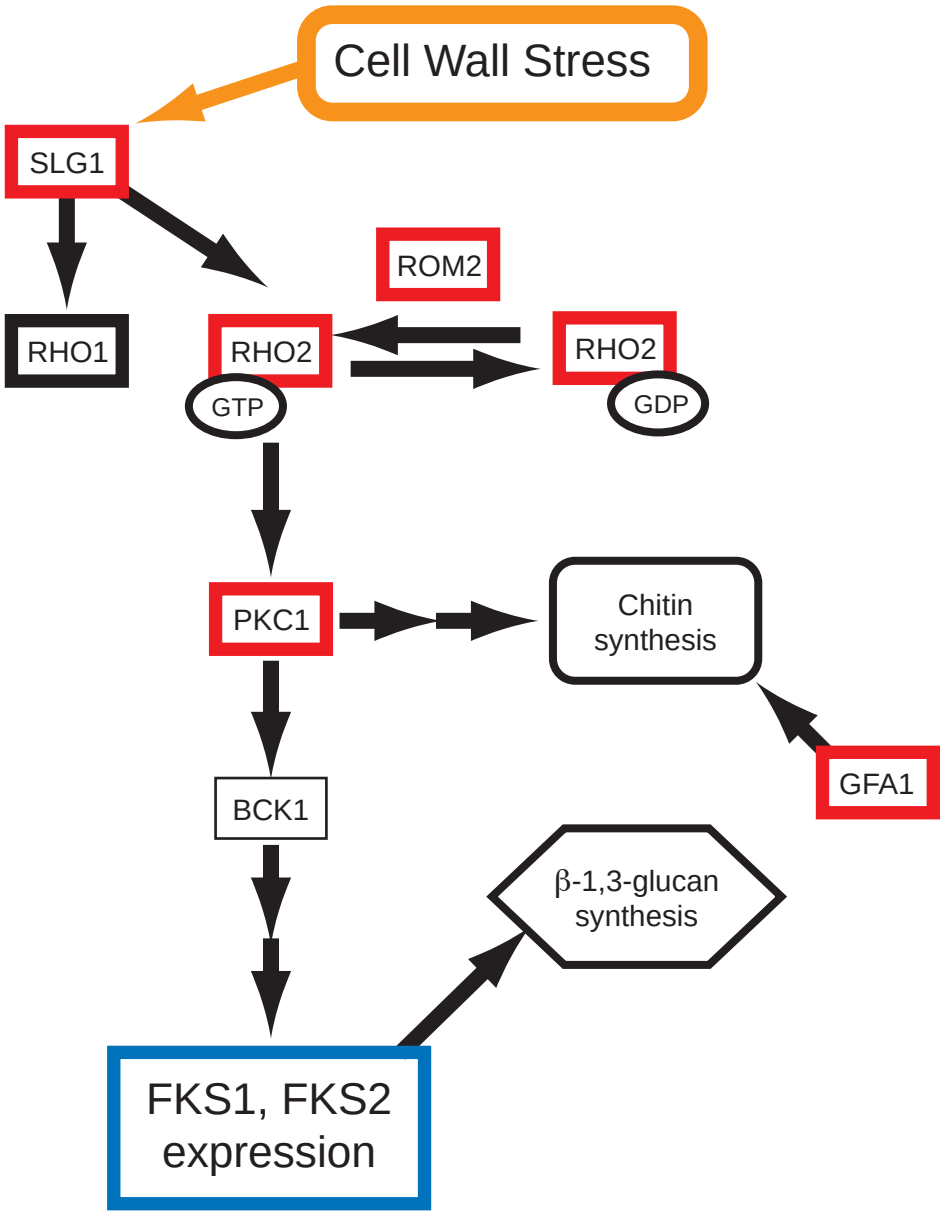

Figure 22. Illustration of Slg1p-Pkc1p pathways

Slg1p-Pkc1p pathways are activated by cell wall stress and enhance the production of cell wall components, such as β-1,3-glucan and chitin. Red squares indicate genes isolated as multicopy suppressors of *gpi7-2*.

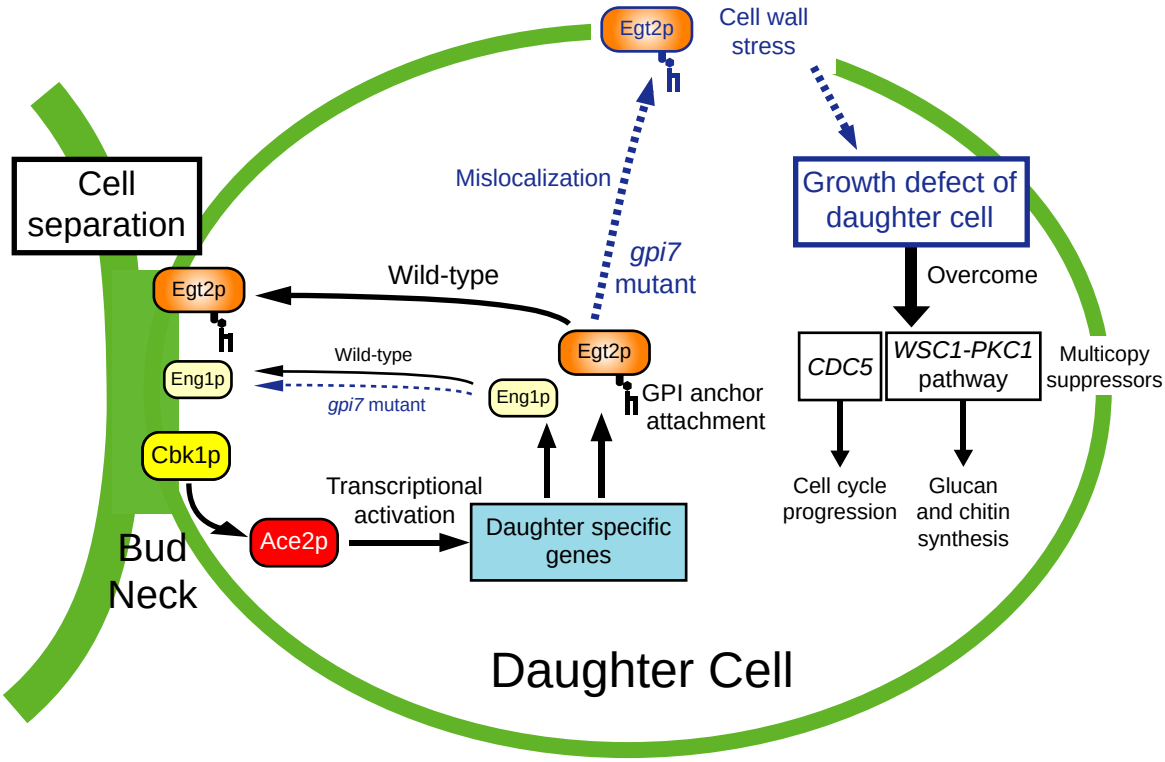

Figure 23. Summary of the regulation of cell separation by *GPI7*

Cbk1p and Ace2p activate the expression of daughter-specific genes. Egt2p, but not Eng1p, is modified by a GPI anchor in the ER. Eng1p and Egt2p are transported to the bud neck. In *gpi7* mutants, Egt2p is transported to the cell surface, but not to the bud neck. Multicopy suppressors overcome the temperature-sensitive growth defect of *gpi7* mutants, but not the cell separation defect.

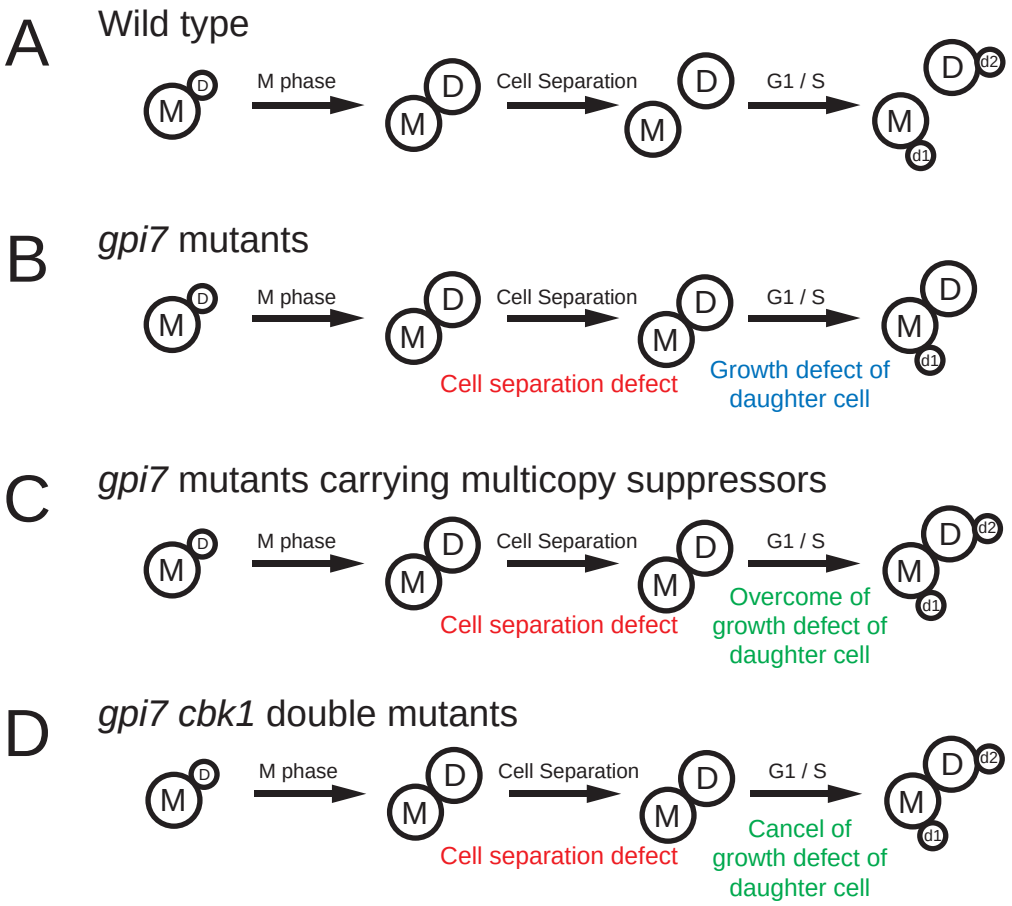

Figure 24 Mechanisms for abnormal cellular morphologies

A, a budding cell separation process of wild type cells; B, that of *gpi7* mutants; C, that of *gpi7* mutants carrying multicopy suppressors; D, that of *gpi7 cbk1* double mutants.
M, D, d1 and d2 indicate mother cell, 1st daughter cell, 2nd daughter cell from mother cell and daughter cell from 1st daughter cell, respectively.

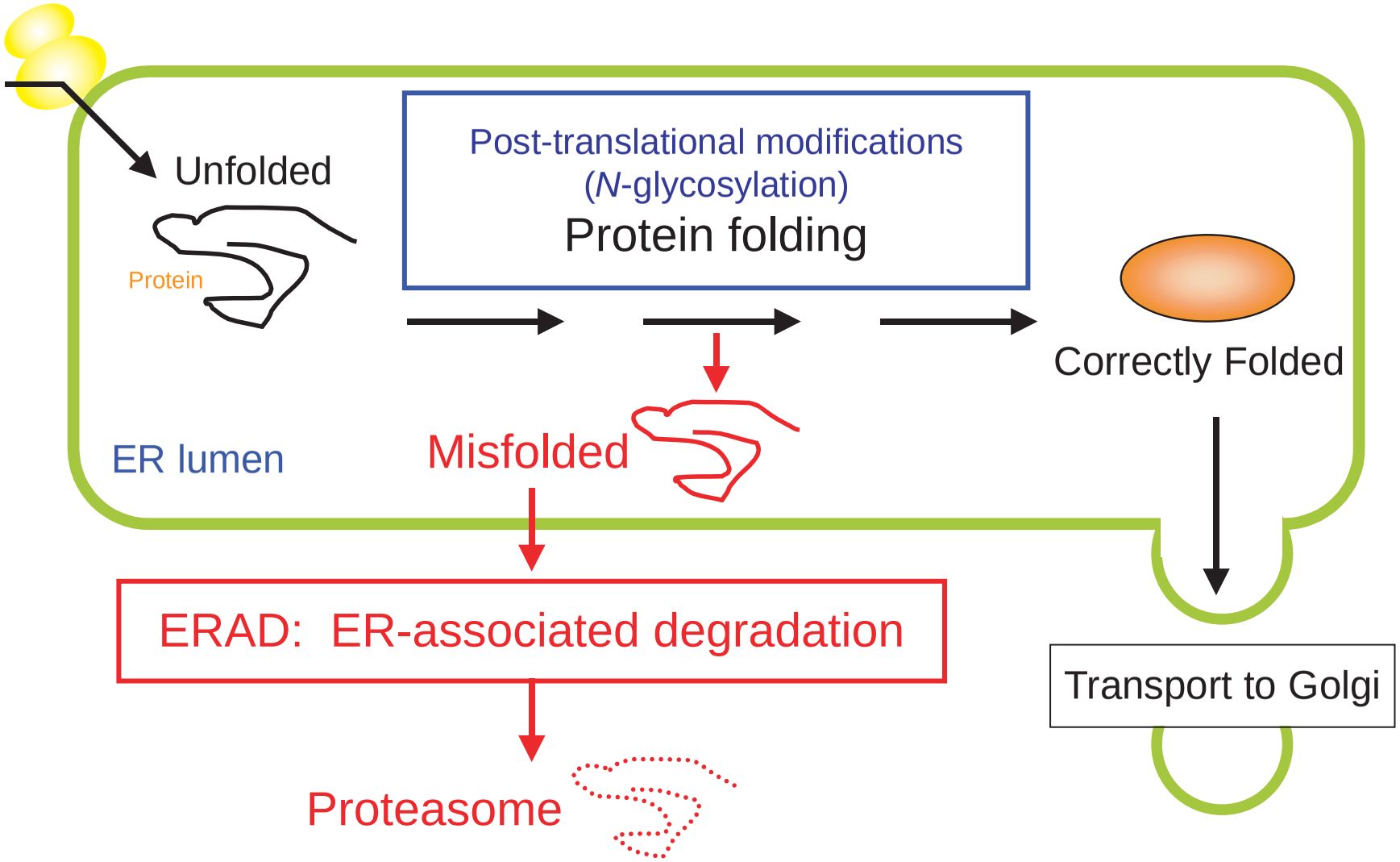

Figure 25. Protein folding and quality control in the ER

Folding of glycoprotein is carried out in the ER. Correctly folded proteins are transported from the ER to the Golgi, whereas aberrantly folded proteins are recognized as misfolded proteins and degraded by ER-associated degradation (ERAD) and proteasome. Post-translational modifications, such as N-glycosylation, play important roles for the quality control of glycoproteins.

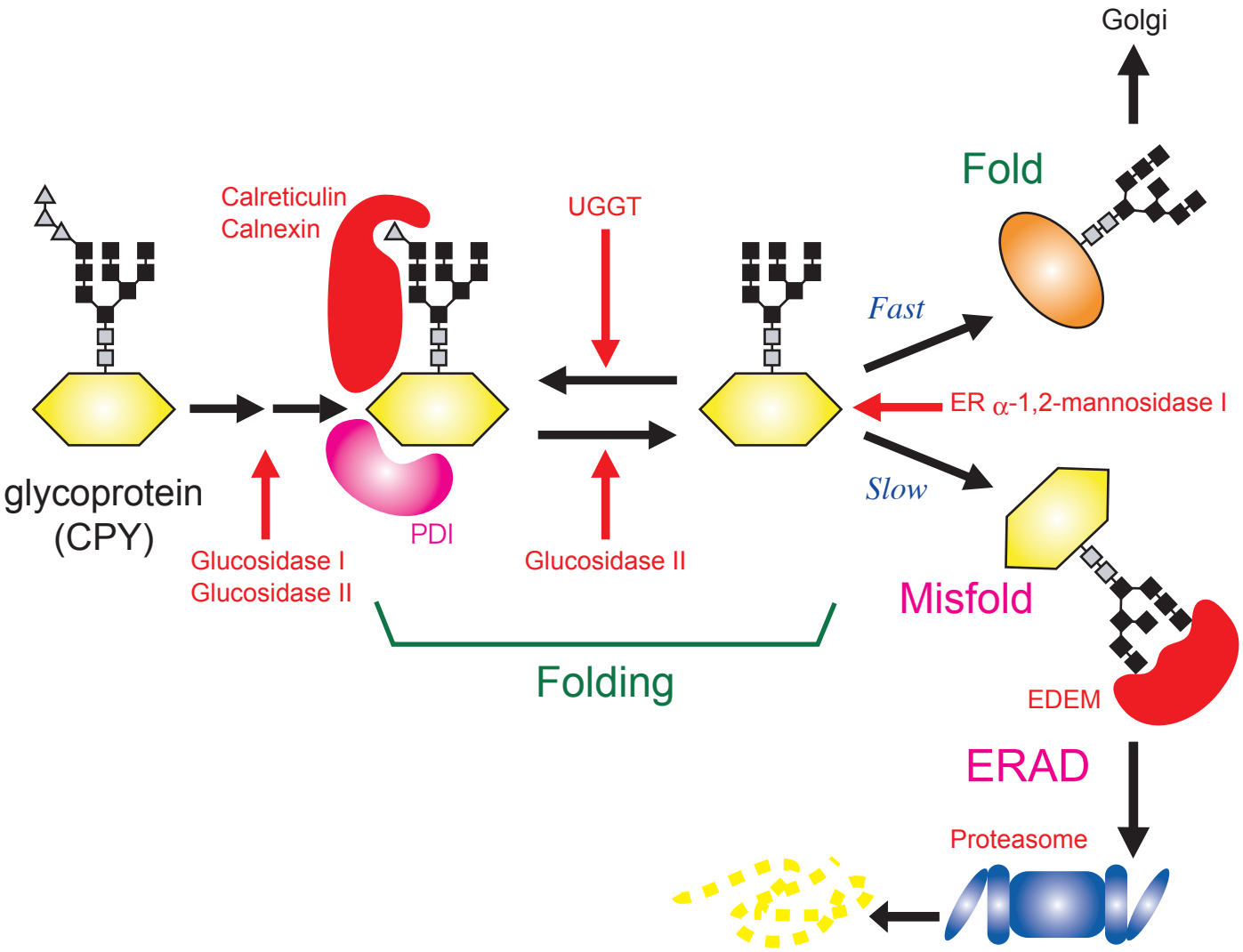
Golgi
Fold
Calreticulin
Calnexin
UGGT
Fast
ER α-1,2-mannosidase I
glycoprotein
(CPY)
Slow
PDI
Glucosidase I
Glucosidase II
Glucosidase II
Misfold
Folding
EDEM
ERAD
Proteasome

Figure 26. Involvement of *N*-glycosylation in the ER quality control

After addition of the core glycan to a growing polypeptide chain by oligosacchride transferase, the outermost of the three glucose residues is removed by glucosidase I. Soon thereafter, glucosidase II removes the middle glucose. Via the monoglucosylated core glycans thus generated, the glycoprotein binds to calnexin and calreticulin. These sequester the nascent or newly synthesized chains and expose them to PDI, a thiol-disulfide oxidoreductase that provides assistance during disulfide bond formation. When glucosidase II removes the remaining glucose, the glycoprotein dissociates from calnexin and calreticulin. The protein now encounters one of three possible fates. If properly folded, mannose residue is trimmed by ER mannosidase I rapidly and the protein leaves the ER. If it is incompletely folded, UDP-Glc:glycoprotein glucosyltransferase (UGGT) uses UDP-glucose transported by a UDP-glucose/UMP exchanger from the cytosol to reglucosylate the high-mannose glycans located in improperly folded regions. Through these glycans, the glycoprotein rebinds to calnexin and calreticulin. The third fate is ER-associated degradation (ERAD) after retrotranslocation of the misfolded glycoprotein to the ER most likely through the translocon complex. ERAD of glycoproteins occurs when they have stayed in the ER lumen for some time and when they are recognized by a putative lectin (EDEM) because they have lost a mannose through the action of ER mannosidase I. Triangles are glucose residues. Black squares are mannose, and Grey squares are N-acetylglucosamine. EDEM, ER degradation-enhancing α-mannosidase-like protein; ERAD, ER-associated protein degradation.

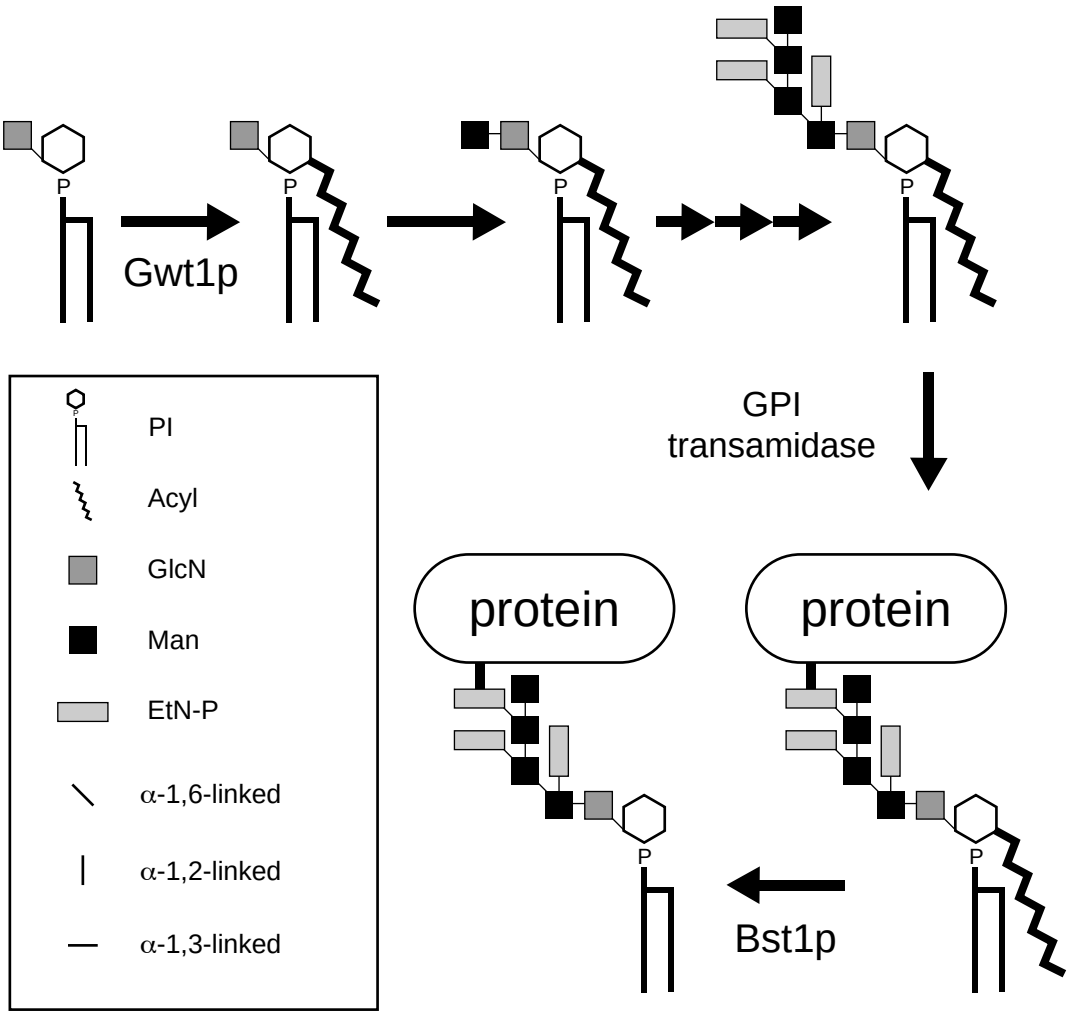

Figure 27. Inositol acylation and deacylation of the GPI moiety during the biosynthesis of GPI in *Saccharomyces cerevisiae*

GPI precursors are synthesized at the ER membrane. Gwt1p is required for the acylation of inositol at an early step in the biosynthesis of GPI. The complete GPI precursor is transferred to a nascent cleaved carboxyl terminus of the GPI-protein precursors. After attachment of GPI to proteins, the acyl group on the inositol is eliminated by Bst1p. PI, phosphatidylinositol; Acyl, acyl group; GlcN, glucosamine; Man, mannose; EtN-P, ethanolamine phosphate.

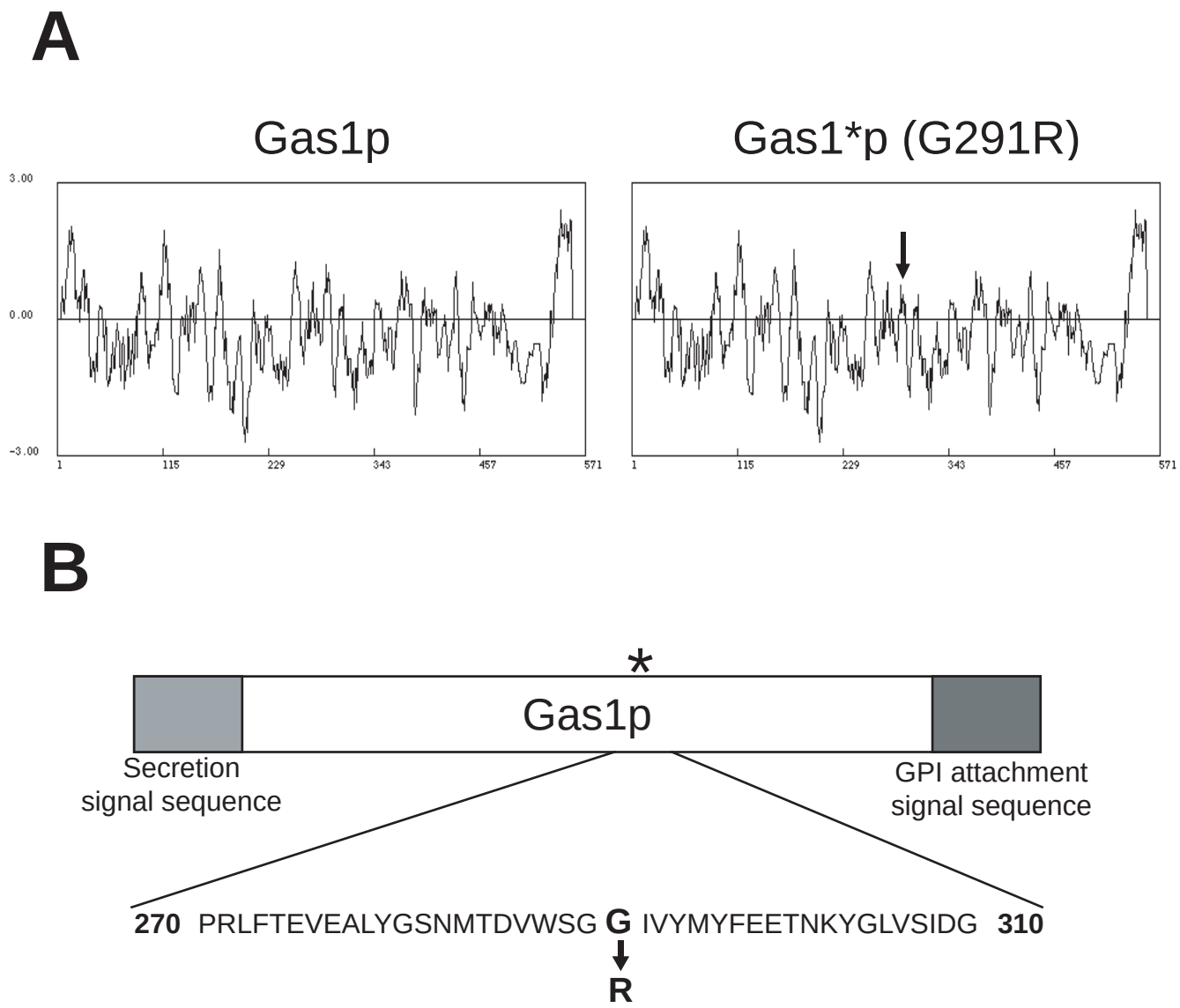

Figure 28. Construction of misfolded Gas1p

(A) Hydropathy plots of wild-type Gas1p (left panel) and mutant Gas1p (right panel; Gas1*p). Hydropathy plots were made using to the Kyte and Doolittle program. The arrows indicate the site of mutation in Gas1*p (G291R). (B) Schematic structure of Gas1p, including the sequence of the mutated form (Gas1*p).

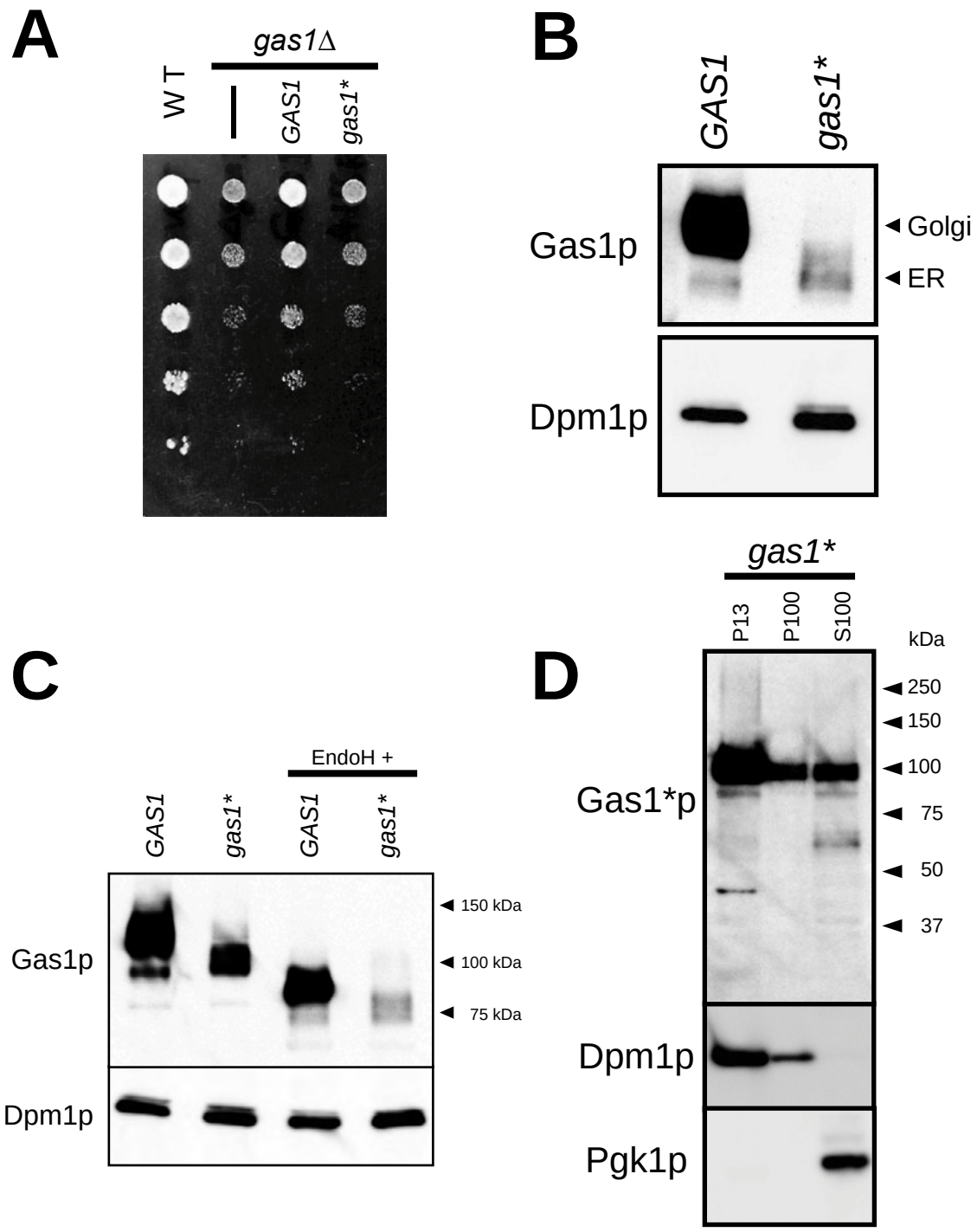

Figure 29. Characterization of Gas1*p

(A) The *gas1** mutant gene does not rescue the slow growth phenotype of *gas1*Δ mutant cells. Isogenic W303-1A (WT), MFY156 (*gas1*Δ), MFY161 (*gas1*Δ *URA3::GAS1*), and MFY163 (*gas1*Δ *URA3::gas1**) cells were spotted in serial dilutions on a YPAD plate and grown at 30°C for 2 days. (B) Gas1*p remains in the ER form, and its level is markedly decreased compared to wild-type Gas1p. MFY161 (*GAS1*) and MFY163 (*gas1**) cells were grown overnight to mid-log phase. Equal cell numbers were disrupted, and total protein extracts were prepared and analyzed by immunoblotting using anti-Gas1p and anti-rabbit HRP-conjugated IgG or with anti-Dpm1p and anti-mouse HRP-conjugated IgG. (C) Gas1*p is correctly *N*-glycosylated. Cell lysates of MFY161 (*GAS1*) and MFY163 (*gas1**) were digested with Endo H. The Endo H-treated or untreated protein extracts were separated by SDS-PAGE and analyzed by immunoblotting using anti-Gas1p or anti-Dpm1p. (F) Fractionation of Gas1*p. Exponentially growing MFY163 cells were broken, and the cell lysate was sedimented by sequential steps of centrifugation and ultracentrifugation. Proteins from the 13,000 X *g* pellet (P13), 100,000 X g pellet (P100), and 100,000 X *g* supernatant (S100) were processed for immunoblotting and detected with anti-Gas1p, anti-Dpm1p, or anti-Pgk1p.

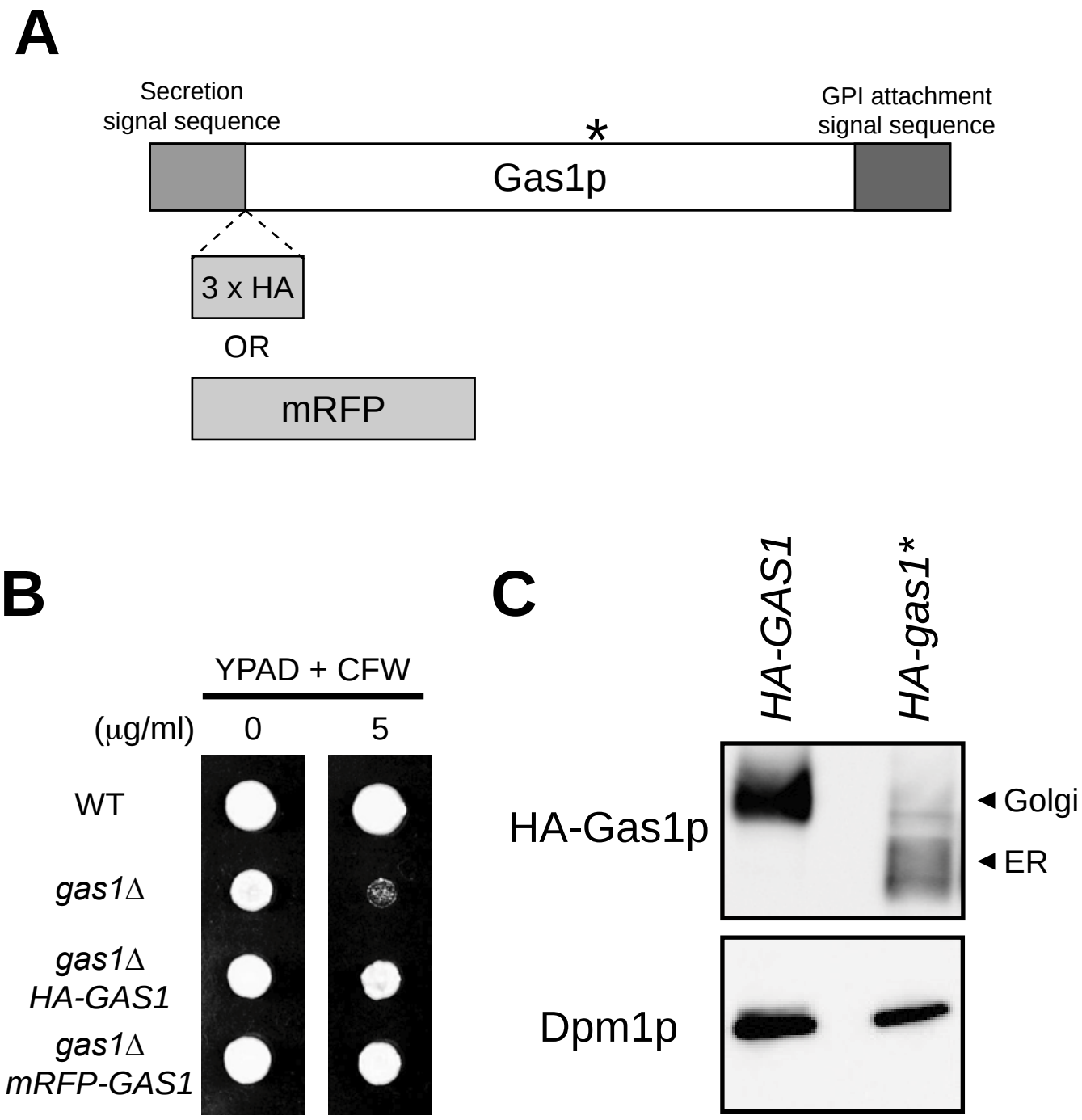

Figure 30. Construction of HA- or mRFP-tagged Gas1p and Gas1*p

(A) Schematic construction of HA-tagged and mRFP-tagged Gas1*p. A 3X HA epitope tag or mRFP sequence was inserted into Gas1p after the secretion signal sequence. (B) Tagged Gas1 proteins are functional and complement the calcofluor white (CFW) sensitivity of gas1 Δ. Isogenic W303-1A (WT), MFY156 (*gas1*Δ), MFY182 (*gas1*Δ *HA-GAS1*), and MFY183 (*gas1*Δ *mRFP-GAS1*) cells were spotted on plates containing YPAD or YPAD with 5 μg/ml CFW and then incubated at 30°C for 2 days. (C) HA-Gas1p behaves like the native form of Gas1p, but the mutant of HA-Gas1p is unstable and remains as the ER form. MFY207 (*HA-GAS1*) and MFY208 (*HA-gas1**) cells were grown overnight to mid-log phase. Equal cell numbers were disrupted, and total protein extracts were prepared and analyzed by immunoblotting using anti-HA and anti-mouse HRP-conjugated IgG, or anti-Dpm1p and anti-mouse HRP-conjugated IgG. ER and Golgi forms of HA-tagged Gas1p are shown by arrowheads.

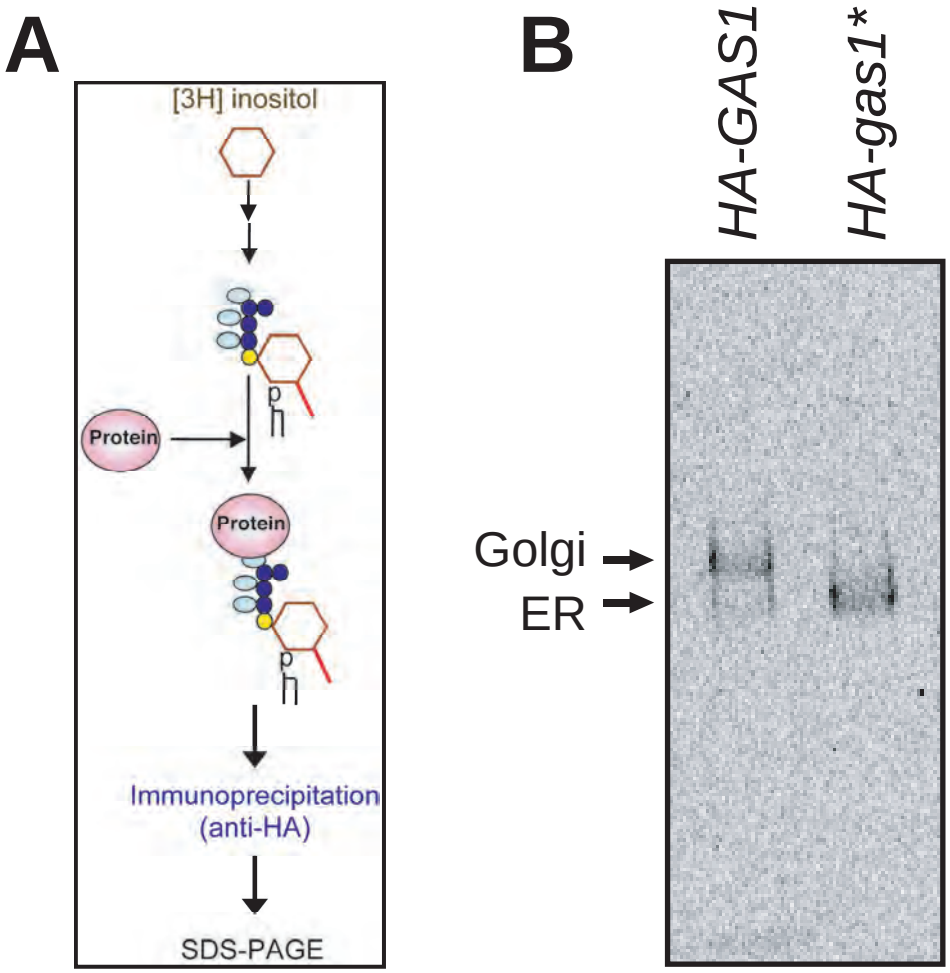

Figure 31. Misfolded Gas1*p is modified by the GPI anchor

(A) Schematic method for the labeling with tritiated inositol of Gas1*p. (B) MFY207 (*HA-GAS1*) and MFY208 (*HA-gas1**) cells were grown to a mid-log phase and labeled with *myo*-[1,2-^{3}H] inositol for 3 h. Gas1p and Gas1*p in cell lysates were then immunoprecipitated with anti-HA-agarose and analyzed by SDS-PAGE, followed by image analysis with a Molecular Imager. The ER and Golgi forms are indicated by arrows.

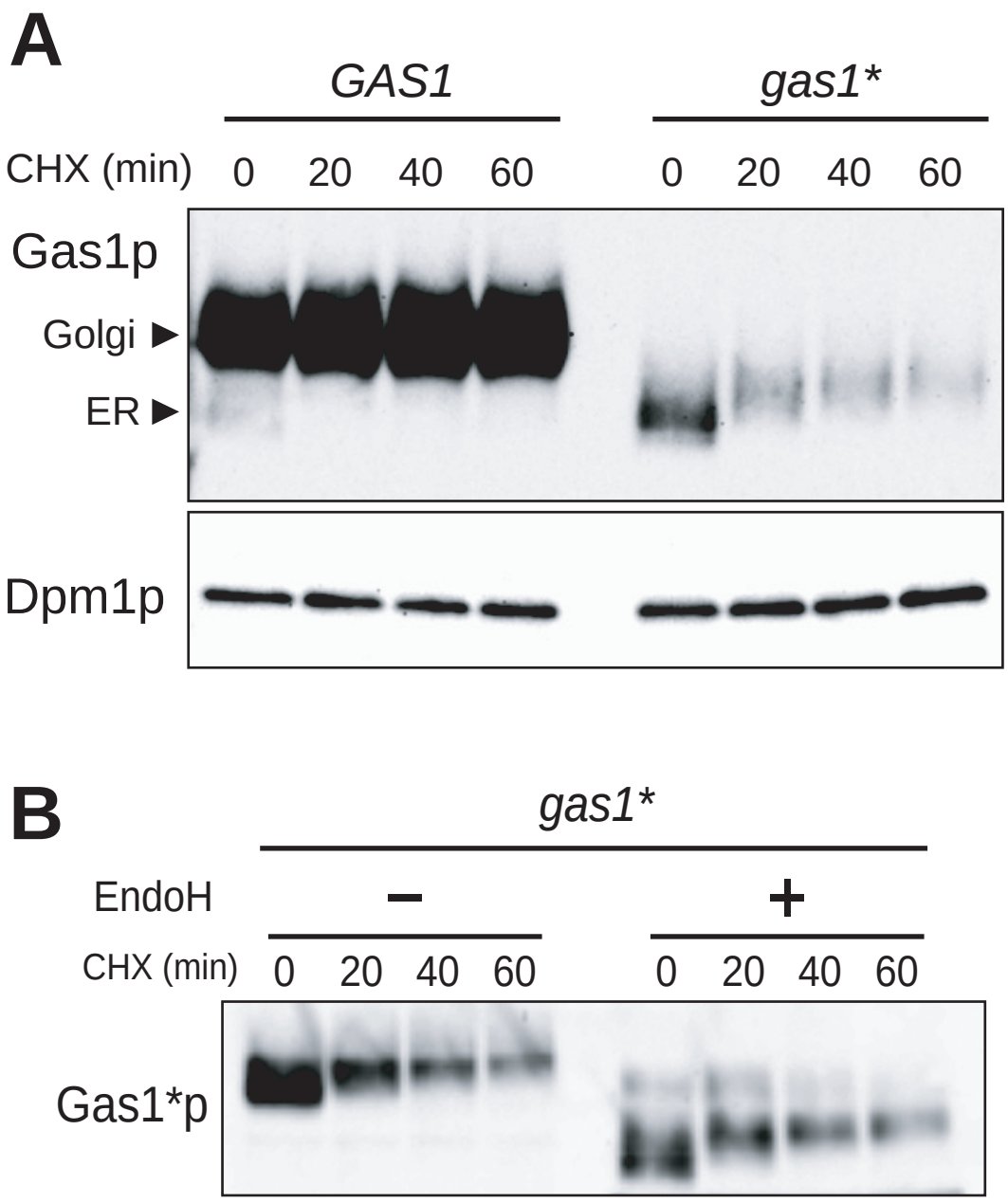

Figure 32. Gas1*p is unstable and rapidly degraded

(A) Isogenic MFY161 (*GAS1*) and MFY163 (*gas1**) cells were grown to 2 X 10^7 cells/ml. Equal cell numbers were then incubated with 200 µg/ml of CHX, and aliquots were removed at the indicated time points. Crude protein extract was separated by SDS-PAGE and analyzed by immunoblotting with anti-Gas1p. The immunoblot was subsequently probed with anti-Dpm1p as a control for loading. (B) Isogenic MFY163 cells were grown to 2 X 10^7 cells/ml, after which CHX chase analysis was performed. Aliquots of the sample were treated for 3 h with Endo H at 37 ° C and then analyzed by immunoblotting with anti-Gas1p.

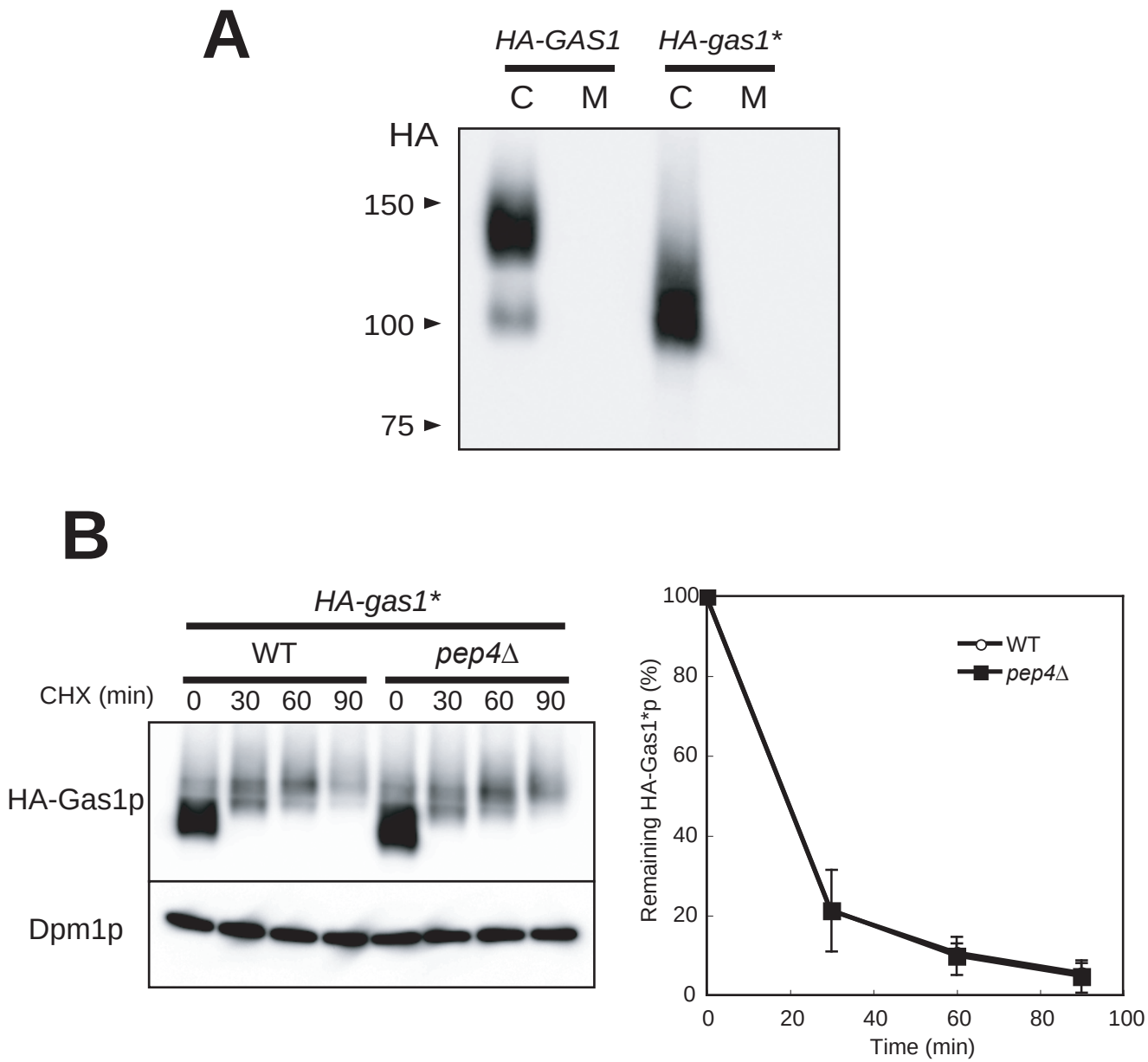

Figure 33. Gas1*p is not secreted into the medium and is not degraded in the vacuole

(A) Cells lysates were prepared from exponentially growing cells. Proteins secreted into the medium were precipitated with 10% trichloroacetic acid. Samples corresponding to 0.5 OD_{600} units of cells per lane were loaded and analyzed by immunoblotting using anti-HA antibodies. C, cell lysate; M, medium. (B) The degradation of Gas1*p was measured in MFY188 (WT) and MFY329 (*pep4*Δ) cells in which *HA-gas1** is integrated at the *URA3* locus, as described in Figure 32A. HA-Gas1p was resolved by electrophoresis and analyzed by immunoblotting with anti-HA. The amounts of Gas1* protein were quantified with an image analyzer and plotted as means values ± SD from three independent experiments, with the quantity at the 0 time point (steady-state level) set at 100%.

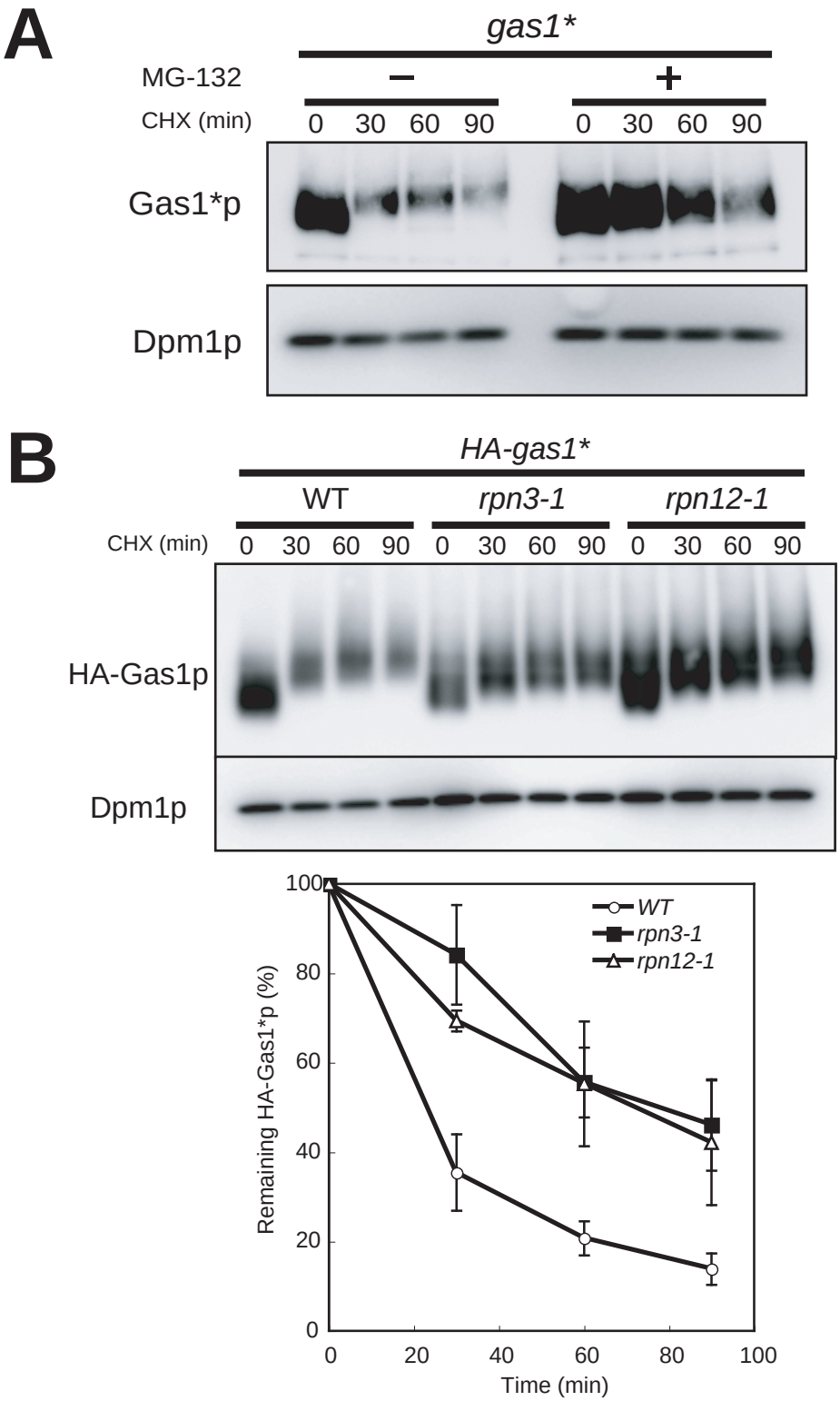

Figure 34. Gas1*p is a substrate for ER-associated degradation via the proteasome

(A) The effect of MG-132, a specific proteasome inhibitor, on the degradation of Gas1*p. MG-132 in DMSO (MG-132 (+)) or DMSO only (MG-132 (–)) was added to cultures of MFY163 cells 10 min before starting CHX chase analysis. (B) The degradation of Gas1*p was measured in MFY188 (WT), MFY337 (*rpn3-1*), and MFY336 (*rpn12-1*) cells, in which *HA-gas1** is integrated at the *URA3* locus. Equal cell numbers (2 X 10^7 cells/ml) were incubated with 200 µg/ml of CHX at 37° C. Cells were chased for the periods indicated. The amounts of Gas1* protein were quantified as described in Figure 33B.

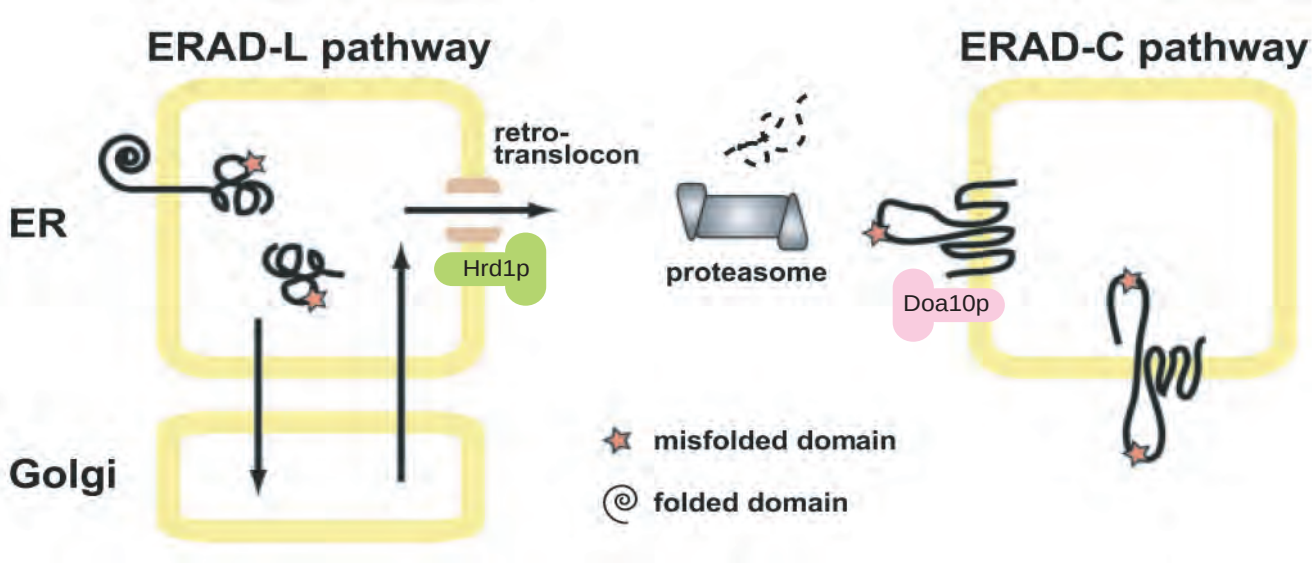

Figure 35. Two distinct ERAD pathways function according to the location of the misfolded domain

The ERAD-L system monitors the folded state of lumenal domains, and degradation of ERAD-L substrates appears to require ER-to-Golgi transport. ERAD-L substrates are ubiquitinated by Hrd1p. The ERAD-C pathway monitors the folded state of cytosolic domains. ERAD substrates with misfolded domains on both sides of the membrane are degraded by the ERAD-C pathway. Doa10p is involved in the ubiquitination for ERAD-C substrates. This figure is modified from a previous report (Nakatsukasa et al., 2005)

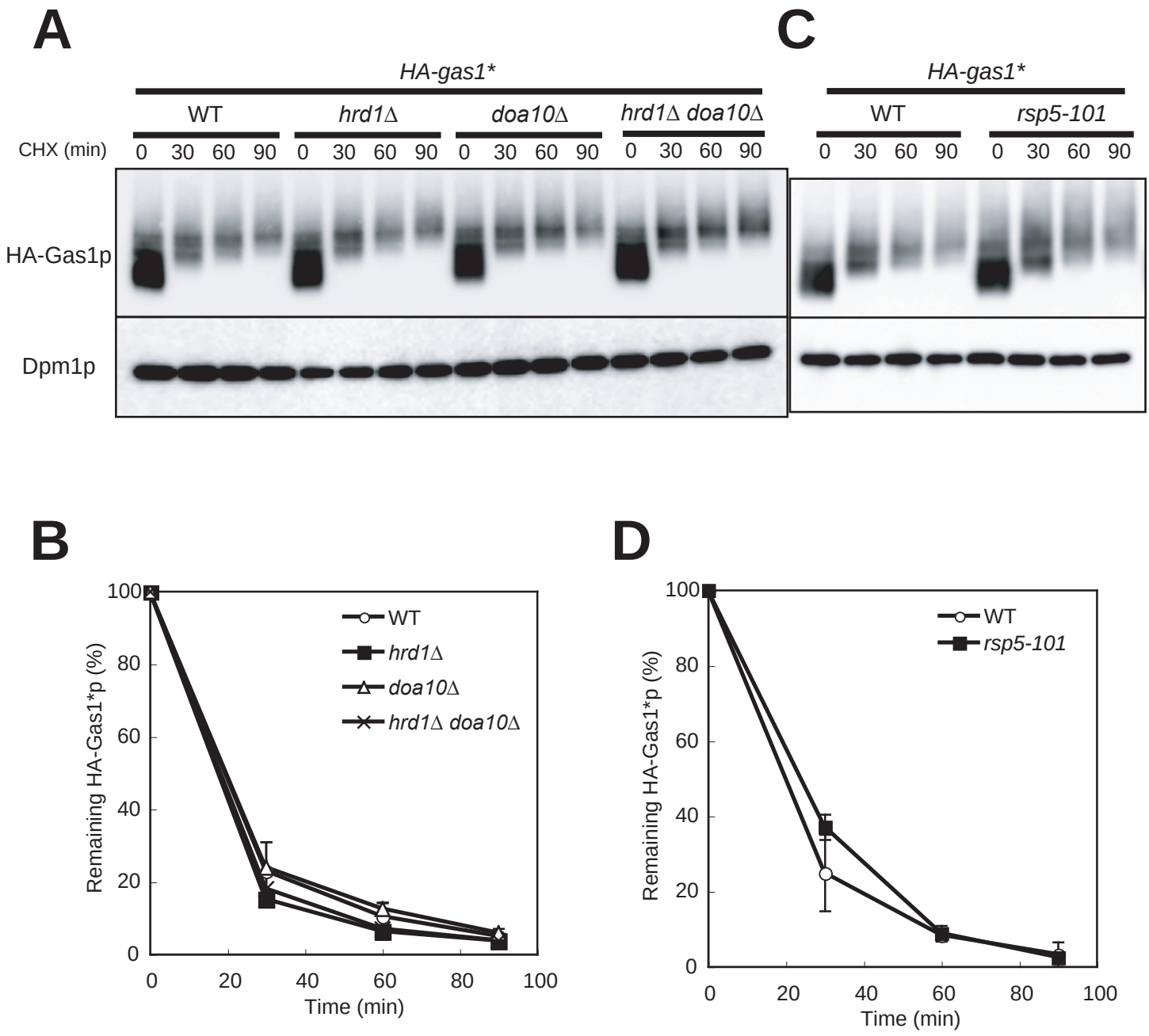

Figure 36. Effects of E3 ubiquitin ligases in the degradation of Gas1*p

(A)(B) The degradation of Gas1*p was measured in MFY188 (WT), MFY327 (*hrd1*Δ), MFY328 (*doa10*Δ), and MFY343 (*hrd1*Δ *doa10*Δ) cells in which *HA-gas1** is integrated at the *URA3* locus, as described in Figure 33B. (C)(D) The degradation of Gas1*p was measured in MFY331 (WT) and MFY332 (*rsp5-101*) cells, in which *HA-gas1** is integrated at the *URA3* locus, as described in Figure 34B.

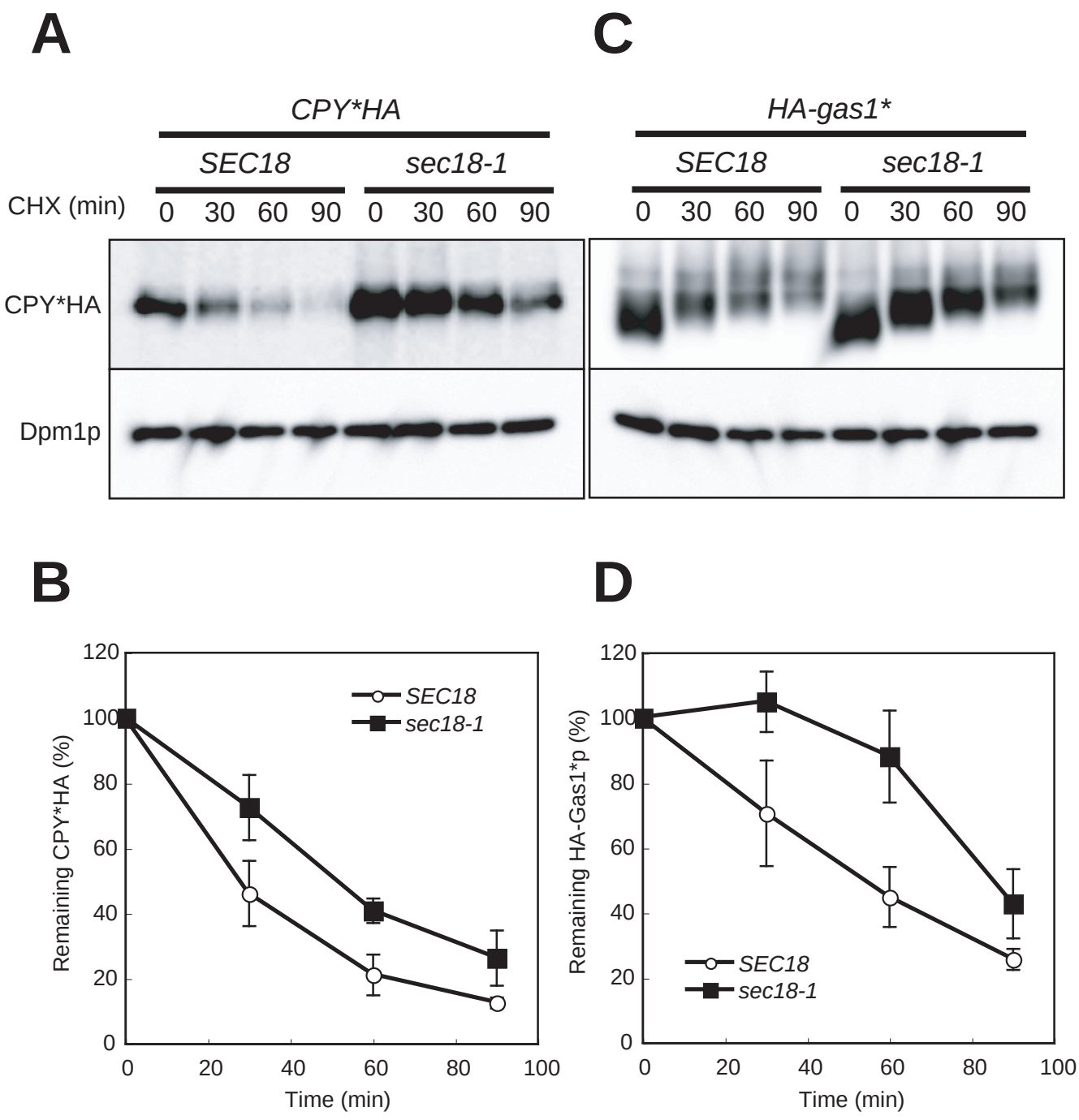

Figure 37. Effects of ER-to-Golgi transport in the degradation of Gas1*p

(A)(B) The degradation of CPY* was measured in YS63-1C cells carrying pRS316-CPY*HA and pRS315-SEC18 (*SEC18*), and YS63-1C cells carrying pRS316-CPY*HA (*sec18-1*), as described in Figure 34B. (C)(D) The degradation of Gas1*p was measured in MFY348 cells carrying pRS315-SEC18 (*SEC18*), and MFY348 cells (*sec18-1*), as described in Figure 34B.

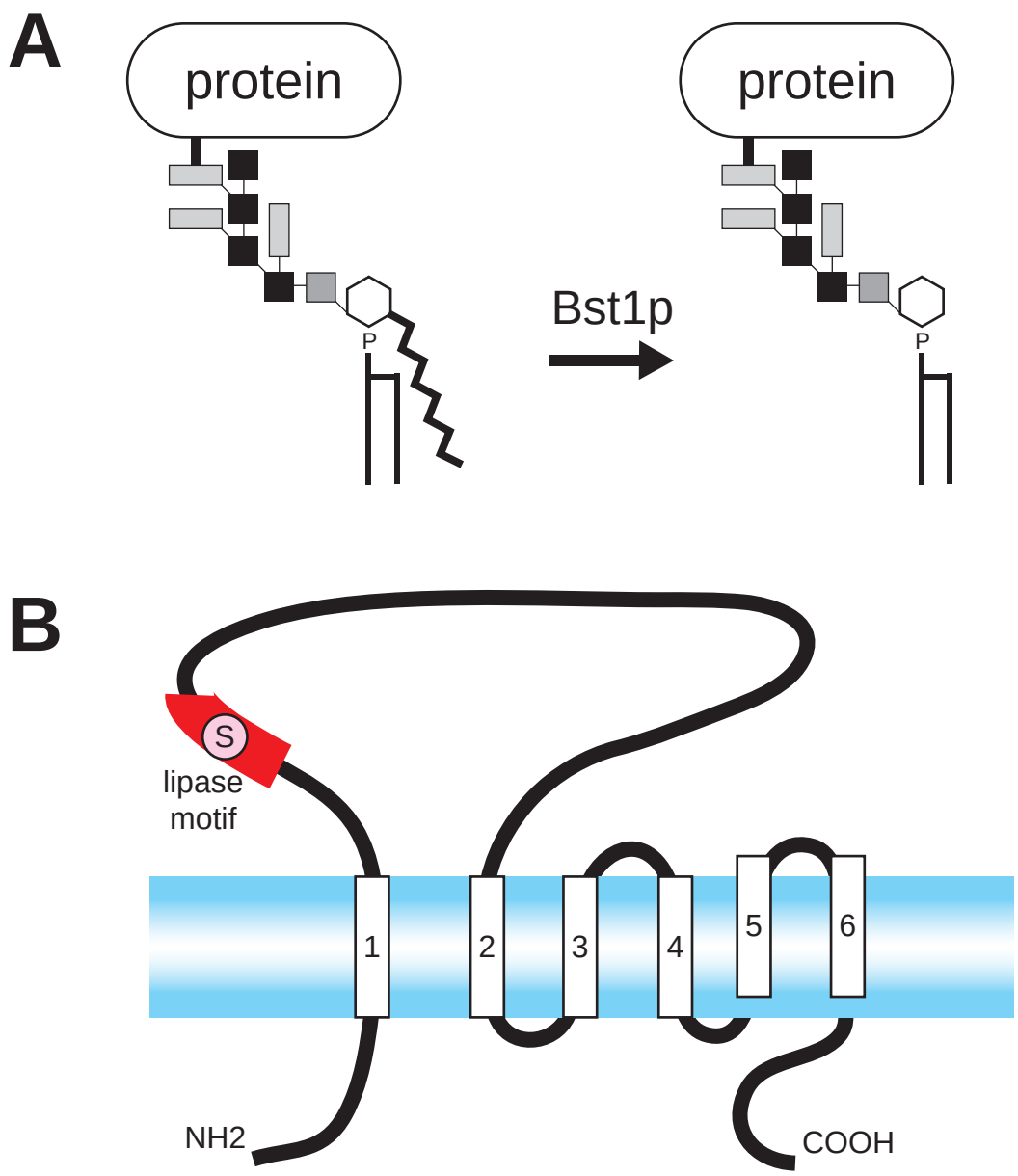

Figure 38. Enzymtic activity and topology of Bst1p

(A) Bst1p is required for the inositol deacylation of GPI after GPI attachment to protein. (B) Bst1p is a multi-spanning membrane protein localized at the ER. Bst1p has a lipase motif, which contain .

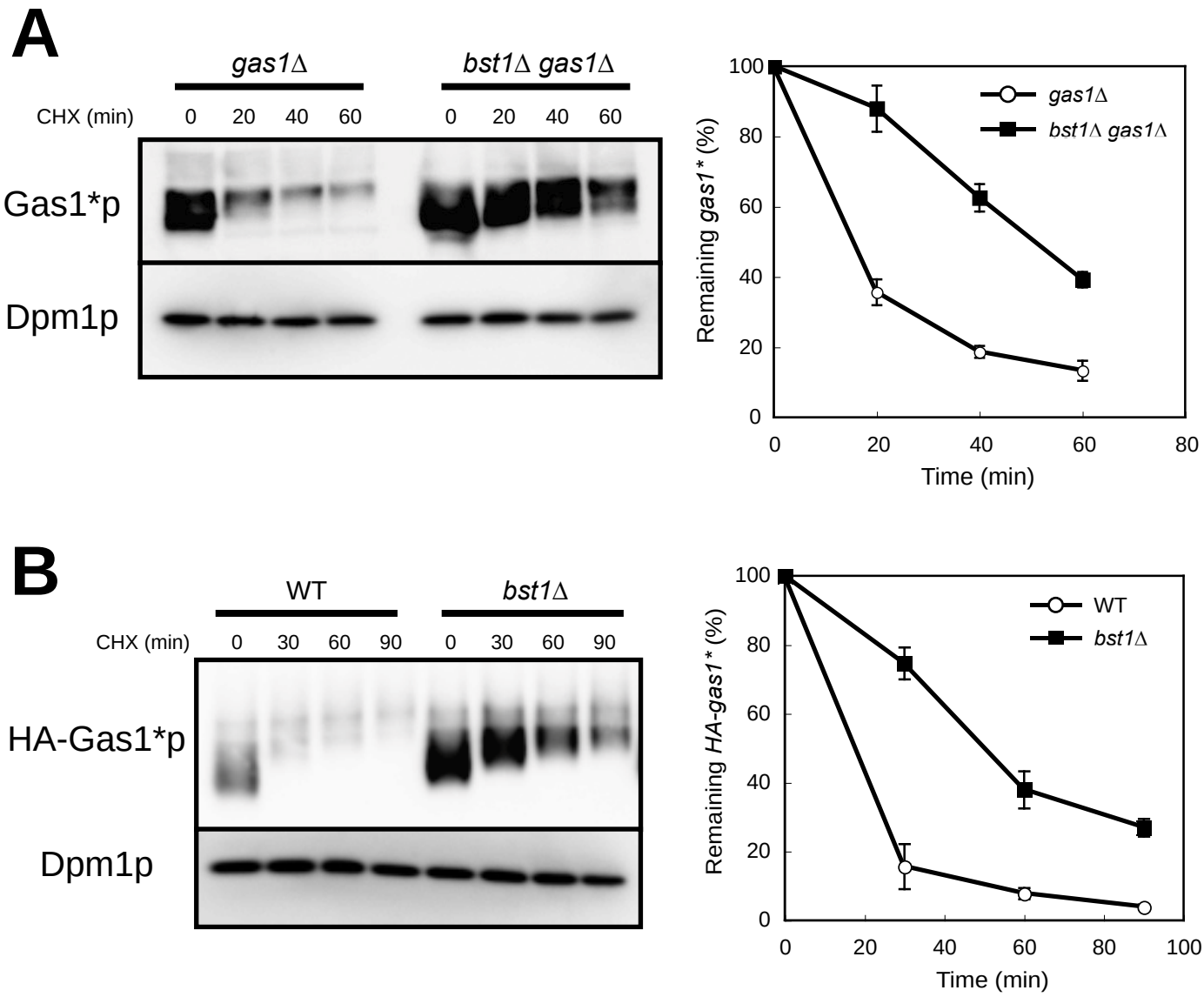

Figure 39. Deletion of *BST1* stabilizes the degradation of misfolded Gas1p

(A) The degradation of Gas1*p in MFY163 (*gas1*Δ *URA3::gas1**) and MFY176 (*bst1*Δ *gas1*Δ *URA3::gas1**) mutant cells. Equal cell numbers (2 X 10^7 cells/ml) were incubated with 200 µg/ml of CHX. Cells were chased for the indicated periods. Gas1p was resolved by electrophoresis and analyzed by immunoblotting with anti-Gas1p. The blot was subsequently probed with anti-Dpm1p as a control for loading. The results were quantified with an image analyzer and are plotted as mean values ± SD from three independent experiments, with the quantity at the 0 time point (steady-state level) set at 100%. (B) The degradation of HA-tagged Gas1*p in MFY188 (WT *URA3::HA-gas1**) and MFY189 (*bst1*Δ *URA3::HA-gas1**). The turnover of HA-Gas1*p in MFY188 (WT) cells and MFY189 (*bst1*Δ) cells was examined as described in (A). The results were quantified with an image analyzer and plotted as mean values ± SD from five independent experiments, with the quantity at the 0 time point (steady-state level) set at 100%.

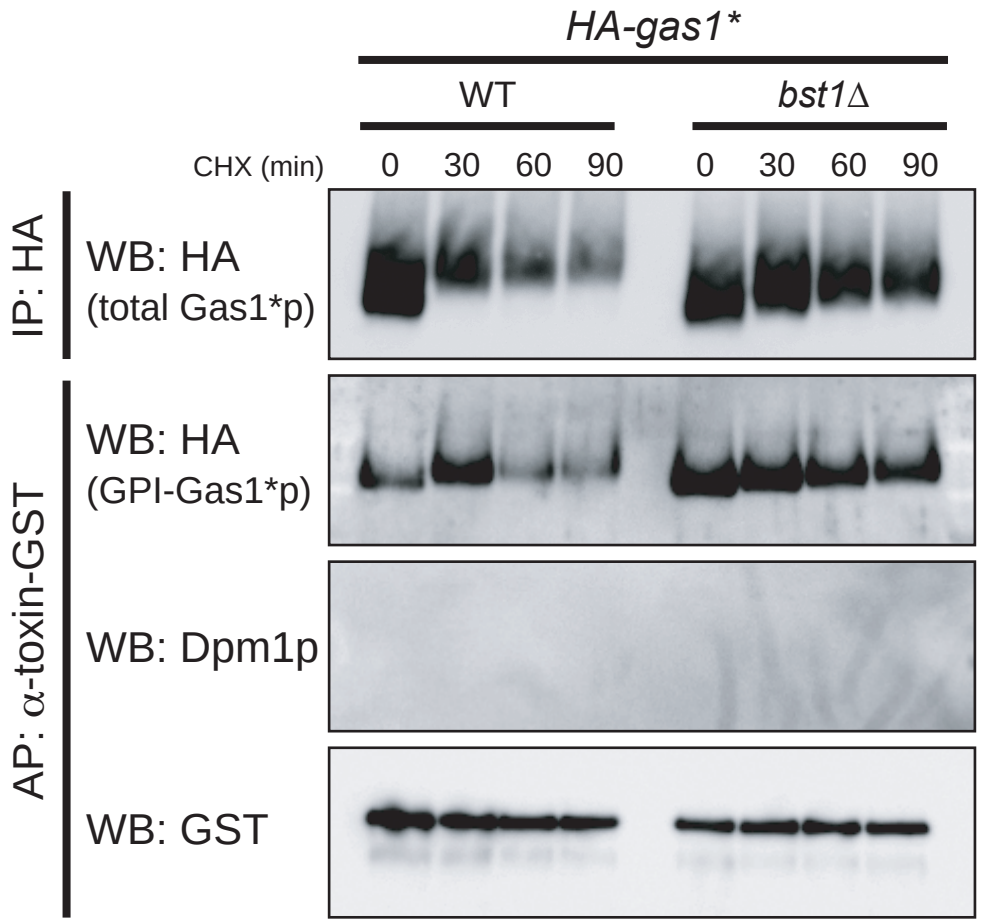

Figure 40. Gas1*p receives a GPI anchor before its degradation

MFY188 (WT) and MFY189 (*bst1*Δ) cells were analyzed by a CHX experiment, followed by immunoprecipitation (IP) with anti-HA-agarose or affinity precipitation (AP) with a-toxin-GST and glutathione-agarose beads. IP fractions were separated by SDS-PAGE and analyzed by immunoblotting with anti-HA, anti-Dpm1p, and anti-GST.

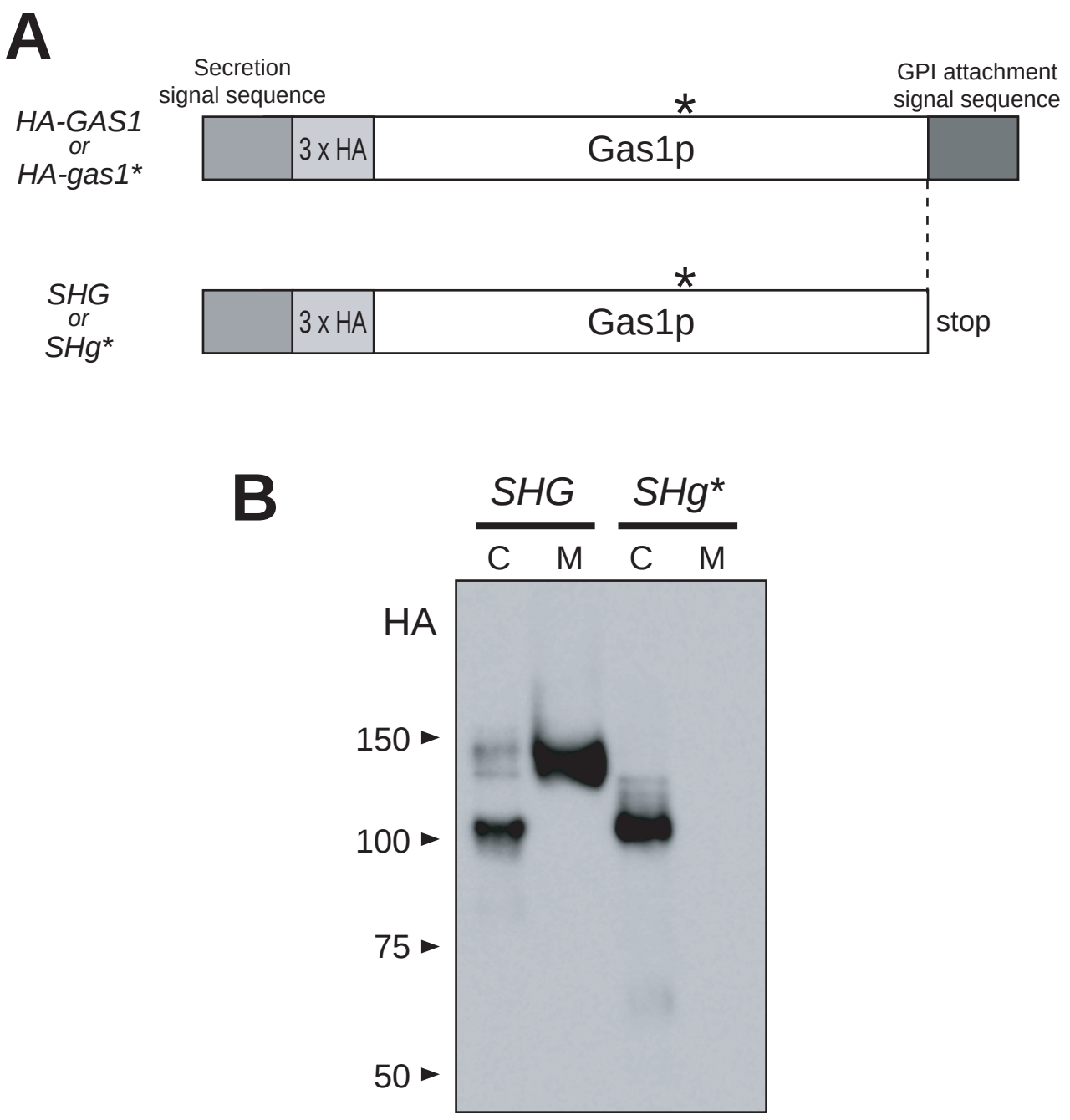

Figure 41. Construction and characterization of soluble forms of Gas1p (SHG) and Gas1*p (SHg*)

(A) SHG and SHg* carry a stop codon instead of an asparagine (N528) just before the GPI anchoring signal of Gas1p. (B) SHG but not SHg* is secreted into the medium. Cell lysates were prepared from exponentially growing cells. Proteins secreted into the medium were precipitated with 10% trichloroacetic acid. Samples corresponding to 0.5 OD_{600} units of cells per lane were analyzed by immunoblotting. C, cell lysate; M, medium.

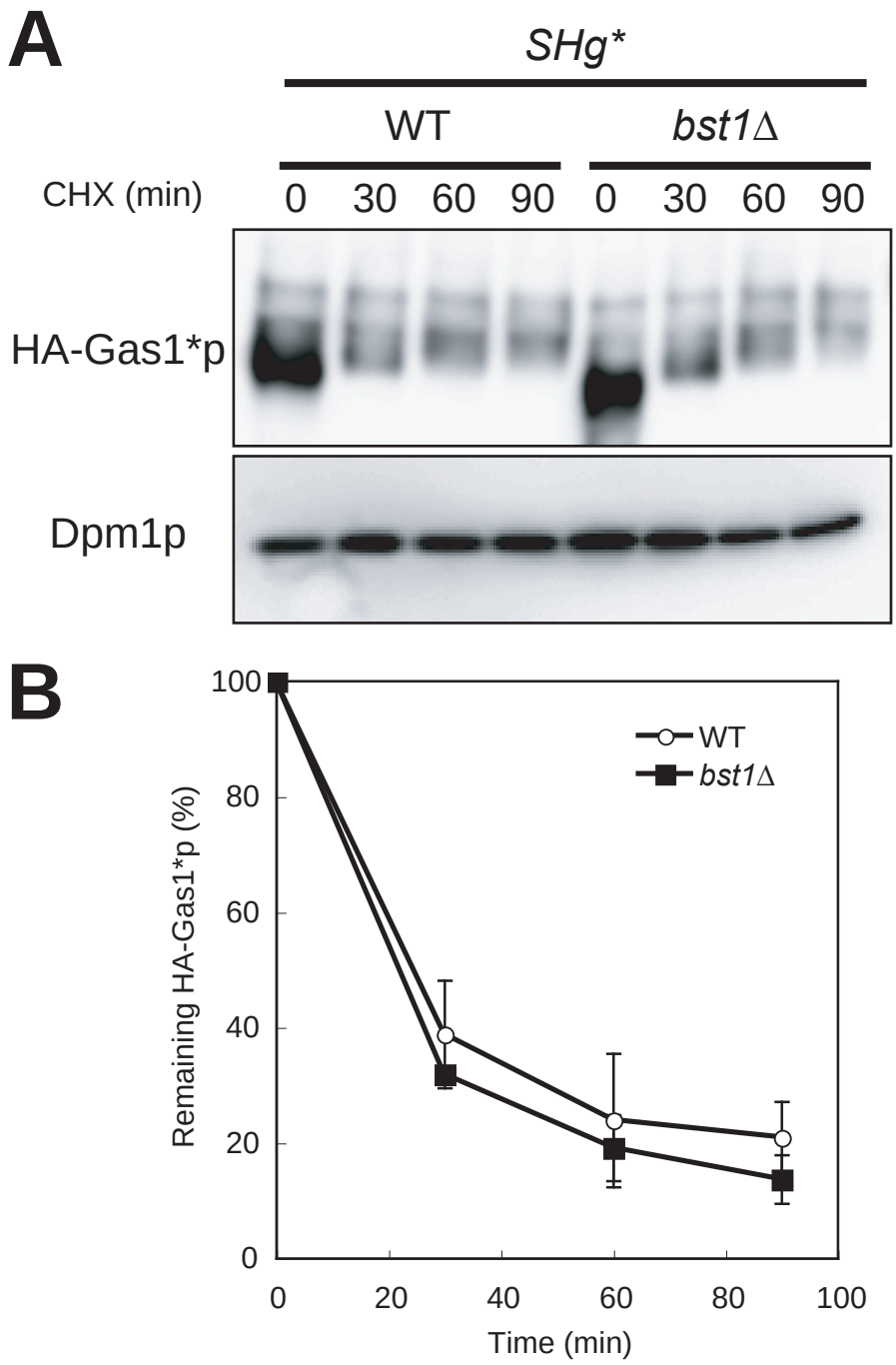

Figure 42. Degradation of a soluble form of Gas1*p is independent of Bst1p function

(A)(B) The degradation of SHg* was measured in MFY325 (WT) and MFY326 (*bst1*Δ) cells, in which SHg* is integrated at the *URA3* locus as described in Figure 38. The results were quantified with an image analyzer, and the mean values ± SDs of three independent experiments are plotted, with the quantity at the 0 time point (steady-state level) set at 100%.

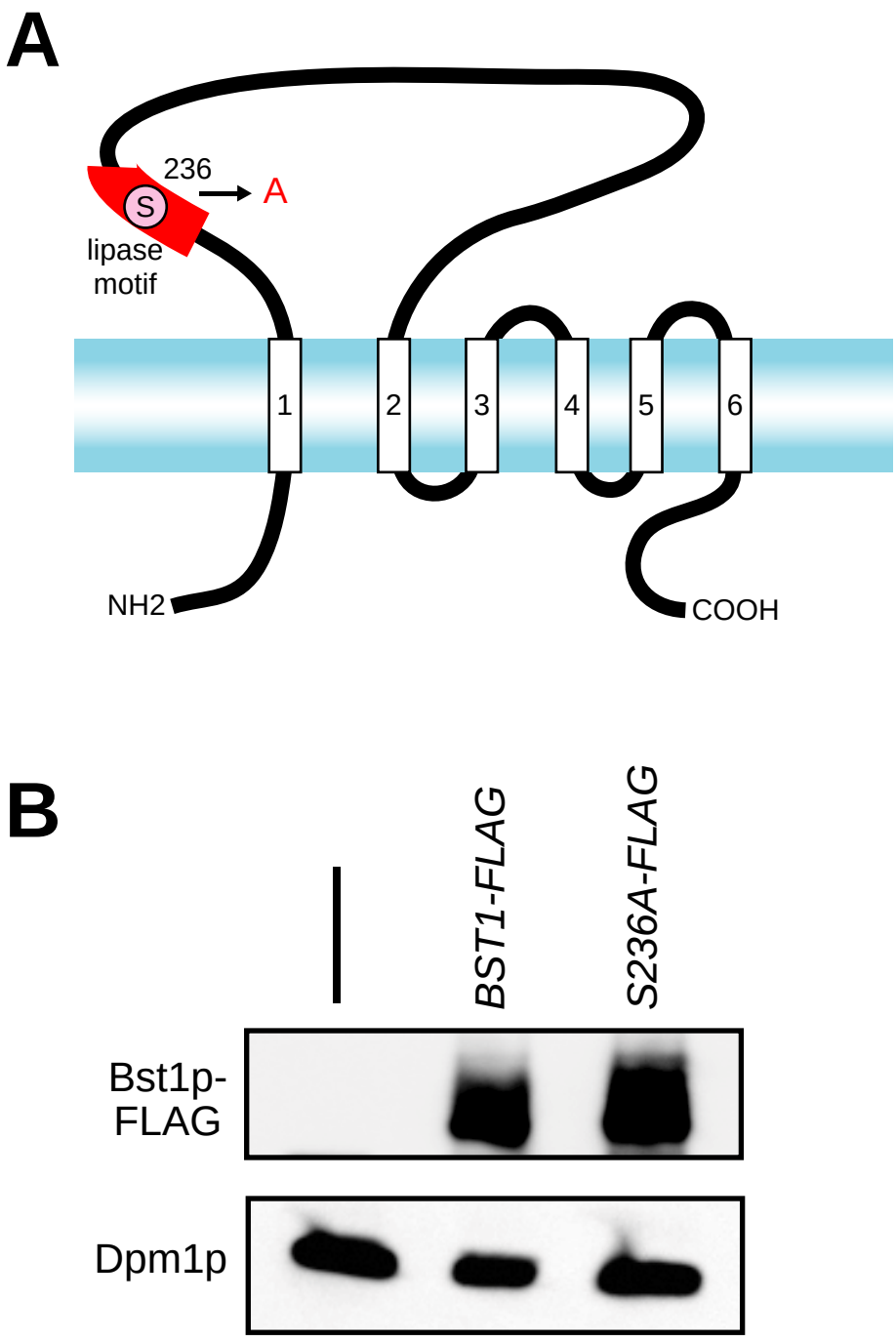

Figure 43. Construction of lipase-dead mutant Bst1p

(A) Schimatic model of mutant Bst1p. Bst1p contains a consensus lipase motif, which is regarded as an active site of deacylase. I replaced the putative catalytic site, serine 236, with alanine in lipase motif of Bst1p (S236A). (B) The expression of an S236A mutant of Bst1p. MFY150 (*bst1*Δ) cells were transformed with the plasmid containing the wild-type (YEp-BST1-FLAG) or S236A mutant (YEp-BST1SA-FLAG) of FLAG-tagged Bst1p. Equal cell numbers were disrupted, and total protein extracts were analyzed by immunoblotting with anti-FLAG antibody and anti-mouse HRP-conjugated IgG or with anti-Dpm1p antibody and anti-mouse HRP-conjugated IgG.

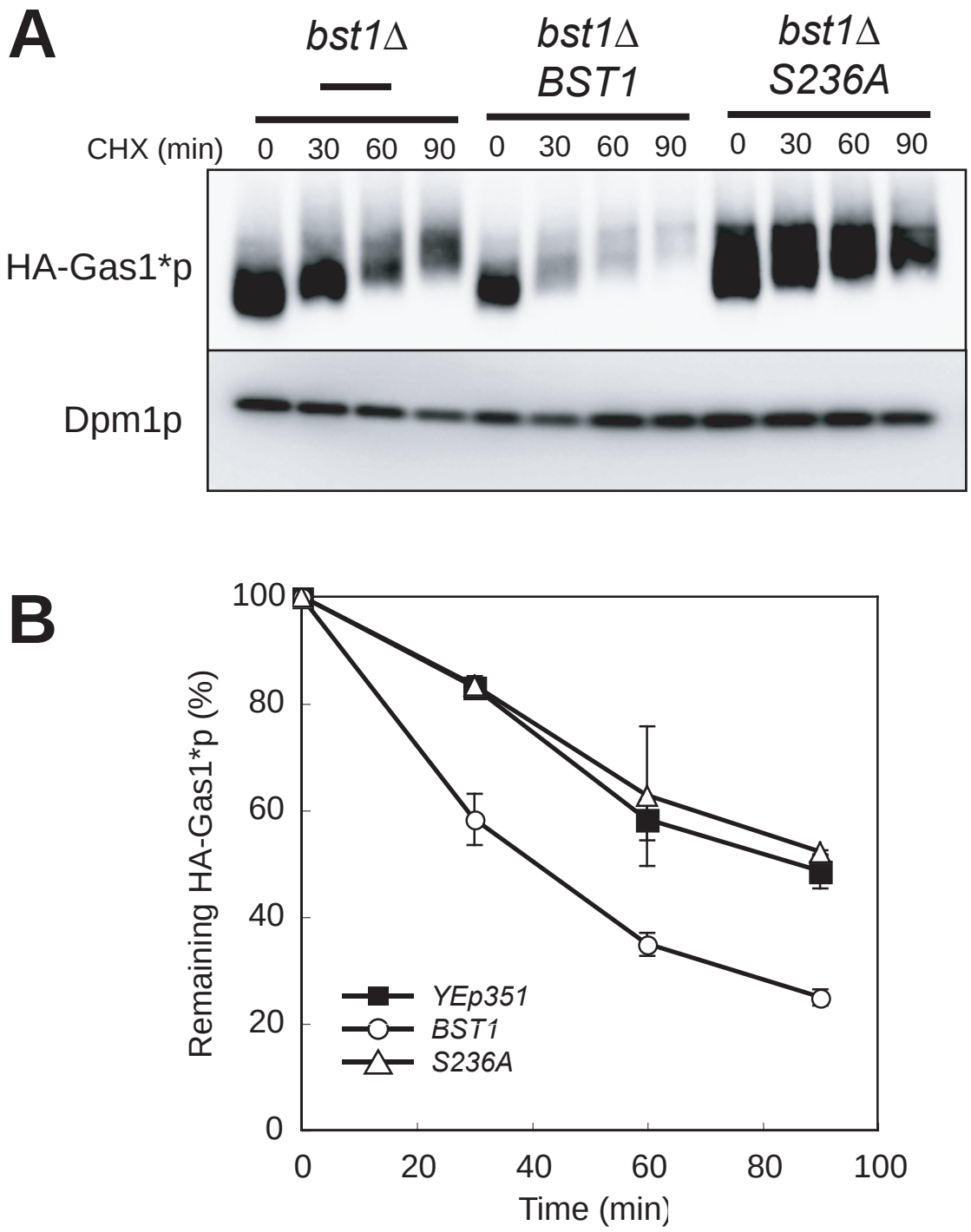

Figure 44. GPI inositol deacylase activity is important for the efficient degradation of misfolded Gas1p

(A)(B) Degradation of HA-Gas1*p was measured in MFY189 cells carrying YEp351 (*bst1*Δ –), YEp351-BST1 (*bst1*Δ *BST1*), or YEp351-BST1S236A (*bst1*Δ *S236A*). The rate of degradation of HA-Gas1*p was determined as described in Figure 33B.

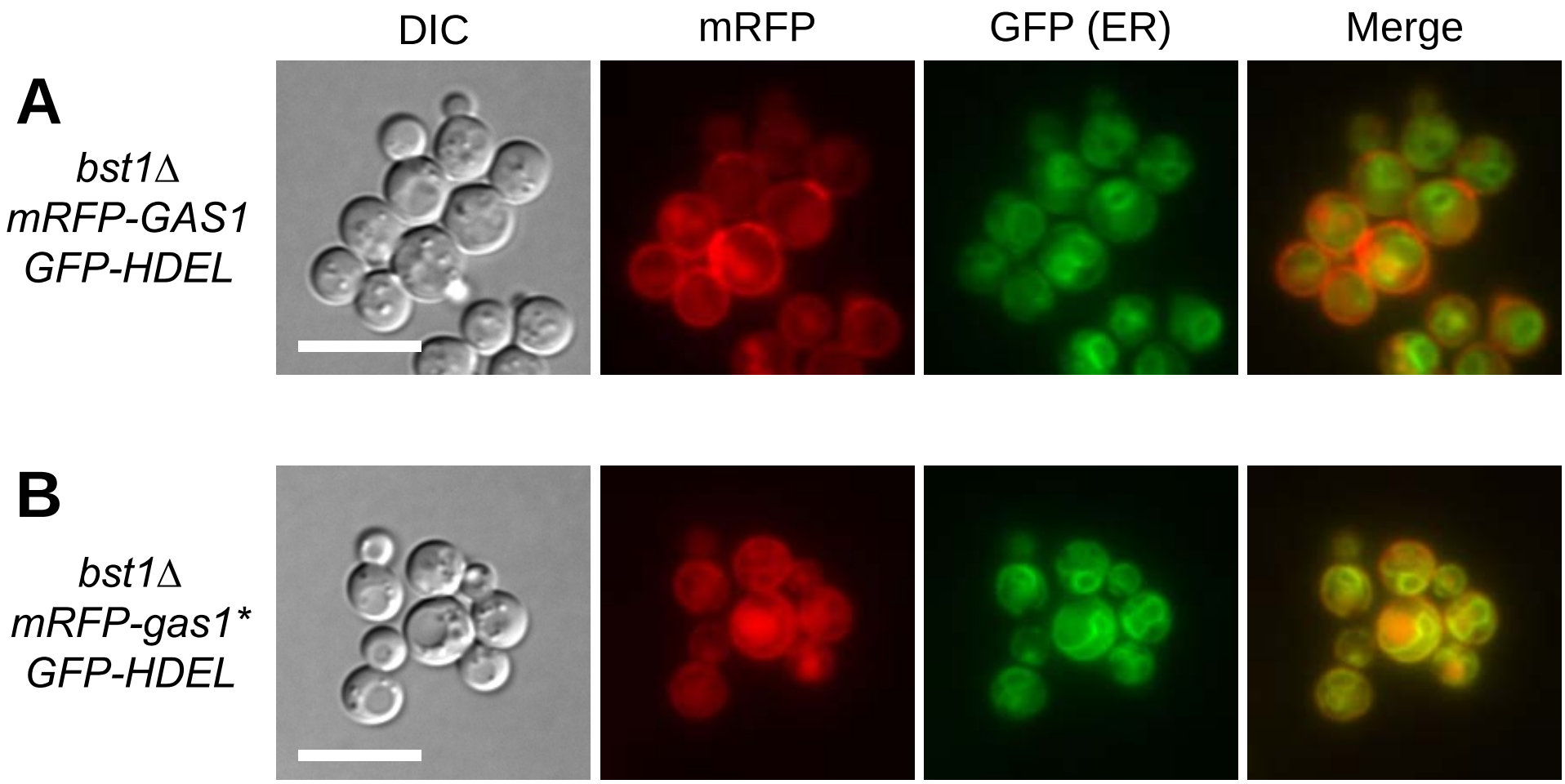

Figure 45. Localization of mRFP-Gas1p and mRFP-Gas1*p in *bst1*Δ cells

(A) MFY213 (*bst1*Δ *mRFP-GAS1*) cells or (B) MFY212 (*bst1*Δ *mRFP-gas1**) cells expressing GFP-HDEL were visualized by fluorescence microscopy. DIC, differential interference contrasts. Bar, 10 µm.

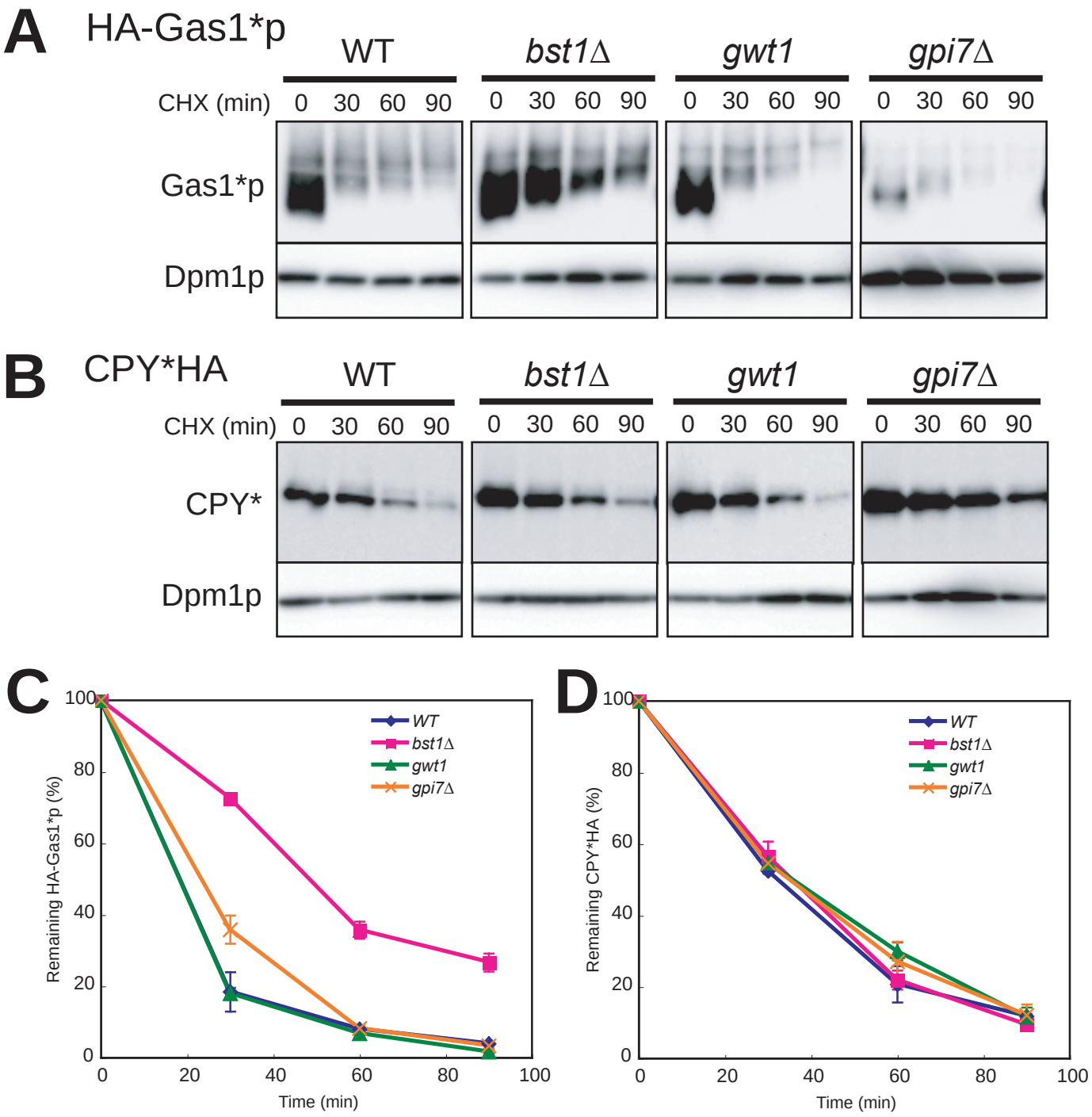

Figure 46. Effects of mutations in GPI biosynthesis on the degradation of Gas1*p and CPY*

(A) The degradation of Gas1*p was measured in MFY188 (WT), MFY189 (*bst1*Δ), MFY191 (*gwt1*), and MFY190 (*gpi7*Δ) cells, in which *HA-gas1** is integrated at the *URA3* locus. The rate of degradation of HA-Gas1*p was determined as described in Figure 33B. (B) The degradation of CPY* was measured in W303-1A (WT), MFY150 (*bst1*Δ), *gwt1-20* (*gwt1*), and MFY11 (*gpi7*Δ) cells, all of which carried pRS316-CPY*HA. The rate of degradation of HA-Gas1*p was determined as described in Figure 33B. (C) The amount of Gas1* protein was quantified and is plotted as the means ± SD of at least two independent experiments, with the quantity at the 0 time point (steady-state level) set at 100%. (D) The amount of CPY* protein was quantified and plotted as described above. CHX, cycloheximide.

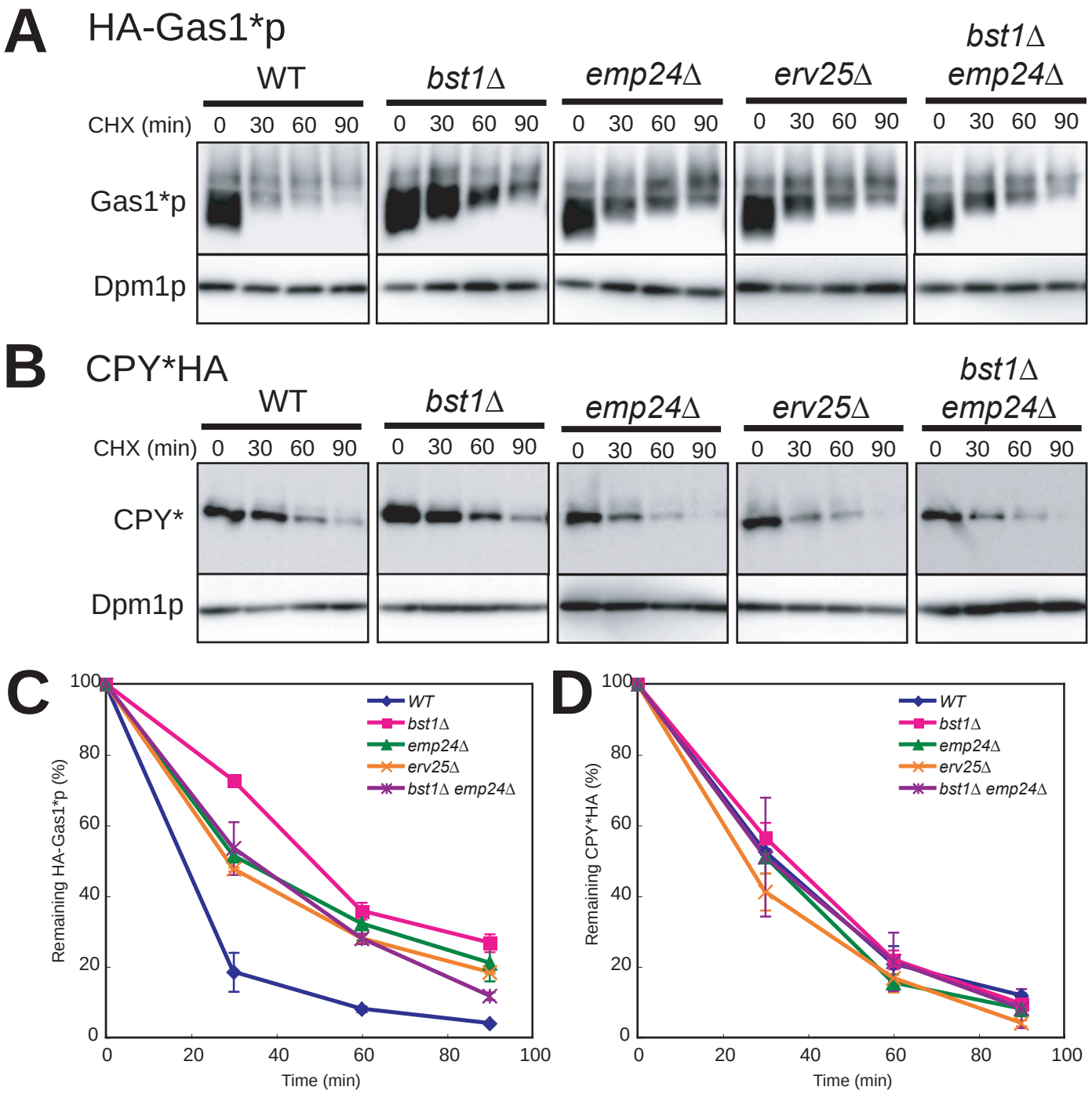

Figure 47. Effects of mutations in cargo receptors for GPI-anchored proteins on the degradation of Gas1*p and CPY*

(A) The degradation of Gas1*p was measured in MFY188 (WT), MFY189 (*bst1*Δ), MFY192 (*emp24*Δ), MFY193 (*erv25*Δ), and MFY195 (*bst1*Δ *emp24*Δ) cells, in which *HA-gas1** is integrated at the *URA3* locus. The rate of degradation of HA-Gas1*p was determined as described in Figure 33B. (B) The degradation of CPY* was measured in W303-1A (WT), MFY150 (*bst1*Δ), MFY157 (*emp24*Δ), MFY167 (*erv25*Δ), and MFY159 (*bst1*Δ *emp24*Δ) cells, all of which carried pRS316-CPY*HA. The rate of degradation of HA-Gas1*p was determined as described in Figure 33B. (C) The amount of Gas1* protein was quantified and is plotted as the means ± SD of at least two independent experiments, with the quantity at the 0 time point (steady-state level) set at 100%. (D) The amount of CPY* protein was quantified and plotted as described above. CHX, cycloheximide.

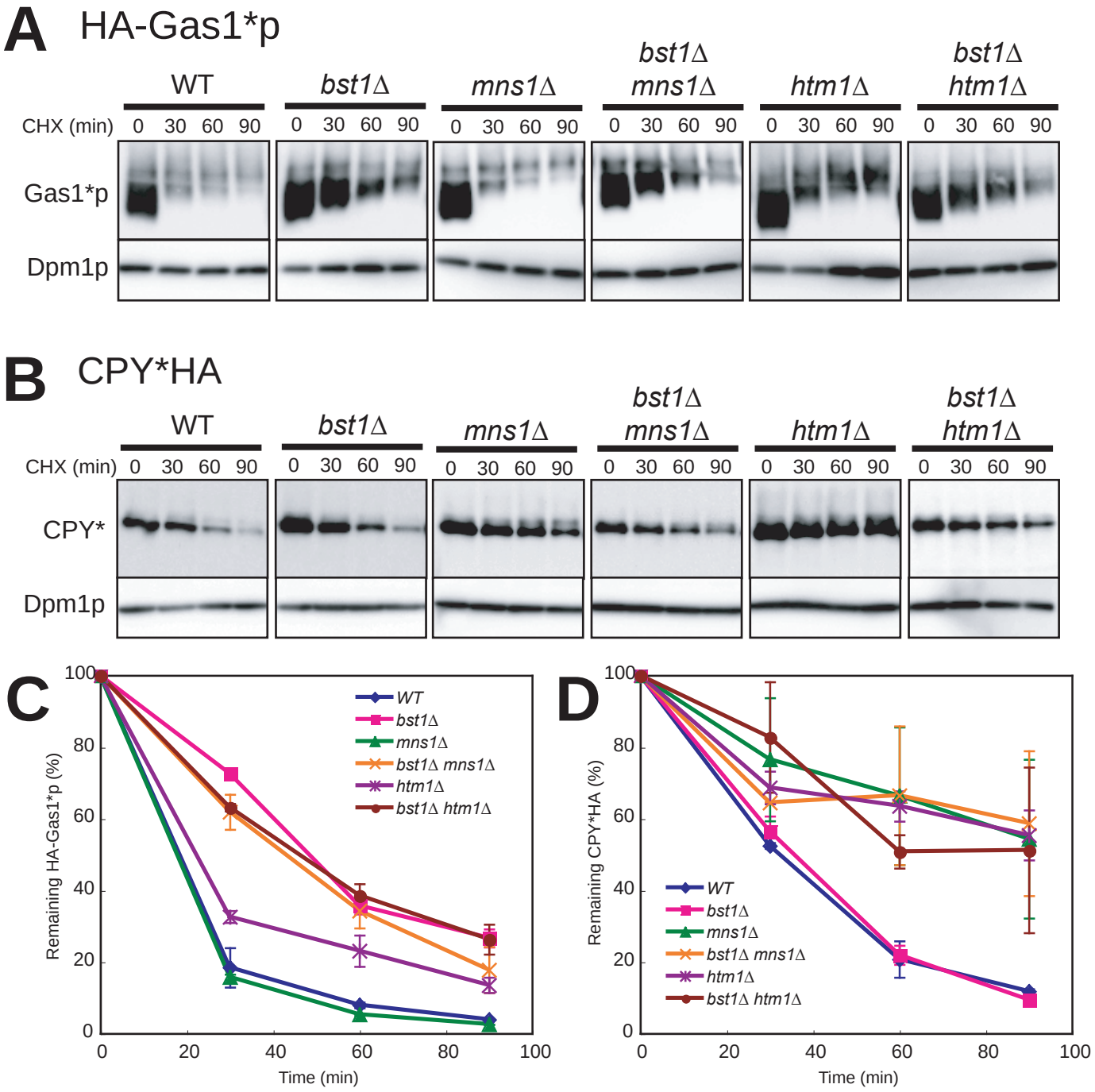

Figure 48. Effects of mutations in *N*-glycan processing on the degradation of Gas1*p and CPY*

(A) The degradation of Gas1*p was measured in MFY188 (WT), MFY189 (*bst1*Δ), MFY194 (*mns1*Δ), MFY196 (*bst1*Δ *mns1*Δ), MFY241 (*htm1*Δ), and MFY242 (*bst1*Δ *htm1*Δ) cells, in which *HA-gas1** is integrated at the *URA3* locus. The rate of degradation of HA-Gas1*p was determined as described in Figure 33B. (B) The degradation of CPY* was measured in W303-1A (WT), MFY150 (*bst1*Δ), MFY165 (*mns1*Δ), MFY168 (*bst1*Δ *mns1*Δ), MFY197 (*htm1*Δ), and MFY198 (*bst1*Δ *htm1*Δ) cells, all of which carried pRS316-CPY*HA. The rate of degradation of HA-Gas1*p was determined as described in Figure 33B. (C) The amount of Gas1* protein was quantified and is plotted as the means ± SD of at least two independent experiments, with the quantity at the 0 time point (steady-state level) set at 100%. (D) The amount of CPY* protein was quantified and plotted as described above. CHX, cycloheximide.

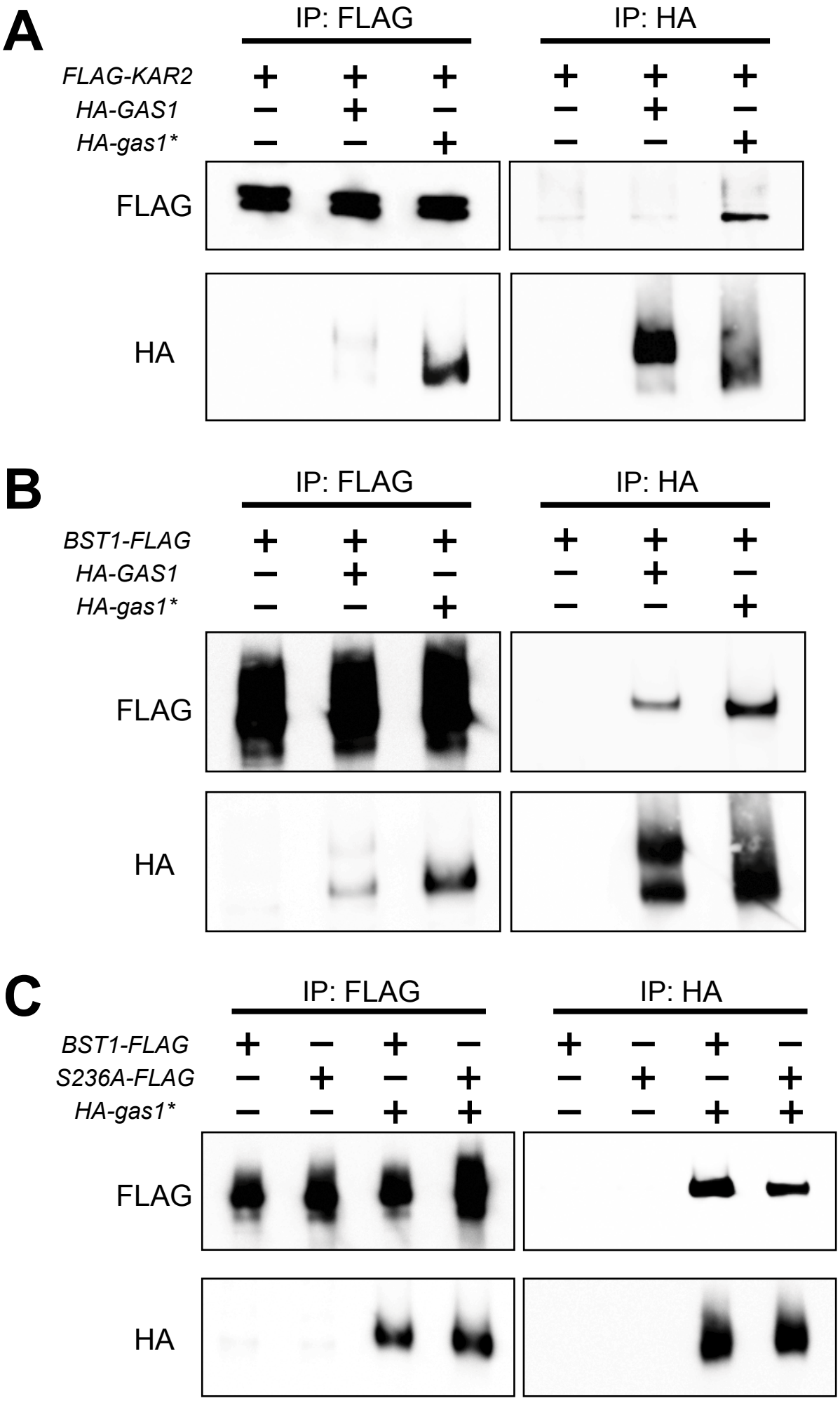
A
IP: FLAG
IP: HA
FLAG-KAR2
HA-GAS1
HA-gas1*
FLAG
HA
B
IP: FLAG
IP: HA
BST1-FLAG
HA-GAS1
HA-gas1*
FLAG
HA
C
IP: FLAG
IP: HA
BST1-FLAG
S236A-FLAG
HA-gas1*
FLAG
HA

Figure 49. BiP/Kar2p and Bst1p associate with Gas1*p *in vivo*

(A) Gas1*p associates with Kar2p. W303-1A (WT), MFY207 (*HA-GAS1*), and MFY208 (*HA-gas1**) cells, all of which carried YEp352-FLAG-KAR2 (*FLAG-KAR2*), were analyzed by immunoprecipitation (IP) with anti-FLAG-agarose or anti-HA-agarose, followed by immunoblotting with anti-FLAG (top) or anti-HA (bottom). (B) Gas1*p associates with Bst1p. W303-1A (WT), MFY207 (*HA-GAS1*), and MFY208 (*HA-gas1**) cells, all of which carried YEp352-BST1-FLAG (*BST1-FLAG*), were analyzed by IP with anti-FLAG-agarose or anti-HA-agarose, followed by immunoblotting with anti-FLAG (top) or anti-HA (bottom). (C) Lipase-inactive Bst1p associates with Gas1*p. W303-1A (WT) cells carrying YEp352-BST1-FLAG (*BST1-FLAG*), WT cells carrying YEp352-BST1S236A-FLAG (*S236A-FLAG*), MFY208 (*HA-gas1**) cells carrying YEp352-BST1-FLAG, and MFY208 cells carrying YEp352-BST1S236A-FLAG were analyzed by IP with anti-FLAG-agarose or anti-HA-agarose, followed by immunoblotting with anti-FLAG (top) or anti-HA (bottom).

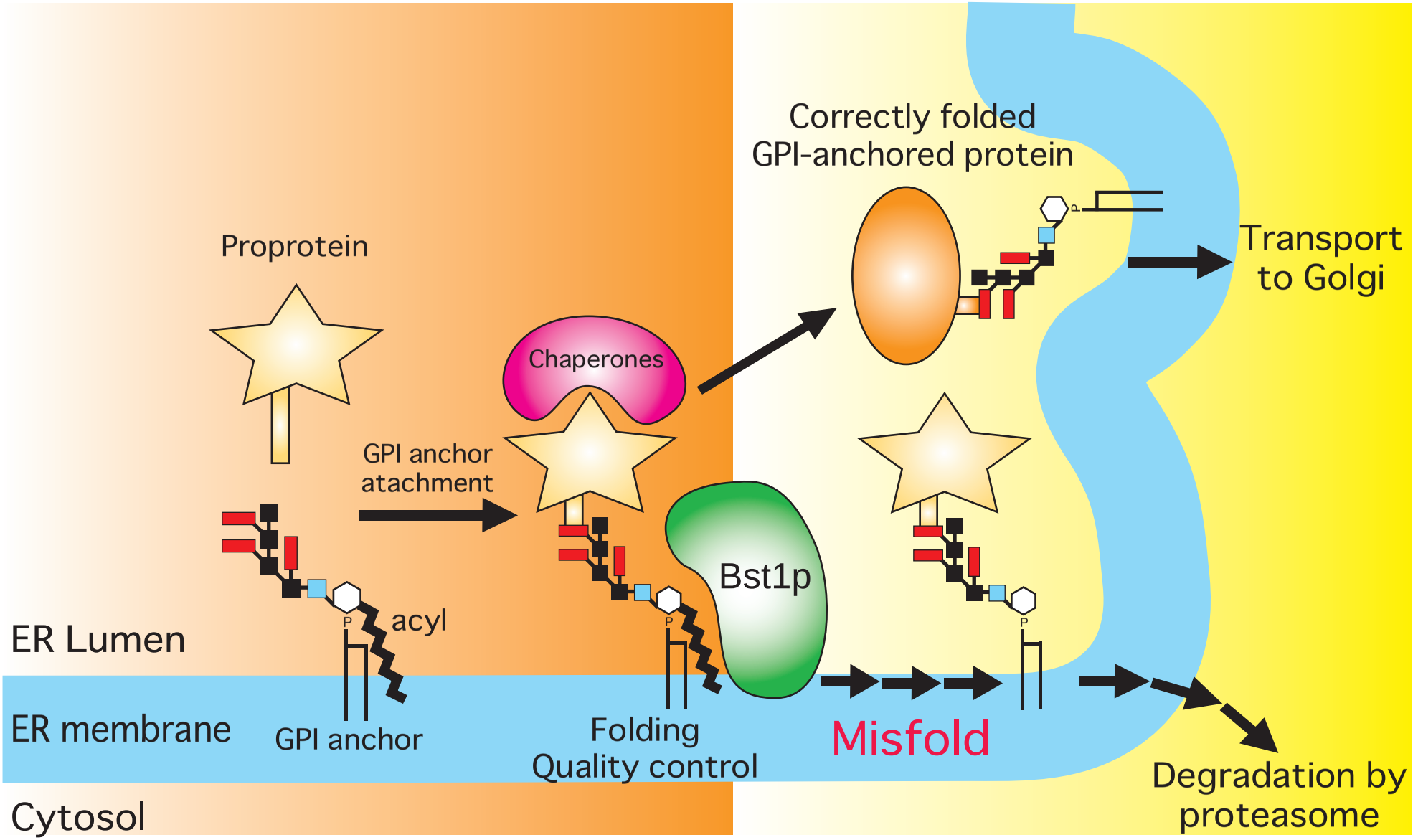

Figure 50. Model for the quality control of GPI-anchored proteins by Bst1p

After proproteins are synthesized, they are transferred to the GPI anchor by the GPI transamidase complex in the ER. Kar2p is one of the components involved in the folding of GPI-anchored proteins. The inositol in correctly folded GPI-anchored proteins is rapidly deacylated by Bst1p, after which the protein is transported to the Golgi. If folding of the GPI-anchored protein is not completed within an appropriate period of time, the GPI-anchored protein is deacylated by Bst1p and targeted for the ERAD pathway. Bst1p act as a gatekeeper that leads GPI-anchored proteiins to the ER exit after receiving some information on their folding status.

Table I: GPI biosynthetic genes

	Pathway	Mammals	*S. cerevisiae*
①	GPI-GlcNAc transferase	PIG-A	*GPI3*
		PIG-H	*GPI15*
		PIG-C	*GPI2*
		GPI1	*GPI1*
		PIG-P	*GPI19*
		PIG-Y	*ERI1*
		DPM2	
			RAS2 (negative)
②	de-*N* -acetylase	PIG-L	*GPI12*
③	flippase		
④	acyltransferase	PIG-W	*GWT1*
⑤	GPI-α-1-4mannosyltransferase	PIG-M	*GPI14*
		PIG-X	*PBN1*
⑥	ethanolamine-P-transferase	PIG-N	*MCD4*
⑦	GPI-α-1-6mannosyltransferase	PIG-V	*GPI18*
⑧	GPI-α-1-2mannosyltransferase	PIG-B	*GPI10*
⑨	GPI-α-1-2mannosyltransferase	(hSMP3)	*SMP3*
⑩	ethanolamine-P-transferase	PIG-O	*GPI13*
		PIG-F	*GPI11*
⑪	ethanolamine-P-transferase	GPI7	*GPI7*
		PIG-F	*GPI11*
⑫	transamidase	GAA1	*GAA1*
		GPI8 (PIG-K)	*GPI8*
		PIG-S	*GPI17*
		PIG-T	*GPI16*
		PIG-U	*GAB1*
⑬	GPI deacylase	PGAP1	*BST1*

Table II. Yeast strains used in this study

Strain	Genotype	Origin
W303-1A	*MAT***a** *ade2-1 his3-11 leu2-3,-112 trp1-1 ura3-1 can1-100*	Sutton *et al.* 1991
W303-1B	*MATα ade2-1 his3-11 leu2-3,-112 trp1-1 ura3-1 can1-100*	Sutton *et al.* 1991
KA31α	*MATα trp1 ura3 leu2 his3*	Yashiroda *et al.* 1996
YAT2-1C	*MATα trp1 ura3 leu2 his3 rsp5-101*	Yashiroda *et al.* 1996
YK109	*MAT***a** *rpn12-1 leu2 his3 trp1 ura3 ade1*	Kominami *et al.* 1995
YAT2579	*MAT***a** *rpn3-1* W303	Dr. Toh-e Laboratory
YS63-1C	*MATα sec18-1 trp1 ura3 leu2 his3*	Laboratory stock
MHY501	*MATα his3-200 leu2-3,-112 ura3-52 lys2-801 trp1-1*	Swanson *et al*. 2001
MHY1703	*MATα hrd1*Δ::*LEU2 doa10*Δ::*HIS3* MHY501	Swanson *et al*. 2001
gwt1-20	*MATα gwt1*Δ::*his5*$^{+}$ *gwt1-20*::*TRP1* W303	Umemura *et al.* 2003
MFY1	*MAT*a *gpi7*Δ::*his5*$^{+}$ W303	This study
MFY11	*MAT***a** *gpi7*Δ::*TRP1* W303	This study
MFY-by38	*MAT*a *gpi7*Δ::*TRP1 cbk1*^{mTn}::*URA3* W303	This study
MFY60	*MAT*a *gpi7*Δ::*TRP1 cbk1*Δ::*his5*$^{+}$ W303	This study
MFY64	*MAT*a *gpi7*Δ::*TRP1 ace2*Δ::*his5*$^{+}$ W303	This study
MFY63	*MAT*a *gpi7*Δ::*TRP1 egt2*Δ::*his5*$^{+}$ W303	This study
MFY75	*MAT*a *gpi7*Δ::*TRP1 bgl2*Δ::*his5*$^{+}$ W303	This study
MFY150	*MAT***a** *bst1*Δ::*TRP1* W303	This study
MFY156	*MAT***a** *gas1*Δ::*his5*$^{+}$ W303	This study
MFY157	*MAT***a** *emp24*Δ::*his5*$^{+}$ W303	This study
MFY159	*MAT***a** *bst1*Δ::*TRP1 emp24*Δ::*his5*$^{+}$ W303	This study
MFY161	*MAT***a** *gas1*Δ::*his5*$^{+}$ *GAS1*::*URA3* W303	This study
MFY163	*MAT***a** *gas1*Δ::*his5*$^{+}$ *gas1**::*URA3* W303	This study
MFY165	*MAT***a** *mns1*Δ::*LEU2* W303	This study
MFY166	*MAT***a** *gas1*Δ::*his5*$^{+}$ *bst1*Δ::*TRP1* W303	This study

MFY167	*MAT***a** *erv25*Δ::*LEU2* W303	This study
MFY168	*MAT***a** *bst1*Δ::*TRP1 mns1*Δ::*LEU2* W303	This study
MFY176	*MAT***a** *bst1*Δ::*TRP1 gas1*Δ::*his5*$^{+}$ *gas1**::*URA3* W303	This study
MFY182	*MAT***a** *gas1*Δ::*his5*$^{+}$ *HA-GAS1*::*LEU2* W303	This study
MFY183	*MAT***a** *gas1*Δ::*his5*$^{+}$ *mRFP-GAS1*::*LEU2* W303	This study
MFY188	*MAT***a** *HA-gas1**::*URA3* W303	This study
MFY189	*MAT***a** *bst1*Δ::*TRP1 HA-gas1**::*URA3* W303	This study
MFY190	*MAT***a** *gpi7*Δ::*TRP1 HA-gas1**::*URA3* W303	This study
MFY191	*MAT***a** *gwt1*Δ::*his5*$^{+}$ *gwt1-20*::*TRP1 HA-gas1**::*URA3* W303	This study
MFY192	*MAT***a** *emp24*Δ::*his5*$^{+}$ *HA-gas1**::*URA3* W303	This study
MFY193	*MAT***a** *erv25*Δ::*LEU2 HA-gas1**::*URA3* W303	This study
MFY194	*MAT***a** *mns1*Δ::*LEU2 HA-gas1**::*URA3* W303	This study
MFY195	*MAT***a** *bst1*Δ::*TRP1 emp24*Δ::*his5*$^{+}$ *HA-gas1**::*URA3* W303	This study
MFY196	*MAT***a** *bst1*Δ::*TRP1 mns1*Δ::*LEU2 HA-gas1**::*URA3* W303	This study
MFY197	*MAT***a** *htm1*Δ::*his5*$^{+}$ W303	This study
MFY198	*MAT***a** *bst1*Δ::*TRP1 htm1*Δ::*his5*$^{+}$ W303	This study
MFY207	*MAT***a** *HA-GAS1*::*LEU2* W303	This study
MFY208	*MAT***a** *HA-gas1**::*LEU2* W303	This study
MFY213	*MAT***a** *bst1*Δ::*TRP1 mRFP-GAS1*::*LEU2* W303	This study
MFY212	*MAT***a** *bst1*Δ::*TRP1 mRFP-gas1**::*LEU2* W303	This study
MFY241	*MAT***a** *htm1*Δ::*his5*$^{+}$ *HA-gas1**::*URA3* W303	This study
MFY242	*MAT***a** *bst1*Δ::*TRP1 htm1*Δ::*his5*$^{+}$ *HA-gas1**::*URA3* W303	This study
MFY215	*MAT***a** *hrd1*Δ::*his5*$^{+}$ W303	This study
MFY278	*MAT***a** *doa10*Δ::*his5*$^{+}$ W303	This study
MFY255	*MAT***a** *pep4*Δ::*his5*$^{+}$ W303	This study
MFY327	*MAT***a** *hrd1*Δ::*his5*$^{+}$ *HA-gas1**::*URA3* W303	This study
MFY328	*MAT***a** *doa10*Δ::*his5*$^{+}$ *HA-gas1**::*URA3* W303	This study
MFY329	*MAT***a** *pep4*Δ::*his5*$^{+}$ *HA-gas1**::*URA3* W303	This study

MFY331	*MATα trp1 ura3 leu2 his3 HA-gas1**::*URA3*	This study
MFY332	*MATα trp1 ura3 leu2 his3 rsp5-101 HA-gas1**::*URA3*	This study
MFY336	*MAT***a** *rpn12-1 HA-gas1**::*URA3 leu2 his3 trp1 ura3 ade1*	This study
MFY337	*MAT***a** *rpn3-1 HA-gas1**::*URA3* W303	This study
MFY324	*MAT***a** *SHG*::*LEU2* W303	This study
MFY325	*MAT***a** *SHg**::*URA3* W303	This study
MFY326	*MAT***a** *bst1*Δ::*TRP1 SHg**::*URA3* W303	This study
MFY341	*MAT***a** *hrd1*Δ::*his5*$^{+}$ *doa10*Δ::*his5*$^{+}$ W303	This study
MFY343	*MAT***a** *hrd1*Δ::*his5*$^{+}$ *doa10*Δ::*his5*$^{+}$ *HA-gas1**::*URA3* W303	This study
MFY348	*MATα sec18-1 trp1 ura3 leu2 his3 HA-gas1**::*URA3*	This study
MFY351	*MATα HA-gas1**::*URA3* MHY501	This study
MFY352	*MATα hrd1*Δ::*LEU2 doa10*Δ::*HIS3 HA-gas1**::*URA3* MHY501	This study

Table III. Plasmids used in this study

Plasmid	Description	Origin
pRS305	*LEU2*	Sikorski and Hieter, 1989
pRS306	*URA3*	Sikorski and Hieter, 1989
pRS315	*CEN, ARS, LEU2*	Sikorski and Hieter, 1989
pRS316	*CEN, ARS, URA3*	Sikorski and Hieter, 1989
YEp351	2μ, *LEU2*	Dr. Jigami Laboratory
YEp351GAPII	2μ, *LEU2, TDH3* promoter and terminator	Abe *et al.*, 2003
YEp352GAPII	2μ, *URA3, TDH3* promoter and terminator	Abe *et al.*, 2003
TOp1014	*GPI7. CEN4, ARS1, URA3*	Dr. Toh-e laboratory
pMO13	*GFP-HDEL, CEN, ARS, URA3*	This study
pMF7	GPI7-HA, pRS316	This study
pMF10	gpi7-2-HA, pRS316	This study
pMF32	gpi7-2-HA, pRS314	This study
YEpROM2	ROM2, YEp352GAPII	This study
YEpCDC5	CDC5, YEp351	This study
YEpWSC1	WSC1, YEp351	This study
YEpGFA1	GFA1, YEp351	This study
YEpRHO2	RHO2, YEp351	This study
pMF297	HA-EGT2, pRS315	This study
pMF310	HA-ENG1, pRS315	This study
pMF357	HA-ENG1-EGT2, pRS315	This study
pMF600	*GAS1*, pRS306	This study
pMF605	*gas1**, pRS306	This study
pMF607	*HA-GAS1*, pRS305	This study
pMF608	*mRFP-GAS1*, pRS305	This study
pMF615	*HA-gas1**, pRS305	This study

pMF616	*HA-gas1**, pRS306	This study
pMF617	*mRFP-gas1**, pRS305	This study
pMF634	*BST1*, YEp351GAPII	This study
pMF636	*BST1(S236A)*, YEp351GAPII	This study
pMF641	*BST1-FLAG*, YEp351GAPII	This study
pMF642	*BST1(S236A)-FLAG*, YEp351GAPII	This study
pMF643	*BST1-FLAG*, YEp352GAPII	This study
pMF644	*BST1(S236A)-FLAG*, YEp352GAPII	This study
pMF834	*FLAG-KAR2*, YEp352GAPII	This study
pMF848	*CPY*HA*, pRS316	This study
pMF874	*SHG*, pRS305	This study
pMF876	*SHg**, pRS306	This study
pMF880	*SEC18*, pRS315	This study